UC Berkeley
UC Berkeley Electronic Theses and Dissertations

**Title**
Supersymmetry, Dark Matter and the Hierarchy of Yukawa Couplings

**Permalink**
https://escholarship.org/uc/item/2658f8gb

**Author**
Mandal, Sourav Kumar

**Publication Date**
2010

Peer reviewed|Thesis/dissertation

eScholarship.org Powered by the California Digital Library
University of California

Supersymmetry, Dark Matter and the Hierarchy of Yukawa Couplings

by

Sourav Kumar Mandal

A dissertation submitted in partial satisfaction of the

requirements for the degree of

Doctor of Philosophy

in

Physics

in the

Graduate Division

of the

University of California, Berkeley

Committee in charge:

Professor Hitoshi Murayama, Chair

Professor Yasunori Nomura

Professor Leo Blitz

Spring 2010

Supersymmetry, Dark Matter and the Hierarchy of Yukawa Couplings

Copyright 2010

by

Sourav Kumar Mandal

Abstract

Supersymmetry, Dark Matter and the Hierarchy of Yukawa Couplings

by

Sourav Kumar Mandal

Doctor of Philosophy in Physics

University of California, Berkeley

Professor Hitoshi Murayama, Chair

While the standard model successfully describes a wide array of phenomena among the fundamental particles and interactions, some significant problems remain. These include the hierarchy problem in the Higgs sector, the hierarchy of the Yukawa couplings, and the nature of dark matter.

These problems are addressed in this thesis. First, the standard model and its problems are reviewed; supersymmetry is identified as possible framework for solving all three problems. Second, brief reviews of supersymmetry and dark matter phenomenology are provided. Then, using gamma rays and neutrinos, novel astrophysical constraints on the dark matter interpretation of the recently observed cosmic-ray $e^{\pm}$ anomalies are developed. Finally, a class of supersymmetric models is described wherein the first and second generation squarks and sleptons are pseudo-Nambu-Goldstone bosons, making their standard model counterparts naturally light, thereby resolving the Yukawa hierarchy problem. We show that this model an be easily identified at the Large Hadron Collider after a few months of running at 14 TeV. This class of models also provides a promising dark matter candidate which evades the derived gamma ray and neutrino bounds, and may be relevant to the cosmic ray $e^{\pm}$ anomalies in a certain parameter region.

To my grandfathers,

On whose shoulders I stand today.

# Contents

# Acknowledgments

First, I would like to thank my family — my father Asim, my mother Manisha, and my younger brother Debarshi — without whose care and support I would not find myself here today. I would also like to thank a new addition to my family, my beautiful wife Shinhyung Ahn, whose empathy and kindness have brought a new joy and strength to my life.

Second, I would like to acknowledge the many mentors who have guided me in my journey. Foremost, I would like to thank my adviser Hitoshi Murayama, who has provided generous support and an example of excellence which I will always remember. I would also like to thank Spencer Klein of the Lawrence Berkeley National Laboratory, Professors Thomas Greytak and Daniel Kleppner of the Massachusetts Institute of Technology (my alma mater), Kenneth Dymond and the late Daryl Yentis of the Naval Research Laboratory, James Ellenbogen at MITRE, and Paul Hertz, formerly of the Naval Research Laboratory, now at NASA.

Finally, I would like to give a special thanks to Drs. Robert Kevess at University Health Services and Jonathan Ellman at the Sutter East Bay Medical Foundation, who got me back on my feet.

This work was supported in part by World Premier International Research Center Initiative, MEXT, Japan, in part by the U.S. DOE under Contract DE-AC03-76SF00098, and in part by the NSF under grant PHY-04-57315.

# Chapter 1

# Introduction

The standard model has stood as a benchmark of predictive power among scientific theories. It explains an array of observations in precision quantum electrodynamics, nuclear physics, collider phenomenology and particle cosmology, and in doing so underlies much of our understanding of nature. However, there remain open questions in the standard model, such as the existence and controlled renormalization of the Higgs, the hierarchy of Yukawa couplings and the nature of dark matter.

In this thesis, these three questions are addressed. In Section 1.1, the standard model is reviewed, and then in Section 1.2 the various problems of the standard model are discussed. Here, supersymmetry is argued to be a framework that may solve all three problems. Then, in Section 1.3 supersymmetry is developed from first principles, installed in curved spacetime backgrounds, then applied to the standard model. Finally, at the end of the Section it is discussed how supersymmetry can explain the hierarchy of the Yukawa couplings. Afterward, in Section 1.4, dark matter is broadly reviewed. Presented are evidence of its existence, possible candidates and certain aspects of its detection, with an emphasis on WIMPs from supersymmetry.

Then, in Chapter 2, the dark matter interpretation of recently observed cosmic-ray $e^{\pm}$ anomalies is put to the test by the development of novel astrophysical constraints from gamma rays and neutrinos. Finally, in Chapter 3, a class of supersymmetric coset theories is presented in which the first and second generation quarks and leptons are the fermionic partners to pseudo-Nambu-Goldstone bosons, thereby

| Symbol | $SU(3)_c$ | $SU(2)_L$ | $U(1)_Y$ | $U(1)_{EM}$ |
|---|---|---|---|---|
| $Q_{L,i} = \begin{pmatrix} u_{L,i} \\ d_{L,i} \end{pmatrix}$ | $\mathbf{3}$ | $\mathbf{2}$ | $+1/6$ | $\begin{pmatrix} +2/3 \\ -1/3 \end{pmatrix}$ |
| $\bar{u}_{R,i} = (u_{R,i})^c$ | $\bar{\mathbf{3}}$ | $\mathbf{1}$ | $-2/3$ | $-2/3$ |
| $\bar{d}_{R,i} = (d_{R,i})^c$ | $\bar{\mathbf{3}}$ | $\mathbf{1}$ | $+1/3$ | $+1/3$ |
| $L_{L,i} = \begin{pmatrix} \nu_{L,i} \\ e_{L,i} \end{pmatrix}$ | $\mathbf{1}$ | $\mathbf{2}$ | $-1/2$ | $\begin{pmatrix} 0 \\ -1 \end{pmatrix}$ |
| $\bar{e}_{R,i} = (e_{R,i})^c$ | $\mathbf{1}$ | $\mathbf{1}$ | $+1$ | $+1$ |

Table 1.1: The representations of one generation of matter in the standard model. Note that all the fields as written such that they are left-handed. The index $i = 1, 2, 3$ denotes the generation.

resolving the problem of the Yukawa hierarchy. It is shown that such a class of models has a number of striking signatures at the Large Hadron Collider (LHC), and that these can be easily seen within a few months of running at 14 TeV. This model scenario also contains a promising dark matter candidate which evades the bounds gamma ray and neutrinos by virtue of its low mass, and in a particular region of parameter space may explain one of the cosmic ray anomalies.

## 1.1 The Standard Model

The standard model of the fundamental particles and interactions is a relativistic (i.e., invariant under the proper isochronous Poincaré transformations) field theory which possesses a local, or gauge, symmetry $SU(3)_c \times SU(2)_L \times U(1)_Y$. The $SU(3)_c$ gauge group describes the strong interaction; this sector of the theory is known as quantum chromodynamics (QCD). $SU(2)_L \times U(1)_Y$ describes the so-called electroweak interactions, and the symbol $L$ denotes that $SU(2)_L$ only acts on left-handed particles or right-handed antiparticles. At low energy ($\lesssim 300$ GeV), the local symmetry is broken down to $SU(3)_c \times U(1)_{EM}$ by the Higgs mechanism, where $U(1)_{EM}$ describes quantum electrodynamics (QED).

The fermionic matter of the theory is arranged in three generations or "flavors" of a single set of representations under the gauge groups, shown in Table 1.1. In

the first generation, $u$ and $d$ are the up and down quarks; in the second generation, they are the charm ($c$) and strange ($s$) quarks, and in the third top ($t$) and bottom ($b$). Similarly, the $\nu$ and $e$ are the electron neutrino ($\nu_e$) and electron ($e$) in the first generation, muon neutrino ($\nu_\mu$) and muon ($\mu$) in the second, and finally tau neutrino ($\nu_\tau$) and tau ($\tau$) in the third. There is no right-handed neutrino in the standard model.

Because of the $SU(2)_L$ interaction, each of the fields is written as left-handed Weyl spinors instead of as Dirac spinors; the left-handed particle fields are arranged in fundamental doublets of $SU(2)_L$. The antiparticle fields (denoted with a " $\bar{}$ ") are left-handed because they are the charge-conjugates (" $(\ )^c$ ") of the right-handed fields, but they are trivial under $SU(2)_L$. So, nominally the electroweak interaction maximally violates parity, but not (charge)×(parity), also denoted CP. This is consistent with the behavior of the weak interactions observed in early experiments. (It will be shown later that a small CP violation can arise in the Yukawa sector.) At low energy nature appears to conserve charge and parity separately, so the electroweak couplings must be very small in order that the effects of $SU(2)_L$ were not visible until the observation of $\beta$ decay. Finally, the hypercharge assignments for the matter fields are such that the fermions have the correct electrical charges at low energy, while also being consistent with the pattern of the electroweak symmetry breaking. In this regime the standard model has proven to be remarkably accurate, giving the anomalous magnetic dipole moment of the electron, $a_e = (g_e - 2)/2$, correctly to ten significant figures [1].

Whereas the electroweak interaction violates parity, the strong interaction $SU(3)_c$ exhibits a chiral symmetry where the left- and right-handed quarks transform independently. Since this interaction is confining at low energies ($\sim$ 200 MeV), pseudo-Nambu-Goldstone boson composites — pions — are formed when the axial part of this $SU(2)_L \times SU(2)_R$ global symmetry is spontaneously broken. Other composite states, the mesons and baryons, are also predicted by the quark model owing to the flavor-blindness of the strong interaction, and most have been found. The first mesons and baryons to be observed are organized as irreducible representations of $SU(3)_F$, in which the three quark species $(d, u, s)$ are in the fundamental representation **3**. The

mesons contain two quarks and compose

$$\mathbf{3} \otimes \mathbf{3}^* = \mathbf{8} \oplus \mathbf{1} \, . \tag{1.1}$$

This results in two nonets, the first containing pions with orbital angular momentum $l = 0$, and the second $\rho$ mesons with orbital angular momentum $l = 1$. The baryons contain three quarks and compose

$$\mathbf{3} \otimes \mathbf{3} \otimes \mathbf{3} = \mathbf{10} \oplus \mathbf{8} \oplus \mathbf{8} \oplus \mathbf{1} \, . \tag{1.2}$$

The states must be antisymmetric under the strong interaction, as well as under the interchange of any two quarks of the same mass. Then one finds that **10** is symmetric under the interchange of any two quarks, while the **1** is antisymmetric; the two **8** are of mixed symmetry (one of these contains the proton and neutron). It should be noted that because $s$ is significantly heavier than $u$ and $d$ the symmetry, $SU(3)_F$ is inexact, and because of the strong confinement involved, it is difficult to make precise numerical predictions analytically; instead, we must rely on lattice computations. Mesons containing $c, b$ and baryons with $c$ have also been observed.

On the other hand, at high energy the strong interaction grows asymptotically free, so deep-inelastic scattering experiments on mesons and baryons induce interactions with constituent quarks and gluons rather than with the composites as a whole. This results in scattering cross-sections in which, at tree level, the momentum distribution of the constituents is independent of the total collision energy. This phenomenon is known as Bjorken scaling [2], has been observed in collider experiments. Moreover, higher-order calculations show that the standard model is consistent with other measurables at colliders (see, for example, Ref. [3]).

The gauge invariant Lagrangian for the theory described so far is

$$\begin{aligned} \mathcal{L} = &- \frac{1}{4} \sum_{a=1}^{8} (G^a)_{\mu\nu} (G^a)^{\mu\nu} - \frac{1}{4} \sum_{a=1}^{3} (W^a)_{\mu\nu} (W^a)^{\mu\nu} - \frac{1}{4} B_{\mu\nu} B^{\mu\nu} \\ &+ \sum_{i=1,2,3} \sum_{f} \bar{f}_i i \gamma^\mu \mathcal{D}_\mu f_i \end{aligned} \tag{1.3}$$

where $a$ is the index over the group generators $\{T^a\}$, $f$ denotes each of the fermions in a generation, and $i$ is the index over generations. In the first line are gauge kinetic

terms expressed in terms of field strength,

$$F^a_{\mu\nu} = \partial_\mu A^a_\nu - \partial_\nu A^a_\mu + g f_{abc} A^b_\mu A^c_\nu \tag{1.4}$$

where $A^a_\mu$ is the gauge connection, $g$ is the gauge coupling and $f_{abc}$ are the structure constants for the group

$$[T_a, T_b] = i f_{abc} T^c \ . \tag{1.5}$$

Since $U(1)_Y$ has only generator, there is no generator index $a$ and the last term in its field strength is absent because it is abelian. The second line in the Lagrangian are the kinetic terms for the matter fields, where

$$\mathcal{D}_\mu f_i = \left( \partial_\mu - i g_s \sum_{a=1}^{8} G^a_\mu T^a_{SU(3)_c} - i g \sum_{a=1}^{3} W^a_\mu T^a_{SU(2)_L} - i g' Y B_\mu \right) f_i \ . \tag{1.6}$$

Here, $g_s$ is the $SU(3)_c$ gauge coupling and $G^a_\mu$ is the $SU(3)_c$ gauge connection; there are corresponding terms for $SU(2)_L$ and $U(1)_Y$. For $U(1)_Y$, the factor of $Y$ is the hypercharge of $f_i$.

Let us now introduce the Higgs mechanism for the symmetry breaking in the electroweak sector. Supposing the Higgs field is the complex $SU(2)_L$ doublet

$$\phi = \begin{pmatrix} \phi^+ \\ \phi^0 \end{pmatrix} \tag{1.7}$$

the gauge-invariant Lagrangian is

$$\mathcal{L} = |\mathcal{D}_\mu \phi|^2 - V(|\phi|^2) \tag{1.8}$$

where

$$V(|\phi|^2) = -\mu^2 |\phi|^2 + \lambda |\phi|^4 \tag{1.9}$$

is the simplest potential that could induce a spontaneous symmetry breaking. For $\mu^2 > 0$, the vacuum expectation value (VEV) is then

$$|\langle \phi \rangle| \equiv v = \left( \frac{\mu^2}{2\lambda} \right)^{1/2} \ . \tag{1.10}$$

Using the freedom of the local $SU(2)_L$ symmetry, we can express the field as

$$\phi(x) = \begin{pmatrix} 0 \\ v + \frac{1}{\sqrt{2}}h(x) \end{pmatrix} \tag{1.11}$$

where $h(x)$ is a real scalar field. Replacing $\phi$ in the potential we find

$$V(h) = \frac{1}{2}m_h^2 h^2 + \sqrt{\frac{\lambda}{2}}m_h h^3 + \frac{1}{4}\lambda h^4 \tag{1.12}$$

where $m_h = \sqrt{2}\mu = 2\sqrt{\lambda}v$. As of this writing, the Higgs boson has not been observed, but a lower bound has been set at $m_h \simeq 114$ GeV [1]. However, from what follows the VEV can be deduced to be $v \simeq 174$ GeV.

Using the Pauli basis for $SU(2)_L$, $\{T^a\} = \{\frac{\sigma^a}{2}\}$, and asserting that the hypercharge of the Higgs is $+1/2$, the kinetic term for the Higgs is then

$$\begin{aligned}
\mathcal{L}_{kin} &= \frac{1}{2}\left[\partial h(x)\right]^2 \\
&\quad + \begin{pmatrix} 0 \\ v + \frac{1}{\sqrt{2}}h(x) \end{pmatrix}^T \left(g\sum_{a=1}^{3} W_\mu^a \frac{\sigma^a}{2} + \frac{1}{2}g' B_\mu\right)^2 \begin{pmatrix} 0 \\ v + \frac{1}{\sqrt{2}}h(x) \end{pmatrix} \\
&= \frac{1}{2}\left[\partial h(x)\right]^2 \\
&\quad + \frac{v^2}{4}\left[g^2\left(W_\mu^1\right)^2 + g^2\left(W_\mu^2\right)^2 + \left(-gW_\mu^3 + g'B_\mu\right)^2\right]\left(1 + \frac{h}{\sqrt{2}v}\right)^2
\end{aligned} \tag{1.13}$$

giving masses to three of the four bosons. Writing those three gauge bosons as

$$\begin{aligned}
W_\mu^\pm &= \frac{1}{\sqrt{2}}\left(W_\mu^1 \mp iW_\mu^2\right) \\
Z_\mu &= \frac{1}{\sqrt{g^2 + g'^2}}\left(gW_\mu^3 - g'B_\mu\right)
\end{aligned} \tag{1.14}$$

we then have

$$\mathcal{L}_{kin} = \frac{1}{2}\left[\partial h(x)\right]^2 + \left[m_W^2 W^+W^- + \frac{1}{2}m_Z^2 Z^2\right]\left(1 + \frac{h}{\sqrt{2}v}\right)^2 \tag{1.15}$$

where

$$m_W = \frac{g}{\sqrt{2}}v \quad , \quad m_Z = \frac{\sqrt{g^2 + g'^2}}{\sqrt{2}}v\ . \tag{1.16}$$

Lastly, the remaining, massless boson is

$$A_\mu = \frac{1}{\sqrt{g^2 + g'^2}} \left( g W_\mu^3 + g' B_\mu \right) . \tag{1.17}$$

Then, if we define the so-called Weinberg angle

$$\cos\theta_W \equiv \frac{g}{\sqrt{g^2 + g'^2}} \quad , \quad \sin\theta_W \equiv \frac{g'}{\sqrt{g^2 + g'^2}} \tag{1.18}$$

the mapping between $(Z_\mu, A_\mu)$ and $(W_\mu^3, B_\mu)$ is given simply by

$$\begin{pmatrix} Z_\mu \\ A_\mu \end{pmatrix} = \begin{pmatrix} \cos\theta_W & -\sin\theta_W \\ \sin\theta_W & \cos\theta_W \end{pmatrix} \begin{pmatrix} W_\mu^3 \\ B_\mu \end{pmatrix} . \tag{1.19}$$

Then, we can rewrite the covariant derivative for the left-handed lepton doublet and right-handed electron, to obtain

$$\begin{aligned} \mathcal{D}_\mu \begin{pmatrix} \nu_L \\ e_L \end{pmatrix} = \Bigg[ \partial_\mu & - i\frac{g}{\sqrt{2}} \begin{pmatrix} 0 & W_\mu^+ \\ W_\mu^- & 0 \end{pmatrix} \\ & - i\frac{g}{\cos\theta_W} Z_\mu \begin{pmatrix} \frac{1}{2} & 0 \\ 0 & -\frac{1}{2} + \sin^2\theta_W \end{pmatrix} \\ & - ieA_\mu \begin{pmatrix} 0 & 0 \\ 0 & -1 \end{pmatrix} \Bigg] \begin{pmatrix} \nu_L \\ e_L \end{pmatrix} \\ \mathcal{D}_\mu e_R = \left[ \partial_\mu - i\frac{g \sin^2\theta_W}{\cos\theta_W} Z_\mu - ieA_\mu(-1) \right] & e_R \end{aligned} \tag{1.20}$$

where $e = g \sin\theta_W$. The corresponding covariant derivative for the quarks is easily deduced.

This result shows that the theory produces the behavior observed in nature: there are charged and neutral current weak interactions, with the former connecting up-type and down-type quarks, and thereby violating isobaric spin ($+1$ for proton, $-1$ for neutron). Moreover, $A_\mu$ can be identified with the photon, the gauge connection of electromagnetism, because it is massless and couples to the various fields by their measured electrical charges. This verifies that the set of hypercharges for all the matter fields (fermions and Higgs) is both consistent and correct.

Now that a Higgs scalar is introduced into the theory, generically there will be Yukawa couplings between the scalar and the fermion fields. This is also an opportunity to give the fermions masses after the Higgs gets a VEV, noting that couplings like $m_e \left(\bar{L}_{L,i}\right)(e_{R,i})$ are not gauge invariant. Beginning with the leptons, the Yukawa couplings are

$$\mathcal{L}_{yuk,e} = -\sum_{i,j} \left(\mathbf{y_e}\right)_{i,j} \left(\bar{L}_{L,i}\right) \phi \left(e_{R,j}\right) + h.c. \tag{1.21}$$

where $h.c.$ denotes the hermitian conjugate and $\left(\mathbf{y_e}\right)_{i,j}$ is a complex matrix with flavor indices. (Again, since there is no $\nu_R$ in the standard model, we omit the neutrino coupling, though their oscillations show they do have mass.) An arbitrary complex square matrix can be diagonalized by two unitary matrices,

$$\mathbf{y_e} \rightarrow \mathbf{U}^\dagger \left(\mathbf{y_e}\right) \mathbf{V} = \begin{pmatrix} y_e & & \\ & y_\mu & \\ & & y_\tau \end{pmatrix} \tag{1.22}$$

and these matrices can just be absorbed into the fields,

$$L_{L,i} \rightarrow \sum_k \left(\mathbf{U}\right)_{i,k} \left(L_{L,k}\right) \quad , \quad e_{R,j} \rightarrow \sum_l \left(\mathbf{V}\right)_{j,l} \left(e_{R,l}\right) \tag{1.23}$$

without affecting any other part of the Lagrangian, since $\mathbf{U}^\dagger\mathbf{U} = \mathbf{1}$ and $\mathbf{V}^\dagger\mathbf{V} = \mathbf{1}$. Then, we find that the lepton mass couplings preserve lepton number for each generation, which is consistent with the lack of lepton flavor changing processes such as $\mu^- \rightarrow e^-\gamma$ [1]. After the Higgs gets a VEV $(0, v)$, the mass of the charged leptons is simply $m_{e,i} = y_{e,i}v$ where $y_{e,i}$ is the eigenvalue of the Yukawa matrix.

Turning to the quarks, the first major difference from the case of the leptons is that, unlike neutrinos, up-type quarks clearly have masses. To include this, we must have a coupling where the scalar has hypercharge $-1/2$ instead of $+1/2$. Then, again in the Pauli basis, this can be done by

$$\phi = \begin{pmatrix} \phi^+ \\ \phi^0 \end{pmatrix} \longrightarrow \tilde{\phi} \equiv i\sigma^2\phi^* = \begin{pmatrix} \phi^0 \\ -\phi^- \end{pmatrix} \tag{1.24}$$

such that

$$\mathcal{L}_{yuk,q} = -\sum_{i,j} \left(\mathbf{y_u}\right)_{i,j} \left(\bar{Q}_{L,i}\right) \tilde{\phi}\left(u_{R,j}\right) - \sum_{i,j} \left(\mathbf{y_d}\right)_{i,j} \left(\bar{Q}_{L,i}\right) \phi\left(d_{R,j}\right) + h.c. \tag{1.25}$$

This time, because there are now two separate mass matrices for the up- and down-type quarks, they cannot simply be rotated away as there is a cross-term connecting them through the $SU(2)_L$ interactions in the kinetic term. If we change basis to the mass eigenstates

$$\begin{aligned} u_{L,i} &\to \sum_k \left(\mathbf{U_u}\right)_{i,k} \left(u_{L,k}\right) \quad , \quad u_{R,j} \to \sum_l \left(\mathbf{V_u}\right)_{j,l} \left(u_{R,j}\right) \\ d_{L,i} &\to \sum_k \left(\mathbf{U_d}\right)_{i,k} \left(d_{L,k}\right) \quad , \quad d_{R,j} \to \sum_l \left(\mathbf{V_d}\right)_{j,l} \left(d_{R,j}\right) \end{aligned} \tag{1.26}$$

then the charged current interaction becomes

$$\mathcal{L}_W = \frac{g}{\sqrt{2}} \sum_{i,j} \left(\bar{u}_{L,i}\right) \gamma^\mu W_\mu^+ \left(\mathbf{U_u U_d}^\dagger\right)_{i,j} \left(d_{L,j}\right) + h.c. \tag{1.27}$$

The theory, however, remains trivial under the rotations of the right-handed quarks.

The matrix $\mathbf{V_{CKM}} \equiv \mathbf{U_u U_d}^\dagger$ is known as the Cabibbo-Kobayashi-Maskawa (CKM) matrix [5, 6]. We observe that the charged current electroweak interaction now may have flavor changing couplings, though the neutral current interactions remain flavor-preserving. This is consistent with a low number of $b \to s\gamma$ events found in experiments [7]. However, the CKM matrix admits a physical complex phase, which creates CP-violating couplings otherwise forbidden by the electroweak interactions.

To see this, we first note that the CKM matrix is an element of the group $U(3)$ with $3 \times 3 = 9$ parameters. Modding out $SO(3)$ which is parameterized by three angles, this leaves six phases. Since we have couplings in the Lagrangian of the form $\bar{q}_L q_L$, $\bar{q}_R q_R$ and $\bar{q}_L q_R$, in principle we have six arbitrary phases $q_L \to e^{i\varphi} q_L$, $q_R \to e^{i\varphi} q_R$, one for each species of quark, which we could use to absorb the phases in the CKM matrix. However, the global phase $\varphi_u = \varphi_d = \varphi_c = \varphi_s = \varphi_t = \varphi_b$ does not change the CKM matrix. Thus, precisely one phase remains. The CKM matrix is then an element of $SO(3)$ extended by a phase.

One common parameterization of the CKM matrix using Euler rotation matrices is

$$\begin{aligned}
\mathbf{V_{CKM}} &= \begin{pmatrix} V_{ud} & V_{us} & V_{ub} \\ V_{cd} & V_{cs} & V_{cb} \\ V_{td} & V_{ts} & V_{tb} \end{pmatrix} \\
&= \begin{pmatrix} 1 & 0 & 0 \\ 0 & c_{23} & s_{23} \\ 0 & -s_{23} & c_{23} \end{pmatrix} \begin{pmatrix} c_{13} & 0 & s_{13}e^{-i\delta} \\ 0 & 1 & 0 \\ -s_{13}e^{-i\delta} & 0 & c_{13} \end{pmatrix} \begin{pmatrix} c_{12} & s_{12} & 0 \\ -s_{12} & c_{12} & 0 \\ 0 & 0 & 1 \end{pmatrix} \\
&= \begin{pmatrix} c_{12}c_{13} & s_{12}c_{13} & s_{13}e^{-i\delta} \\ -s_{12}c_{23} - c_{12}s_{23}s_{13}e^{i\delta} & c_{12}c_{23} - s_{12}s_{23}s_{13}e^{i\delta} & s_{23}c_{13} \\ s_{12}s_{23} - c_{12}c_{23}s_{13}e^{i\delta} & -c_{12}s_{23} - s_{12}c_{23}s_{13}e^{i\delta} & c_{23}c_{13} \end{pmatrix}
\end{aligned} \tag{1.28}$$

where $c_{ij} \equiv \cos(\theta_{ij})$ and $s_{ij} \equiv \sin(\theta_{ij})$. A more useful parameterization where all of the parameters are $\mathcal{O}(1)$ is the Wolfenstein parameterization [8],

$$\begin{pmatrix} 1 - \lambda^2/2 & \lambda & A\lambda^3(\rho - i\eta) \\ -\lambda & 1 - \lambda^2/2 & A\lambda^2 \\ A\lambda^3(1 - \rho - i\eta) & -A\lambda^2 & 1 \end{pmatrix} + \mathcal{O}(\lambda^4) \tag{1.29}$$

where $\lambda \approx s_{12} \approx 0.22$ is roughly the Cabibbo angle, which gives the flavor mixing between the first and second generations [5]. Then, it is manifest that the CP violating effects are small because they are suppressed $\mathcal{O}(\lambda^3)$. Finally, we should observe that if there were only two generations of quarks, then there would be no CP violation: a $2 \times 2$ unitary matrix has one angle and three phases, but in this case there would be four quark species with arbitrary phases, so all the phases could be eliminated.

Then, finally, let us recapitulate the standard model after symmetry breaking in

the mass eigenbasis:

$$\begin{aligned}\mathcal{L} = &-\frac{1}{4}\sum_{a=1}^{8}(G^a)_{\mu\nu}(G^a)^{\mu\nu} - \frac{1}{4}\sum_{a=1}^{3}(W^a)_{\mu\nu}(W^a)^{\mu\nu} - \frac{1}{4}B_{\mu\nu}B^{\mu\nu} \\ &+ \left[m_W^2 W^+W^- + \frac{1}{2}m_Z^2 Z^2\right]\left(1+\frac{h}{\sqrt{2}v}\right)^2 \\ &+ \frac{1}{2}\left[\partial h(x)\right]^2 - \left[\frac{1}{2}m_h^2 h^2 + \sqrt{\frac{\lambda}{2}}m_h h^3 + \frac{1}{4}\lambda h^4\right] \\ &+ \sum_i \left[\bar{L}_{L,i}\left(i\gamma^\mu \mathcal{D}_\mu\right) L_{L,i} + \bar{e}_{R,i}\left(i\gamma^\mu\mathcal{D}_\mu\right) e_{R,i}\right] + \sum_i \bar{q}_{R,i}\left(i\gamma^\mu\mathcal{D}_\mu\right) q_{R,i} + h.c. \\ &+ \sum_{i,j}\left(\bar{Q}_{L,i}\right)\left(i\gamma^\mu\mathcal{D}_\mu\delta_{i,j}\right)\left[\left(\mathbf{V_{CKM}}\right)_{i,j}\left(Q_{L,j}\right)\right] + h.c. \\ &+ \sum_f m_f \bar{f}_L f_R + h.c.\end{aligned} \tag{1.30}$$

where

$$\begin{aligned}\mathcal{D}_\mu = \partial_\mu &- ig_s\sum_{a=1}^{8}G_\mu^a T_s^a \\ &- i\frac{g}{\sqrt{2}}\left(W_\mu^+ T^+ + W_\mu^- T^-\right) - i\frac{g}{\cos\theta_W}Z_\mu\left(T^3 - \sin^2\theta_W Q\right) \\ &- ieA_\mu Q\end{aligned} \tag{1.31}$$

in which $Q = T^3 + Y$ is the electric charge of the interacting fermion, and

$$T^+ = \begin{pmatrix} 0 & 1 \\ 0 & 0 \end{pmatrix} \quad , \quad T^- = \begin{pmatrix} 0 & 0 \\ 1 & 0 \end{pmatrix} \quad , \quad T^3 = \begin{pmatrix} \frac{1}{2} & 0 \\ 0 & -\frac{1}{2} \end{pmatrix} \tag{1.32}$$

for the left-handed fermions and $T^+ = T^- = T^3 = 0$ for the right-handed fermions. All the parameters for this Lagrangian are given in Table 1.2, from Ref. [1].

Some of these values are given implicitly, most notably $g$ is contained within $G_F$, known as the Fermi constant. $G_F$ comes from the effective Lagrangian first proposed by Fermi for a four-fermion contact interaction,

$$\mathcal{L}_{int} = \frac{G_F}{\sqrt{2}}\left[\bar{p}\gamma^\mu\left(1 - \frac{g_A}{g_V}\gamma_5\right)n\right]\left[\bar{e}\gamma_\mu\nu\right] + h.c. \tag{1.33}$$

where $g_A/g_V \simeq 1.26$. Reinterpreting the interaction as an the exchange of a massive $W$ boson, this now reads

$$\mathcal{L}_{int} = \frac{g^2}{m_W^2}J_W^{\mu-}J_{\mu W}^+ \tag{1.34}$$

| | | | |
|---|---|---|---|
| $\alpha_s(m_Z) = g_s^2/4\pi$ | 0.1176(20) | $m_e$ | $0.510998910 \pm 0.000000013$ MeV |
| $G_F = \frac{g^2}{4\sqrt{2}m_W^2}$ | $1.16637(1) \times 10^{-5}$ GeV$^{-2}$ | $m_\mu$ | $105.658367 \pm 0.000004$ MeV |
| $\sin^2\theta_W(m_Z)$ | 0.23119(14) ($\overline{\rm MS}$) | $m_\tau$ | $1776.84 \pm 0.17$ MeV |
| $m_W = \frac{g}{\sqrt{2}}v$ | 80.398(25) GeV | $m_u$ | 1.5 to 3.3 MeV |
| $m_Z = \frac{m_W}{\cos\theta_W}$ | 91.1876(21) GeV | $m_d$ | 3.5 to 6.0 MeV |
| $\lambda$ | $0.2257^{+0.0009}_{-0.0010}$ | $m_s$ | $105^{+25}_{-35}$ MeV |
| $A$ | $0.814^{+0.021}_{-0.22}$ | $m_c$ | $1.27^{+0.07}_{-0.11}$ GeV |
| $\bar\rho \simeq \rho$ | $0.135^{+0.031}_{-0.016}$ | $m_b$ | $4.20^{+0.17}_{-0.07}$ GeV($\overline{\rm MS}$) |
| $\bar\eta \simeq \eta$ | $0.349^{+0.015}_{-0.017}$ | $m_t$ | $171.3 \pm 1.1 \pm 1.2$ GeV |

Table 1.2: Parameters for the standard model after symmetry breaking, from Ref. [1].

where the factor of $m_W^2$ in the denominator is from the weak boson propagator, and where $\left(J_W^-\right)^\mu$ is the current of the leptons and quarks,

$$\left(J_W^-\right)^\mu = \frac{1}{\sqrt{2}}\left[\sum_i \bar{e}_{L,i}\gamma^\mu\nu_{L,i} + \sum_{i,j}\bar{d}_{L,i}\gamma^\mu\left(\mathbf{V_{CKM}}^\dagger\right)_{i,j}u_{L,j}\right] \tag{1.35}$$

and $\left(J_W^+\right)_\mu$ is its hermitian conjugate. Then, we see that the strength of the interaction $\propto m_W^{-2}$, illustrating why these interactions were originally called "weak" and not visible until $\beta$ decay was observed. By comparison the effective Lagrangian for baryon scattering mediated by pion exchange is roughly $\propto m_\pi^{-2} \approx (140\text{ MeV})^{-2}$, a coupling over $10^6$ times stronger.

Finally, it is interesting to observe that $m_W \approx m_Z$. In the limit $m_W = m_Z$, $\cos\theta_W = 1$ or equivalently $\sin\theta_W = g' = 0$. We can see then from Eq. 1.13 that $Z_\mu$ would be pure $W_\mu^3$ and all the $W_\mu^a$ bosons would have the same mass. This means that in addition to the gauged $SU(2)_L$ symmetry which ensures that $W_\mu^1$ and $W_\mu^2$ have the same mass when $g' \neq 0$, there exists a global $SU(2)$ under which all three transform as a triplet when $g' = 0$.

It is precisely the gauging of the $U(1)$ in this $SU(2)$ to form hypercharge which splits this triplet. This additional $SU(2)$ can be identified as the $SU(2)_R$ in the Higgs potential (Eq. 1.9), where the Higgs transforms as the bifundamental, $(i\sigma_2\phi)^\dagger\,\phi \to L\left[(i\sigma_2\phi)^\dagger\,\phi\right]R^\dagger$ under $SU(2)_L \times SU(2)_R$. Upon spontaneous symmetry breaking, of the four real degrees of freedom in the bifundamental of $SU(2)_L \times SU(2)_R$, three

becomes a triplet under the diagonal $SU(2)_V$, and the fourth becomes the real Higgs scalar. This $SU(2)_V$ is known as "custodial" symmetry.

If $g'$ as well as the ratio $\rho \equiv m_W/m_Z$ and its corrections are well-specified by measurements, this leaves no room for additional terms in the potential which lack this $SU(2)_R$ symmetry. One example is $\left|\phi^\dagger \mathcal{D}_\mu \phi\right| / \Lambda^2$, which is excluded by precision electroweak tests for $\Lambda < \mathcal{O}(1 \text{ TeV})$ [4]. This is a significant restriction on new physics at TeV scales. These precision electroweak tests also put severe limits on additional generations of fermions and too high of a Higgs mass.

## 1.2 Problems of the Standard Model

While the standard model has met with tremendous success in precision electroweak tests, in predicting the array of QCD bound states, as well as in matching observations in higher energy QCD processes, there still remain significant problems which prevent the standard model from being a complete description of nature. Most prominently, there is no mention of gravity in the standard model. This is not problematic for the phenomenology described by the standard model, as the expected scale of quantum gravity is the Planck mass

$$m_{pl} = \sqrt{\frac{\hbar c}{G}} \simeq 1.2209 \times 10^{19} \text{ GeV}, \tag{1.36}$$

far too great to influence measurements at $\mathcal{O}(\text{TeV})$ or below. In any event, incorporating gravity into the standard model has proven to be an immense challenge because a quantum field theory with a spin-2 field is not renormalizable. String theory is the most notable effort in devising a self-consistent theory of quantum gravity, while also providing hope of reproducing the standard model at lower energies (see, for example, Ref. [9]).

### 1.2.1 Hierarchy problem in the Higgs sector

There are, however, other problems which are of concern at TeV-scale or below. Foremost is the so-called hierarchy problem, which does involve the Planck scale. If

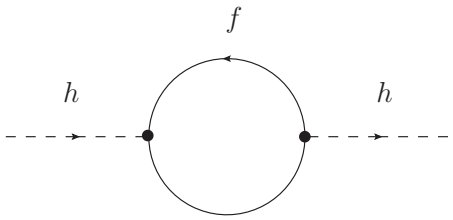


Figure 1.1: Contribution to Higgs mass from fermion loop, through Yukawa coupling.

we consider the contribution to the running of the Higgs mass from Yukawa couplings to the fermions (see Figure 1.1),

$$\Delta m_h^2 = \sum_i \sum_f -\frac{|y_{f_i}|^2}{8\pi^2}\Lambda_{UV}^2 + \dots \tag{1.37}$$

we see that there is a quadratic dependence on the cutoff scale, rather than the logarithmic one characteristic of bosonic corrections to fermion masses. The largest correction to the Higgs mass is obviously from the top quark, whose Yukawa coupling is $y_t \approx 1$. If we take $\Lambda_{UV} = m_{pl}$, and assume that $\lambda$ and $\mu$ are $\mathcal{O}(1)$, then the Higgs mass must be the result of a miraculous cancellation precise to one part in $10^{34}$. In fact, if $\Lambda_{UV}$ is as small as $\mathcal{O}(\text{TeV})$, the correction is still one part in $10^2$, considered unacceptable by many.

One obvious solution is to develop new physics at TeV-scale, but this is rather difficult due to the severe constraints of electroweak precision tests mentioned above. An example of a theory in this class is technicolor, where the Higgs is a condensate arising from QCD-like dynamics at this scale (see, for example, Ref. [10]). This framework has gone through several renditions in an effort to satisfy these tests and constraints from flavor changing neutral currents. The latest is "walking" technicolor, in which the theory is nearly conformal and lattice computations are ongoing to determine its fitness [11]. Another class are little Higgs theories, where the Higgs is a pseudo-Nambu-Goldstone boson from the breaking of product groups $SU(2) \times SU(2) \times ...$ which are generated by dimensional deconstruction [12].

Another strategy is to reduce the scale of quantum gravity from Planck scale to

TeV scale. Let us consider Gauss's law for gravitation in $3+1$ dimensions,

$$\vec{g} = -\frac{GM}{r^2}\hat{r} \tag{1.38}$$

where $M$ is a point-like source mass. Now suppose that the universe is in fact $3+1+\delta$ dimensions, where the extra $\delta$ dimensions are compactified with a scale $R \ll r$. Then, Gauss's law becomes

$$\vec{g}_\delta = -\frac{G_\delta M}{r^2 R^\delta}\hat{r} \tag{1.39}$$

such that taking $\vec{g}_\delta = \vec{g}$ we have $G_\delta \equiv R^\delta G$ (geometric factors are absorbed into $G_\delta$). Now supposing that $r \ll R$, Gauss's law is rewritten

$$\vec{g}_\delta = -\frac{G_\delta M}{r^{2+\delta}}\hat{r} \tag{1.40}$$

and so

$$m_{pl} \to m_{pl}\left(\frac{r}{R}\right)^{\delta/2} \quad . \tag{1.41}$$

To reduce $m_{pl}$ from $10^{19}$ GeV to $\sim$ 1 TeV at experimental energies of $\sim$ 1 TeV (corresponding to $r \sim 10^{-18}$ m), for $\delta = 2$ we require $R$ to be a few millimeters. Therefore, models using this strategy are known as large extra dimension models [13].

Yet another strategy using extra dimensions, proposed by Randall-Sundrum [14], supposes that the Universe is a 5-dimensional anti-de Sitter space bounded at one end by a "brane" with negative energy and at the other end by a brane with positive energy. The standard model fields resides on the negative energy brane, whereas gravitons propagate freely in the bulk. The difference in brane energies "warps" space along the extra dimension $y$, giving a metric

$$ds^2 = \frac{1}{k^2 y^2}\left(dy^2 + g_{\mu\nu}dx^\mu dy^\nu\right) \tag{1.42}$$

such that the energy scale corresponding to the curvature of space (i.e., quantum gravity) is naturally much greater at one end than the other, resolving the hierarchy.

However, perhaps the most widely-regarded solution for the hierarchy problem is "supersymmetry," a symmetry between bosons and fermions. Suppose that every fermionic field $f$ in the standard model has two scalar counterparts $\tilde{f}$ (one for each degree of freedom), and each boson in the standard model has a Majorana fermion

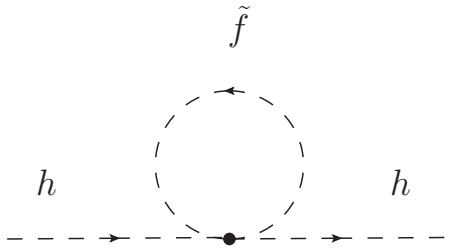


Figure 1.2: Contribution to Higgs mass from scalar loop, through Yukawa coupling.

counterpart. Moreover, suppose that the quantum numbers and Yukawa couplings are identical. Then, we have the additional contribution to the Higgs mass running from the scalar four-point coupling (see Figure 1.2),

$$\Delta m_h^2 = \sum_i \sum_f 2 \times \frac{|y_{f,i}|^2}{16\pi^2} \left[\Lambda_{UV}^2 - 2m_s^2 \log\left(\Lambda_{UV}/m_s\right) + ...\right] \tag{1.43}$$

where $m_s$ is the mass of the scalar counterparts. This perfectly cancels the quadratic divergence in Figure 1.1 [15]. The scalar top must be the largest contribution just like the fermionic top since they have the same Yukawa couplings, so its mass cannot be too big ($\lesssim 1$ TeV) otherwise the logarithmic correction would spoil the cancellation. If the scalar top is too heavy, this reintroduces a fine tuning in order to obtain a small Higgs mass favored by electroweak precision tests. Nonetheless, the masses of these supersymmetric partners are sufficiently high that they have yet to be observed in experiments. How, and at what energy, to break supersymmetry is an open issue.

The particulars of supersymmetry — supersymmetry breaking, the low energy spectrum, and coupling to gravity — will be discussed in Section 1.3.

### 1.2.2 Hierarchy of Yukawa couplings

Another problem at low scale presented by the standard model is the vast hierarchy of fermion Yukawa couplings. Dividing through the fermion masses by the Higgs VEV $v$, the resulting Yukawa couplings are shown in Table 1.3. These follow a

| | | | | | |
|---|---|---|---|---|---|
| $y_u$ | $\sim 10^{-5}$ | $y_c$ | $7.3 \times 10^{-3}$ | $y_t$ | $\approx 1$ |
| $y_d$ | $\sim 3 \times 10^{-5}$ | $y_s$ | $\approx 6 \times 10^{-4}$ | $y_b$ | $2.4 \times 10^{-2}$ |
| $y_e$ | $2.9 \times 10^{-6}$ | $y_\mu$ | $6.1 \times 10^{-4}$ | $y_\tau$ | $1.0 \times 10^{-2}$ |

Table 1.3: Yukawa couplings of the fermions in the standard model.

rough pattern

$$\begin{pmatrix} \epsilon^5 & \epsilon^3 & 1 \\ \epsilon^5 & \epsilon^4 & \epsilon^2 \\ \epsilon^6 & \epsilon^4 & \epsilon^2 \end{pmatrix} \tag{1.44}$$

where $\epsilon \sim 0.1$. It is clear that on a linear scale, the coupling of the top quark is vastly larger than those of the bottom quark and tau, and the couplings of the third generation are vastly larger than those of first and second generations, while the difference in the couplings between the first and second generations is not so great. This structure of dimensionless parameters spanning six orders of magnitude requires some explanation.

There have been a number of proposed solutions to this problem. One uses a relatively low scale of supersymmetry breaking ($\mathcal{O}(10^7)$ GeV), giving masses to a scalar field, which in turn gives masses to fields subject to the Froggatt-Nielsen mechanism [16]. These in turn drive the masses of "flavon" fields negative through two-loop running, creating a set of vacuum expectation values containing the desired hierarchy [17].

Another idea uses extra dimensions, asserting a 4D domain wall where the standard model fields reside, and this wall is positioned along these extra dimensions. If the left- and right-handed fields for each fermion are "stuck" at different positions relative to one another along these extra dimensions inside the wall, then the effective 4D Yukawa coupling depends on the overlap of their higher-dimensional wavefunctions. If these fields are highly peaked, then one can obtain a Yukawa hierarchy with the required six orders of magnitude [18].

There are also avenues for creating the Yukawa hierarchy using string compactifications [19] and a kind of "seesaw" mechanism [20].

Yet another possibility using supersymmetry is the notion that the scalar superparticles are pseudo-Nambu-Goldstone bosons of some broken global symmetry. These have protected small masses due to the famous low-energy theorem [21], with most of their mass coming from the running of supersymmetry breaking terms. Then, the standard model fermionic partners of these fields are naturally light for the same reason, resolving the hierarchy. The third generation set of fields are taken to be fundamental, so they are considerably heavier as desired. This hypothesis is described in more detail at the end of Section 1.3, and the prospects for testing it at the Large Hadron Collider (LHC) are studied in Chapter 3.

### 1.2.3 Neutrino mass

The problem of neutrino mass is one of omission from the standard model, but unlike gravity has direct bearing at low energies. The mass of neutrinos is evidenced by their flavor oscillations. This is analogous to two-state oscillations in ordinary quantum mechanics, which require non-zero energy eigenvalues. Considering only two neutrino flavors, the unitary matrix for flavor mixing is in $U(1) \sim SO(2)$,

$$\begin{pmatrix} \nu_\alpha \\ \nu_\beta \end{pmatrix} = \begin{pmatrix} \cos\theta & \sin\theta \\ -\sin\theta & \cos\theta \end{pmatrix} \begin{pmatrix} \nu_1 \\ \nu_2 \end{pmatrix} \tag{1.45}$$

where $\theta$ is the mixing angle and $\alpha, \beta$ are one of $e$, $\mu$ or $\tau$; $\nu_1$ and $\nu_2$ are the mass eigenstates. Computing the probability for (anti)neutrinos of one flavor to convert to another, we find

$$P(\nu_\alpha \to \nu_\beta) \simeq 1.267 \times \sin^2 2\theta \times \sin^2 \left[ \frac{\Delta m^2}{\mathrm{eV}^2} \frac{L}{\mathrm{km}} \frac{\mathrm{GeV}}{E} \right] \tag{1.46}$$

where $\Delta m^2$ is the (mass)$^2$ splitting between the eigenstates, $L$ is the distance traveled (at the speed of light) and $E$ is beam energy. The dependence on finite neutrino mass is now explicit.

Extending to three flavors, similar to the CKM matrix, we have the so-called

Pontecorvo-Maki-Nakagawa-Sakata (PMNS) matrix [22],

$$\begin{aligned}\mathbf{U} &= \begin{pmatrix} U_{e1} & U_{e2} & U_{e3} \\ U_{\mu 1} & U_{\mu 2} & U_{\mu 3} \\ U_{\tau 1} & U_{\tau 2} & U_{\tau 3} \end{pmatrix} \\ &= \begin{pmatrix} 1 & 0 & 0 \\ 0 & c_{23} & s_{23} \\ 0 & -s_{23} & c_{23} \end{pmatrix} \begin{pmatrix} c_{13} & 0 & s_{13}e^{-i\delta} \\ 0 & 1 & 0 \\ -s_{13}e^{-i\delta} & 0 & c_{13} \end{pmatrix} \begin{pmatrix} c_{12} & s_{12} & 0 \\ -s_{12} & c_{12} & 0 \\ 0 & 0 & 1 \end{pmatrix} \\ &= \begin{pmatrix} c_{12}c_{13} & s_{12}c_{13} & s_{13}e^{-i\delta} \\ -s_{12}c_{23} - c_{12}s_{23}s_{13}e^{i\delta} & c_{12}c_{23} - s_{12}s_{23}s_{13}e^{i\delta} & s_{23}c_{13} \\ s_{12}s_{23} - c_{12}c_{23}s_{13}e^{i\delta} & -c_{12}s_{23} - s_{12}c_{23}s_{13}e^{i\delta} & c_{23}c_{13} \end{pmatrix}\end{aligned} \tag{1.47}$$

where the phase $\delta$ induces CP violation in the neutrino sector. There is an additional matrix factor to the right

$$\begin{pmatrix} e^{i\alpha_1/2} & 0 & 0 \\ 0 & e^{i\alpha_2/2} & 0 \\ 0 & 0 & 1 \end{pmatrix} \tag{1.48}$$

if the neutrinos are Majorana particles, where $\alpha_1$ and $\alpha_2$ are additional phases. Neutrino oscillation was first observed as a dearth of neutrinos from the sun, later understood to be due to the oscillations combined with the Mikheyev-Smirnov-Wolfenstein effect [23]. Bounds have been placed on the mixing angles in the matrix by long baseline experiments, such as those using neutrinos emitted by nuclear power plants or accelerators. The total size of the neutrino mass hierarchy is limited by cosmic microwave background (CMB) measurements [24, 25] to $\sum_{i=1}^{3} m_i < 1.3$ eV; additional data such as that from large scale structure in the universe can make this bound more severe.

This opens the question of how to obtain a mass this small in a natural way. A Yukawa coupling to achieve this mass would make the hierarchy another factor of $10^6$ wider, and the same kind of coupling as the other fermions

$$\mathcal{L}_\nu = y_\nu \bar{\nu}_L \tilde{\phi} \nu_R + h.c. \tag{1.49}$$

assumes the existence of a right-neutrino which has yet to be observed. However, if we dispense with lepton number conservation, we can also assume that there are

Majorana mass terms in addition to Dirac, giving

$$\mathcal{L}_\nu = \frac{1}{2} m_R \bar{\nu}_R^c \nu_R + h.c. \tag{1.50}$$

which mixes $\bar{\nu}$ and $\nu$. Using a seesaw mechanism [110] there are left- and right-handed neutrinos with both Majorana and Dirac mass terms, which together can explain the observed low neutrino mass. This is achieved with a mass matrix

$$\mathcal{L}_\nu = -\frac{1}{2} \begin{pmatrix} \bar{\nu}_L & \bar{\nu}_R^c \end{pmatrix} \begin{pmatrix} 0 & m \\ m & M \end{pmatrix} \begin{pmatrix} \nu_L^c \\ \nu_R \end{pmatrix} + h.c. \tag{1.51}$$

whose eigenvalues are approximately $M$ and $-m^2/M$. Choosing $M$ near the grand unification scale of the gauge fields $\mathcal{O}(10^{16}$ GeV) and $m$ near the weak scale $v$ gives the lighter eigenvalue $\mathcal{O}(1$ meV). Thus, we have lepton-number-conserving Dirac mass couplings with a low eigenvalue (consistent with experiment) and a heavy, lepton-number-violating Majorana mass coupling which may play an important role in the very early universe in driving lepton genesis. Moreover, $m \sim v$ resolves the hierarchy associated with creating light neutrinos — the effective coupling to the Higgs is the same strength as the heavy standard model fermions. If, on the other hand, there are Majorana mass terms at a low scale, this may be revealed in searches for neutrino-less double-$\beta$ decay.

Neutrino oscillations are a concern in our study of neutrino signals from dark matter decay and annihilation in the next Chapter.

### 1.2.4 Dark matter and other problems

Assuming that $\nu_L$ is Dirac and there is no $\nu_R$, the standard model contains every allowed renormalizable term given the gauge symmetries and the matter content, save for CP-violating gauge surface terms of the form

$$-\theta \frac{g^2}{64\pi^2} \sum_a \epsilon^{\mu\nu\rho\sigma} F^a_{\mu\nu} F^a_{\rho\sigma} = -\theta \frac{g^2}{16\pi^2} \sum_a F^a_{\mu\nu} \tilde{F}^{a\mu\nu} \tag{1.52}$$

where $\theta$ is a free parameter on the interval $[0, 2\pi)$. Because $SU(3)_c$ can have a non-trivial vacuum structure [27], this term cannot be ignored for the strong interaction.

However, the measured CP violation is very small, with $\theta < 10^{-10}$ from bounds on the neutron electric dipole moment [28]. One solution is to promote $\theta$ to a scalar field (called the "axion") which is the result of broken $U(1)$ global symmetry, known as the Peccei-Quinn symmetry [29]. As a Nambu-Goldstone boson, the ground state is at $\theta = 0$, explaining why $\theta$ should be so small.

Turning to cosmology, the TeV-scale frameworks relevant to the two hierarchy problems also come to bear on another problem of the standard model: what is the composition of 80% of the mass in the universe? Most of the mass of the universe is known to be "dark," i.e. not subject to electromagnetic or strong interactions, according to CMB measurements [24, 25]. Then, the dark matter can have at most weak charges, or charges arising from some hidden sector. So far, all the evidence for the existence for dark matter, while overwhelming, remains circumstantial because of this characteristic.

TeV scale frameworks, to not have been discovered already, rely on $\mathbb{Z}_2$ parities to demarcate the standard model fields from the fields special to this framework. These parities arise from other considerations, such as conserving lepton and baryon number in supersymmetry, or restricting TeV-scale fields from tree-level interactions with standard model fields in technicolor, or generating chiral fermions in theories of extra dimensions. However, if the the lightest $\mathbb{Z}_2$-odd particle has only weak charges, it can be dark matter. A compelling reason for thinking that dark matter would be of this mass scale is that thermal production in the early universe gives the abundance observed today. Along with the hierarchy problems, this leads further credence to the notion that there must be new physics at the TeV scale; it should be noted however, the axion is also dark matter candidate, but is not related to TeV physics. Particle dark matter candidates and their detection will be covered in Section 1.4.

There is another "dark" quantity missing from the standard model, dark energy. Established by observing the magnitude-redshift relationship of supernovae [30], showing that the expansion of the universe is accelerating. Together with CMB dark matter constraints, it is determined that the fraction of the energy density of the universe currently due to dark energy is $\simeq 72\%$, which corresponds to $\simeq 5 \times 10^{-6}\ \mathrm{GeV\,cm^{-3}} = 3.8 \times 10^{-47}\ \mathrm{GeV}^4$. To cause acceleration, dark energy must

have a negative pressure. This can be due to a scalar field, such as the Higgs. However, the Higgs VEV is $v = 174$ GeV, giving an energy density $\sim 10^9$ GeV$^4$, a factor of $10^{56}$ too large; if we presume that the standard model is valid to Planck scale, then the expected energy density is $m_{pl}^4 \sim 10^{76}$ GeV$^4$, a factor of $10^{123}$ too big. By comparison, the Higgs hierarchy problem only requires a cancellation that one part in $10^{34}$. Ironically, global supersymmetric models require the cosmological constant, the simplest model of dark energy, to be precisely zero, which is certainly too small.

Given these difficulties, the remainder of this thesis will refrain from discussing solutions to the dark energy problem. Instead, we will show how astrophysical gamma rays and neutrinos can constrain models of dark matter. Then, we will describe a class of supersymmetric models which provide a viable dark matter candidate and a solution to the Yukawa hierarchy problem, demonstrating how they can be easily detected at the LHC. But first, in the remainder of this Chapter, brief overviews of supersymmetry and particle dark matter are provided.

## 1.3 A Brief Tour of Supersymmetry

### 1.3.1 A new symmetry

Let us first quickly review the formal aspects of supersymmetry. This will follow Ref. [31]; for more details see the text and the references therein.

The Coleman-Mandula theorem states that the most general Lie algebra consistent with the $S$-matrix of relativistic quantum field theory contains the operators of the homogeneous Poincaré group as well as a finite number of Lorentz scalar operators which must transform under a compact Lie group. The familiar structure of Lagrangians in particle physics, such as that of the standard model, is consistent with these requirements.

The set of algebras satisfying the theorem can be extended to include a certain class of graded Lie algebras (i.e., algebras whose operator spaces can be decomposed into subspaces) known as supersymmetry algebras, which have the following operator

relations in addition to those of the Lorentz and compact Lie groups:

$$\begin{aligned} \left\{Q_\alpha, \bar{Q}_{\dot{\beta}}\right\} &= 2\sigma^\mu_{\alpha\dot{\beta}} P_\mu \\ \{Q_\alpha, Q_\beta\} &= \left\{\bar{Q}_{\dot{\alpha}}, \bar{Q}_{\dot{\beta}}\right\} = 0 \\ [P_\mu, Q_\alpha] &= \left[P_\mu, \bar{Q}_{\dot{\alpha}}\right] = 0 \end{aligned} \tag{1.53}$$

where $\{,\}$ and $[,]$ are the anticommutator and commutator, respectively, and $\alpha, \beta$ and $\dot{\alpha}, \dot{\beta}$ are equal to one or two and denote the components of a Weyl spinor. $P_\mu$ is the energy-momentum operator, and $Q$, $\bar{Q}$ are new operators. This algebra can be extended to an arbitrary number of $Q$, $\bar{Q}$ operator pairs, as well as to include central charges.

There exist quantum field theories which contain conserved currents that fall in a representation of the supersymmetry algebra. The mass operator $P^2$ commutes with $Q$ and $P$, so the irreducible representations of the algebra are of equal mass. It can be easily proven that every representation contains an equal number of bosonic and fermionic degrees of freedom. Defining the fermionic annihilation and creation operators in the rest frame

$$a_\alpha = \frac{1}{\sqrt{2M}} Q_\alpha \quad , \quad (a_\alpha)^\dagger = \frac{1}{\sqrt{2M}} \bar{Q}_{\dot{\alpha}} \tag{1.54}$$

then the states in the fundamental representation are the Clifford vacuum $\Omega$, the symmetrized spin-$\frac{1}{2}$ fermionic state $(a_\alpha)^\dagger \Omega$ and the two antisymmetrized spin-0 bosonic states

$$\frac{1}{\sqrt{2}} (a_\alpha)^\dagger (a_\beta)^\dagger \Omega = -\frac{1}{2\sqrt{2}} \epsilon^{\alpha\beta} (a^\gamma)^\dagger (a_\gamma)^\dagger \Omega \, . \tag{1.55}$$

In the massless case in the lightlike frame $(-E, 0, 0, E)$ the algebra is modified

$$\left\{Q_\alpha, \bar{Q}_{\dot{\beta}}\right\} = 2 \begin{pmatrix} 2E & 0 \\ 0 & 0 \end{pmatrix} \tag{1.56}$$

so $Q_2$ and $\bar{Q}_{\dot{2}}$ are represented by zero. Therefore, there is only one bosonic state and one fermionic state, with helicities $\lambda_0$ and $\lambda_0 + \frac{1}{2}$, respectively; $\lambda_0$ is the helicity of the vacuum. (For CPT-completeness, the number of states must in fact be doubled.)

To formulate a field theory, the algebra must be given in terms of fields without mass-shell conditions. Using the anticommuting parameters $\xi^\alpha$ and $\bar{\xi}_{\dot{\alpha}}$, the algebra can be expressed entirely in commutators

$$\begin{aligned} \left[\xi Q, \bar{\xi}\bar{Q}\right] &= 2\xi\sigma^\mu\bar{\xi}P_\mu \\ [\xi Q, \xi Q] &= \left[\bar{\xi}\bar{Q}, \bar{\xi}\bar{Q}\right] = 0 \\ [P^\mu, \xi Q] &= \left[P^\mu, \bar{\xi}\bar{Q}\right] = 0 \end{aligned} \tag{1.57}$$

where the sums are implied. Considering a multiplet in the fundamental representation with components $(A, \psi, \dots)$, where $A$ is a complex scalar and $\psi$ is a spinor, let us define the infinitesimal transformation

$$\begin{aligned} \delta_\xi A &= \left(\xi Q + \bar{\xi}\bar{Q}\right) \times A \\ \delta_\xi \psi &= \left(\xi Q + \bar{\xi}\bar{Q}\right) \times \psi \\ &\vdots \end{aligned} \tag{1.58}$$

where $\delta_\xi$ then satisfies the commutator

$$\left(\delta_\eta\delta_\xi - \delta_\xi\delta_\eta\right) A = 2\left(\eta\sigma^\mu\bar{\xi} - \xi\sigma^\mu\bar{\eta}\right) P_\mu A \,. \tag{1.59}$$

From the algebra, $Q$ has mass dimension $1/2$, so the transformation turns the scalar into a spinor. Then, we define

$$\begin{aligned} \delta_\xi A &= \sqrt{2}\xi\psi \\ \delta_\xi \psi &= i\sqrt{2}\sigma^\mu\bar{\xi}\partial_\mu A + \sqrt{2}\xi F \\ \delta_\xi F &= i\sqrt{2}\bar{\xi}\bar{\sigma}^\mu\partial_\mu\psi \end{aligned} \tag{1.60}$$

such that the commutator above closes for $A$, $\psi$ and $F$. These three fields form a so-called supersymmetric chiral multiplet, with dimensions 1, 3/2 and 2, respectively. $F$ is an auxiliary field which transforms only into a space derivative, i.e. a surface term.

To obtain a Lagrangian, we write terms that also only transform into space derivatives,

$$\mathcal{L} = -i\partial_\mu\bar{\psi}\bar{\sigma}^\mu\psi - A^*\Box A + F^*F + mAF + mA^*F^* - \frac{1}{2}m\psi\psi - \frac{1}{2}m\bar{\psi}\bar{\psi} \tag{1.61}$$

giving the equations of motion

$$\begin{aligned} -i\bar{\sigma}^{\mu}\partial_{\mu}\psi + m\bar{\psi} &= 0 \\ F + mA^{*} &= 0 \\ -\Box A + mF^{*} &= 0 \end{aligned} \tag{1.62}$$

which describe a spinor and complex scalar, each of mass $m$. It can be shown that the expectation value of the stress-energy tensor of this theory vanishes as long as the vacuum is supersymmetric. This gives a cosmological constant of zero, which is at once desirable and problematic as described in the previous section.

We now define a "superfield," a compact description for the supersymmetry multiplet. Considering the supersymmetry algebra as a Lie algebra with anticommuting parameters, a finite transformation is given by

$$G(x,\theta,\bar{\theta}) = \exp\left[i(-x^{\mu}P_{\mu} + \theta Q + \bar{\theta}\bar{Q})\right] \tag{1.63}$$

then the infinitesimal transformation $\xi Q + \bar{\xi}\bar{Q}$ can be expressed in the parameter basis by

$$Q_{\alpha} = \frac{\partial}{\partial\theta^{\alpha}} - i\sigma^{\mu}_{\alpha\dot{\alpha}}\bar{\theta}^{\dot{\alpha}}\partial_{\mu} \quad , \quad \bar{Q}_{\dot{\alpha}} = \frac{\partial}{\partial\bar{\theta}^{\dot{\alpha}}} - i\theta^{\alpha}\sigma^{\mu}_{\alpha\dot{\beta}}\epsilon^{\dot{\beta}\dot{\alpha}}\partial_{\mu} \; . \tag{1.64}$$

This is for left multiplication. For right multiplication, we define

$$D_{\alpha} = \frac{\partial}{\partial\theta^{\alpha}} + i\sigma^{\mu}_{\alpha\dot{\alpha}}\bar{\theta}^{\dot{\alpha}}\partial_{\mu} \quad , \quad \bar{D}_{\dot{\alpha}} = -\frac{\partial}{\partial\bar{\theta}^{\dot{\alpha}}} - i\theta^{\alpha}\sigma^{\mu}_{\alpha\dot{\alpha}}\partial_{\mu} \tag{1.65}$$

which have the same algebra as $Q$ and $\bar{Q}$, up to a sign.

Then, on the "superspace" $(x,\theta,\bar{\theta})$ we can define any superfield by the full expansion

$$\begin{aligned} F(x,\theta,\bar{\theta}) = f(x) &+ \theta\phi(x) + \bar{\theta}\bar{\chi}(x) \\ &+ \theta\theta m(x) + \bar{\theta}\bar{\theta}n(x) + \theta\sigma^{\mu}\bar{\theta}v_{\mu}(x) \\ &+ \theta\theta\bar{\theta}\bar{\lambda}(x) + \bar{\theta}\bar{\theta}\theta\psi(x) + \theta\theta\bar{\theta}\bar{\theta}d(x) \end{aligned} \tag{1.66}$$

which transforms as $F \to (\xi Q + \bar{\xi}\bar{Q})F$. Then, a chiral superfield corresponding to the chiral multiplet above is

$$\begin{aligned} \Phi &= A(y) + \sqrt{2}\theta\psi(y) + \theta\theta F(y) \\ \Phi^{\dagger} &= A^{*}(y^{\dagger}) + \sqrt{(}2)\bar{\theta}\bar{\psi}(y^{\dagger}) + \bar{\theta}\bar{\theta}F^{*}(y^{\dagger}) \end{aligned} \tag{1.67}$$

where $y^\mu = x^\mu + i\theta\sigma^\mu\bar{\theta}$. Explicit calculation shows that $A$, $\psi$ and $F$ here transform the same way as those in the chiral multiplet. Explicit calculation also shows that $\Phi_i\Phi_j$ and $\Phi_i\Phi_j\Phi_k$ are superfields, but $\Phi^\dagger\Phi$ is not.

Next, a vector multiplet $V$ satisfies the condition $V = V^\dagger$, which gives the gauge freedom $V \to V + \Phi + \Phi^\dagger$. Then, with a gauge choice known as Wess-Zumino gauge, the superfield can be expressed simply as

$$V = -\theta\sigma^\mu\bar{\theta}v_\mu(y) + i\theta\theta\bar{\theta}\bar{\lambda}(y) - i\bar{\theta}\bar{\theta}\theta\lambda(y) + \frac{1}{2}\theta\theta\bar{\theta}\bar{\theta}\left[D(y) - i\partial_\mu v^\mu(y)\right] . \tag{1.68}$$

This gauge fixing breaks supersymmetry, but still permits the gauge transformation $v_\mu \to v_\mu + \partial_\mu a$. Because

$$V^2 = -\frac{1}{2}\theta\theta\bar{\theta}\bar{\theta}v_\mu v^\mu \quad , \quad V^3 = 0 \tag{1.69}$$

we may interpret $V$ as a gauge potential. Then, the corresponding field strength is

$$W_\alpha = -\frac{1}{4}\bar{D}\bar{D}e^{-V}D_\alpha e^V V \quad , \quad \bar{W}_{\dot{\alpha}} = -\frac{1}{4}DDe^V\bar{D}_{\dot{\alpha}}e^{-V}V \tag{1.70}$$

Under gauge interactions, $\Phi \to e^{-i\Lambda}\Phi$, where $\Lambda$ is a multiplet containing $\lambda$, and $\Lambda = \sum_a \Lambda^a T^a$ where $T^a$ are the gauge group generators. The kinetic terms for $\Phi$ and $W_\alpha$ are invariant when $e^V \to e^{-i\Lambda^\dagger}e^V e^{i\Lambda}$, so then the most general, gauge-invariant, renormalizable Lagrangian with chiral and vector superfields is

$$\begin{aligned}\mathcal{L} =& \frac{1}{16g^2}\mathrm{Tr}_a(W^\alpha W_\alpha|_{\theta\theta} + \bar{W}_{\dot{\alpha}}\bar{W}^{\dot{\alpha}}\big|_{\bar{\theta}\bar{\theta}}) + \Phi^\dagger e^V\Phi\big|_{\theta\theta\bar{\theta}\bar{\theta}} \\ &+ \left[\left(\frac{1}{2}m_{ij}\Phi_i\Phi_j + \frac{1}{3}g_{ijk}\Phi_i\Phi_j\Phi_k\right)\Big|_{\theta\theta} + h.c.\right] .\end{aligned} \tag{1.71}$$

where $X|_{\theta\theta\ldots}$ denotes the $\theta\theta\ldots$ component of the superfield.

Of course, since supersymmetry is not observed at low energies, it must be broken at some scale. From the supersymmetry algebra, one can find

$$H = \frac{1}{4}(\bar{Q}_1Q_1 + Q_1\bar{Q}_1 + \bar{Q}_2Q_2 + Q_2\bar{Q}_2) \tag{1.72}$$

which shows that $\langle\Psi|H|\Psi\rangle \geq 0$ for any state $\Psi$. Moreover, it shows that the ground state is $H = 0$, and that it is supersymmetric since $Q|0\rangle = \bar{Q}|0\rangle = 0$. However, if

$H > 0$ is the ground state, then supersymmetry is broken. One strategy for breaking supersymmetry is to have a spontaneous breaking which gives a VEV.

As an example, let us consider so-called O'Raifeartaigh breaking, with the potential

$$\mathcal{L}_{PE} = (\lambda_k \Phi_k + m_{ik} \Phi_i \Phi_k + g_{ijk} \Phi_i \Phi_j \Phi_k)|_{\theta\theta} + h.c. \tag{1.73}$$

In components,

$$F_k^* = -(\lambda_k + m_{ik} A_i + g_{ijk} A_i A_j) \ . \tag{1.74}$$

The scalar potential is $\mathcal{V} = F_k^* F_k$; if this has a non-zero expectation value, supersymmetry is broken. For the appropriate choices of $\lambda$, $m$ and $g$ there is no solution for the VEV $a_i$ of $A_i$ in

$$0 = \lambda_k + m_{ik} a_i + g_{ijk} a_i a_j \ . \tag{1.75}$$

Since supersymmetry is a spacetime symmetry, we now consider how to extend supersymmetry to curved spacetime backgrounds. This will eventually provide a phenomenologically attractive way of breaking supersymmetry.

### 1.3.2 Supergravity

Let us define the collective superspace coordinate $z^M \sim (x^\mu, \theta^\alpha, \bar{\theta}_{\dot{\alpha}})$, where $M$ is a collective index. These coordinates obey the relation $z^M z^N = (-)^{nm} z^N z^M$, where $n$ and $m$ take the values zero or one depending on whether $N$ and $M$ are vector or spinor indices. Then, we can define a differential form

$$\Omega = dz^{M_1} \wedge \cdots \wedge dz^{M_p} W_{M_p \ldots M_1}(z) \tag{1.76}$$

which if it has an odd number of spinorial indices is fermionic, or bosonic with an even number of spinorial indices. The usual properties of differential forms follow; in particular, the superspace analogue of the Bianchi identity is

$$\mathcal{D}_L F_{NM} + (-)^{l(n+m)} \mathcal{D}_N F_{ML} + (-)^{m(n+l)} \mathcal{D}_M F_{LN} = 0 \tag{1.77}$$

where $\mathcal{D}$ is the covariant derivative and $F$ is the rank-2 Ricci tensor.

Unfortunately, in the basis $d_z^N$ the exterior derivative does not commute with the supersymmetry generators. However, $D_\mu = \frac{\partial}{\partial x^\mu}$, $D_\alpha$ and $\bar{D}^{\dot{\alpha}}$ do commute with the generators. Taking $D_A \equiv (D_\mu, D_\alpha, \bar{D}^{\dot{\alpha}})$, we define a new basis

$$e^A(z) = dz^M e_M^A(z) \tag{1.78}$$

such that the exterior derivative is $e^A D_A$, where

$$D_A = e_A^N \frac{\partial}{\partial z^N} \ . \tag{1.79}$$

Then, the Bianchi identity becomes

$$\frac{1}{2} e^A e^B e^C \mathcal{D}_C F_{BA} + \frac{1}{2} e^A de^B F_{BA} - \frac{1}{2} de^A e^B F_{BA} = 0 \ . \tag{1.80}$$

Since supersymmetry is spacetime symmetry, to make contact with gravity we must gauge it. So, we promote the superspace coordinates to

$$\begin{aligned} x^\mu &\to x^\mu - i(\theta\sigma^\mu \bar{\xi}(x) - \xi(x)\sigma^\mu \bar{\theta}) \\ \theta^\alpha &\to \theta^\alpha - \xi^\alpha(x) \\ \bar{\theta}_{\dot{\alpha}} &\to \bar{\theta}_{\dot{\alpha}} - \bar{\xi}_{\dot{\alpha}}(x) \end{aligned} \tag{1.81}$$

which generate coordinate transformations $z^M \to z^M - \xi^M(z)$, with vielbein $E$. Taking the Lorentz group $L$ as the local structure group, one can construct the standard Ricci and torsion tensors. It is interesting to note that in flat space the torsion is not zero:

$$T_{\alpha\dot{\beta}}^\mu = T_{\dot{\beta}\alpha}^\mu = 2i\sigma_{\alpha\dot{\beta}}^\mu \ . \tag{1.82}$$

The vielbein transforms as

$$E_M^A \to E_M^A - \mathcal{D}_M \xi^A - \xi^B T_{BM}^A + E_M^B L_B^A \tag{1.83}$$

and has the physical degrees of freedom

$$E_M^A(z)\big|_{\theta=\bar{\theta}=0} = \begin{pmatrix} e_\mu^\nu(x) & \frac{1}{2}\psi_\mu^\alpha(x) & \frac{1}{2}\bar{\psi}_{\mu\dot{\alpha}}(x) \\ 0 & \delta_\beta^\alpha & 0 \\ 0 & 0 & \delta_{\dot{\alpha}}^{\dot{\beta}} \end{pmatrix} . \tag{1.84}$$

Here, $e_\mu^\nu$ is the spin-2 graviton and $\psi_\mu^\alpha$ and $\bar{\psi}_\mu^{\dot{\alpha}}$ are the spin-$\frac{3}{2}$ gravitino.

After considerable work in solving the Bianchi identity, it can be shown that the torsion and curvature tensors can be expressed in terms of the lowest components of three superfields,

$$\begin{aligned} R(z)|_{\theta=\bar{\theta}=0} &= -\frac{1}{6}M(x) \\ G_\mu(z)|_{\theta=\bar{\theta}=0} &= -\frac{1}{3}b_\mu(x) \end{aligned} \tag{1.85}$$

and the vielbein $E$, indicating that they are the only physical supergravity degrees of freedom. These four degrees of freedom form a multiplet.

Now that supersymmetry is local, we must promote the superspace coordinate $\theta$ to $\Theta^\alpha$, such that the chiral superfield has covariant components

$$\Phi = A(x) + \sqrt{2}\Theta^\alpha\chi_\alpha(x) + \Theta^\alpha\Theta_\alpha F(x)\ . \tag{1.86}$$

Then, the supergravity Lagrangian is

$$\mathcal{L}_{SG} = -6\int d^2\Theta\mathcal{E}R + h.c. \tag{1.87}$$

where $\mathcal{E}$ is the vierbein determinant (i.e, the Jacobian of superspace) and the gravitational coupling $\kappa^2 = 8\pi G$ has been set to one. In components, this is

$$\begin{aligned} \mathcal{L}_{SG} = &-\frac{1}{2}e\mathcal{R} - \frac{1}{3}eM^*M + \frac{1}{3}eb^a b_a \\ &+ \frac{1}{2}e\epsilon^{\mu\nu\rho\sigma}\left(\bar{\psi}_\mu\bar{\sigma}_\nu\tilde{\mathcal{D}}_\rho\psi_\sigma - \psi_\mu\sigma_\nu\tilde{D}_\rho\bar{\psi}_\sigma\right) \end{aligned} \tag{1.88}$$

where $\mathcal{R}$ is the Riemann curvature and $\tilde{D}_\rho$ is the covariant derivative. We see that this expression contains the Rarita-Schwinger action for a spin-$\frac{3}{2}$ gravitino, and that $b^a$ and $M$ are not dynamical. Then, combining with the full Lagrangian in Eq. 1.71, but omitting gauge interactions for simplicity, we find in curved space

$$\mathcal{L} = \int d^2\Theta 2\mathcal{E}\left[-\frac{1}{8}(\bar{\mathcal{D}}\bar{\mathcal{D}} - 8R)\Omega(\Phi,\Phi^\dagger) + P(\Phi)\right] + h.c. \tag{1.89}$$

where

$$\begin{aligned} \Omega(\Phi,\Phi^\dagger) &= \Phi_i^\dagger\Phi_i + c_i\Phi_i + \bar{c}_i\Phi_i^\dagger - 3 \\ P(\Phi) &= d + a_i\Phi_i + \frac{1}{2}m_{ij}\Phi_i\Phi_j + \frac{1}{3}g_{ijk}\Phi_i\Phi_j\Phi_k \end{aligned} \tag{1.90}$$

are the superspace kinetic term and potential term, respectively, in which $c$ and $d$ arise from shifts in the superfields. Expanding in components, one finds that

$$\Omega(\Phi, \Phi^\dagger) = -3 \exp\left[-\frac{1}{3}K(\Phi, \Phi^\dagger)\right] \tag{1.91}$$

where $K(\Phi, \Phi^\dagger)$ is a hermitian function, known as the Kähler potential. The kinetic terms are invariant under the simultaneous transformations

$$\begin{aligned} K(A, A^*) &\to K(A, A^*) + F(A) + F^*(A^*) \\ \chi^i &\to \exp\left[\frac{i}{2}(\mathrm{Im}F)\chi^i\right] \\ \psi_\mu &\to \exp\left[-\frac{i}{2}(\mathrm{Im}F)\psi_\mu\right] \end{aligned} \tag{1.92}$$

known as the Kähler-Weyl transformations. The first reflects an isometry of the $(\Phi, \Phi^\dagger)$ manifold, the latter two compensate for the spinor phase under the action of this isometry group on curved backgrounds. The Kähler potential features prominently in Chapter 3, and we will return to at the end of this chapter.

### 1.3.3 Minimal supersymmetric standard model

We now consider the low energy consequences of formal supersymmetry, following Ref. [32].

Starting from the standard model Lagrangian before electroweak symmetry breaking, we must promote each chiral field to a chiral superfield, and every vector field to a vector superfield. First, let us examine the additional terms to the standard model kinetic terms from gauge invariant kinetic terms in the supersymmetric Lagrangian (for each gauge field):

$$\begin{aligned} \mathcal{L} =& \mathcal{L}_{\text{chiral}} + \mathcal{L}_{\text{gauge}} \\ &- \sqrt{2}g(\phi^* T^a \psi)\lambda^a - \sqrt{2}g\lambda^{\dagger a}(\psi^\dagger T^a \phi) - \frac{g^2}{2}(\phi^* T^a \phi)(\phi^* T^a \phi) \, . \end{aligned} \tag{1.93}$$

Here $\phi$ is the scalar partner to a chiral fermion $\psi$, and $\lambda$ is the fermionic partner to a gauge field. For example, the scalar partners of $L_L$ and $\bar{e}_R$ are denoted $\tilde{\nu}$, $\tilde{e}_L$ and $\tilde{e}_R^*$ respectively, and are called "sneutrino" and "selectron;" in general the

scalar partner of some fermion "foo" is "sfoo." The new terms in the Lagrangian are "supersymmetrizations" of the normal gauge interactions, where one or more standard model legs are replaced by superpartner legs.

Next, ignoring the shift term and the singlet term (which can also be shifted away), the superpotential $P(\Phi)$ (henceforth denoted $W$) is purely in the Yukawa sector,

$$W = \bar{u}\mathbf{y_u}QH_u - \bar{d}\mathbf{y_d}QH_d - \bar{e}\mathbf{y_e}LH_d + \mu H_u H_d \ . \tag{1.94}$$

As explained earlier, due to the great hierarchy in the Yukawa couplings, conventionally only the third generation couplings are taken to be non-zero. There are a few oddities in this potential. First, there a two Higgs doublets, not just one. This is because $W$ is holomorphic, so terms like $\bar{u}QH_d^*$ are forbidden. Moreover, Higgs mass terms like $(H_u^*H_u + H_d^*H_d)$ are also forbidden, so the term $\mu H_u H_d$ gives the Higgs bosons mass. It is also true that two Higgs doublets are required for anomaly cancellation, now that there are extra degrees of freedom running in the loops. Before proceeding, let us remark that the size of $\mu$ is completely undetermined, and naive considerations would set it to the Planck mass. However, we know it must be roughly weak scale to give the right masses to the Higgs. This contradiction is known as the "$\mu$ problem."

Then, the additional Lagrangian terms in the Yukawa sector are

$$\begin{aligned}
\mathcal{L}_{\tilde{H}} =& -\mu(\tilde{H}_\mu^+\tilde{H}_d^- - \tilde{H}_u^0\tilde{H}_d^0) + c.c. \\
\mathcal{L}_H =& -|\mu|^2(|H_u^0|^2 + |H_u^+|^2 + |H_d^0|^2 + |H_d^-|^2) \\
\mathcal{L}_{(\text{scalar})^3} =& \mu^*(\tilde{\bar{u}}\mathbf{y_u}\tilde{u}H_d^{0*} + \tilde{\bar{d}}\mathbf{y_d}\tilde{d}H_u^{0*} + \tilde{\bar{e}}\mathbf{y_e}\tilde{e}H_u^{0*} \\
&+ \tilde{\bar{u}}\mathbf{y_u}\tilde{d}H_d^{-*} + \tilde{\bar{d}}\mathbf{y_d}\tilde{u}H_u^{+*} + \tilde{\bar{e}}\mathbf{y_e}\tilde{\nu}H_u^{+*}) + c.c.
\end{aligned} \tag{1.95}$$

The first term gives mass to the "Higgsinos," the second gives mass to the new Higgses, and the third gives mass to the "sfermions" while also creating new doublet interactions. There are also numerous $(\text{scalar})^4$ interactions which also contribute to the sfermion masses; these are all possible terms which are symmetric combinations of scalars proportional to $\mathbf{y_f}^\dagger\mathbf{y_{f'}}$. For example, the interactions with coupling $\mathbf{y_e}^\dagger\mathbf{y_e}$

are

$$\begin{aligned}\mathcal{L}_{(\text{scalar})^4,e^2} = &\frac{1}{2}|\tilde{\bar{e}}\mathbf{y_e}\tilde{e}|^2 + (\tilde{\bar{e}}^* H_u^{0*})\mathbf{y_e}^\dagger\mathbf{y_e}(\tilde{\bar{e}}H_u^0) + (\tilde{e}^* H_u^{0*})\mathbf{y_e}^\dagger\mathbf{y_e}(\tilde{e}H_u^0) \\ &+ \frac{1}{2}|\tilde{\bar{e}}\mathbf{y_e}\tilde{\nu}|^2 + (\tilde{\bar{e}}^* H_u^-)\mathbf{y_e}^\dagger\mathbf{y_e}(\tilde{\bar{e}}H_u^+) + (\tilde{\nu}^* H_u^-)\mathbf{y_e}^\dagger\mathbf{y_e}(\tilde{\nu}H_u^+) \\ &+ (\tilde{\nu}^* H_u^-)\mathbf{y_e}^\dagger\mathbf{y_e}(\tilde{e}H_u^0) + c.c.\end{aligned} \tag{1.96}$$

One may notice that the superpotential is missing the renormalizable, gauge-invariant lepton- and baryon-violating terms,

$$\begin{aligned}W_{\Delta L=1} =&\frac{1}{2}\lambda^{ijk}L_iL_j\bar{e}_k + \lambda'^{ijk}L_iQ_j\bar{d}_k + \mu'^iL_iH_u \\ W_{\Delta B=1} =&\frac{1}{2}\lambda''^{ijk}\bar{u}_i\bar{d}_j\bar{d}_k\end{aligned} \tag{1.97}$$

where $i$, $j$ and $k$ are family indices written explicitly. These terms are quite dangerous. For example, if $\lambda'$ and $\lambda''$ are both non-zero, then the proton can decay $p^+ \to e^+\pi^0$ through the exchange of a $\bar{s}_R^*$. If the couplings are of order unity, then the proton lifetime would be a fraction of a second, when in fact the experimental lower bound is $10^{34}$ years. To preclude these kind of terms, we introduce a $\mathbb{Z}_2$ parity called R-parity,

$$P_R = (-1)^{3(B-L)+2s} \tag{1.98}$$

which is $+1$ for standard model particles and $-1$ for superpartners. Then, the lightest supersymmetric particle (LSP) is perfectly stable. If it has no electric charge or color, it can be dark matter (described in the next section). Moreover, each superpartner must eventually decay into an odd number of LSPs, and collider experiments can only produce superpartners in even numbers. While this parity may seem ad hoc, it could be the result of some breaking of a continuous $U(1)_{B-L}$ at high scale.

We now revisit the breaking of supersymmetry. In order not to spoil the cancellation of quadratic divergences in the Higgs running, the breaking method itself should not contribute such divergences. In other words, the breaking must be "soft." Moreover, if there is some mass scale $m_{\text{soft}}$ in the breaking sector, as $m_{\text{soft}} \to 0$ supersymmetry should be restored. Thus, the corrections to the Higgs mass from the breaking sector should go like

$$\Delta m_H^2 = m_{\text{soft}}^2\left[\frac{\lambda}{16\pi^2}\log\left(\frac{\Lambda_{UV}}{m_{\text{soft}}}\right) + \dots\right] . \tag{1.99}$$

The way to achieve this is simply to give the superpartners masses differently than their standard model counterparts. Unfortunately, renormalizable tree-level mass terms would create severe phenomenological problems. Foremost, the tree-level masses in spontaneously broken supersymmetric theories obey "sum rules," deriving from the so-called supertrace

$$\mathrm{STr}(m^2) \equiv \sum_s (-1)^s (2s+1)\mathrm{Tr}(m_s^2) \tag{1.100}$$

where $s$ is the particle spin and the trace is over all the gauge and flavor indices. This gives a sum rule

$$\mathrm{Tr}(\mathbf{m_B^2}) - 2\mathrm{Tr}(\mathbf{m_F}^\dagger \mathbf{m_F}) + 3\mathrm{Tr}(\mathbf{m_V^2}) = 0 \tag{1.101}$$

where $\mathbf{m_B^2}$, $\mathbf{m_F}$ and $\mathbf{m_V^2}$ are the boson, fermion and vector mass matrices. In the limit that lepton number, quark flavor, etc. are conserved then the supertraces for each lepton and quark sector are separately equal to zero, e.g.

$$m_{\tilde{e}_L}^2 + m_{\tilde{e}_R}^2 + m_{\tilde{\nu}}^2 - 2m_e^2 - 2m_\nu^2 = 0 \; . \tag{1.102}$$

Then, to make some superpartners heavy, the squared-masses for the others would have to be driven negative. One way to avoid this is to place the breaking in a hidden sector, so that the mass is generated at loop-level instead of tree-level; another is to use nonrenormalizable mass terms instead of renormalizable ones.

The latter option is useful for supergravity, since the Planck scale is a natural choice for the suppression scale. At $\mathcal{O}(F/m_{pl})$, we can have terms such as

$$\begin{aligned} \mathcal{L}_{NR} = &- \frac{1}{m_{pl}} F \left( \frac{1}{2} f_a \lambda^a \lambda^a + \frac{1}{6} y'^{ijk} \phi_i \phi_j \phi_k + \frac{1}{2} \mu'^{ij} \phi_i \phi_j \right) + c.c. \; . \\ &- \frac{F F^*}{m_{pl}^2} k_j^i \phi_i \phi^{*j} \; . \end{aligned} \tag{1.103}$$

The first term is for gauginos, the second for the Yukawa couplings, and the last is for the scalars. Under the assumption that these terms are universal for the different gauge symmetries, standard model generations, etc., the soft masses are

$$m_{1/2} = f \frac{\langle F \rangle}{m_{pl}} \; , \; m_0^2 = k \frac{|\langle F \rangle|^2}{m_{pl}^2} \; , \; A_0 \propto \frac{\langle F \rangle}{m_{pl}} \; , \; B_0 \propto \frac{\langle F \rangle}{m_{pl}} \; . \tag{1.104}$$

To obtain superpartners $\mathcal{O}$(0.1-1) TeV, the scale of supersymmetry breaking should be $\sim 10^{11}$ GeV. However, there is some flexibility, depending on the details of the running of the theory down to electroweak scale.

Due to the simplicity of the soft masses in universal minimal supergravity, and the gentle running in broken supersymmetry, the low-energy spectrum of the sfermions is parameterized to good approximation as

$$\begin{array}{lllll} m_Q^2 & = m_0^2 & +K_3 & +K_2 & +\frac{1}{36}K_1 \\ m_{\bar{u}}^2 & = m_0^2 & +K_3 & & +\frac{4}{9}K_1 \\ m_{\bar{d}}^2 & = m_0^2 & +K_3 & & +\frac{1}{9}K_1 \\ m_L^2 & = m_0^2 & & +K_2 & +\frac{1}{4}K_1 \\ m_{\bar{e}}^2 & = m_0^2 & & & +K_1 \end{array} \tag{1.105}$$

where

$$K_1 \approx 0.15 m_{1/2}^2 \quad , \quad K_2 \approx 0.5 m_{1/2}^2 \ , \ K_3 \approx (4.5 \text{ to } 6.5) m_{1/2}^2 \ . \tag{1.106}$$

There are also mass rules for the Higgs bosons and Higgsinos, and for the charged and neutral weak gauginos. These are subject to the constraints of electroweak symmetry breaking and the ratio $\tan\beta \equiv v_u/v_d$, where $v_u$ and $v_d$ are the VEVs for $H_u$ and $H_d$. Usually, $\tan\beta$ is specified instead of the $B_0$ soft mass as a high-energy boundary condition for the renormalization; $B_0$, or equivalently, $\mu$ is then solved for. The charged states mix into "charginos" denoted $\tilde{\chi}^{\pm}_{1,2}$, and the neutral states into "neutralinos" denoted $\tilde{\chi}^0_{1,2,3,4}$. There exists a "small $\mu$ region" in which the $\mu$ parameter is found to be small, and thus the weak gauginos are light and of which the lightest higgsinos are large components.

Finally, the mass of the gluino is roughly six times that of the lightest neutralino, though more precise predictions can be made by accounting for the running of squark loops.

In Chapter 3, an example spectrum for universal soft masses can be seen in Figure 3.3. The chapter also describes how to reconstruct the masses in a gluino or squark decay chain at the LHC. Moreover, we will see that a higher breaking scale and non-universal soft masses are phenomenologically sound. Next, we will discuss the motivation for these non-universal soft masses.

### 1.3.4 Coset spaces

As discussed in the previous section, the hierarchy of Yukawa couplings is an outstanding problem of the standard model, and one solution is to have the first and second generation quarks and leptons be the supersymmetric fermionic partners to the pseudo-Nambu-Goldstone bosons (NGBs) of some broken global symmetry. These fermions may be called "quasi-Nambu-Goldstone" fermions (QNGFs). Because the lower bound on the compositeness scale of standard model leptons established at colliders is $\mathcal{O}$(1-10 TeV) [1], they must be effectively massless at the supersymmetry breaking scale for renormalization to not make them too heavy. The fermions reside in the same supermultiplet as the NGBs, so their masses are protected by the low energy theorem [21]. If the QNGFs have the correct quantum numbers, then both the Yukawa hierarchy and the representations of the standard model generations would have a dynamical motivation. Here we present some of basic aspects of this theory (see, for example Ref. [33]).

When there is a breaking $G \to H$, the resulting NGB fields continue to reside in a linear representation under $H$, but compose a nonlinear realization of the coset space $G/H$. They are described by the Lagrangian

$$\mathcal{L}^{NL}_{NGB} = -\left(\partial^\mu \pi_i\right) g^{ij}(\pi/f_\pi) \left(\partial_\mu \pi_j\right) \tag{1.107}$$

where $g^{ij}$ is the metric of the coset space and $f_\pi$ is scale fixed by the underlying dynamics [34]. (This Lagrangian is very similar to that for pions, which produced by the breaking of the global chiral symmetry in standard model QCD.) The corresponding Lagrangian for the QNGFs is

$$\mathcal{L}^{NL}_{QNGF} = \frac{c_{ijkl}}{f_\pi^2}(\bar{\psi}_i \gamma^\mu \psi_j)(\bar{\psi}_k \gamma^\mu \psi_l) \tag{1.108}$$

where $c_{ijkl}$ is fixed by both the coset space and the underlying dynamics. Under supersymmetry, each multiplet is required to have the same number of bosonic and fermionic degrees of freedom, so we require

$$2n_{QNGF} = n_{NGB} + n_{QNGB} \tag{1.109}$$

where "QNGB" denotes additional bosons from other sources that may fill the multiplets. The case in which $n_{NGB} < 2n_{QNGF}$ thus requires some dynamical justification.

For a given breakdown $G \to H$ the pattern of QNGFs, i.e. which fermions go in what multiplets, is a dynamical question. If the NGBs are in real representation $r$, then the QNGFs transform like $r$ and so another set of QNGBs which transform the same way is required; the same is true for a vector representation $i + \bar{i}$. However, if $G/H$ is a Kähler manifold, then one can have QNGFs which transform like $i$ and no QNGBs are required.

This can be understood by considering the supersymmetric generalization of the nonlinear Lagrangian above, which is just the Kähler potential [34]

$$\mathcal{L}^{NL}_{SUSY} = K(\Phi, \Phi^\dagger)\big|_{\theta\theta\bar{\theta}\bar{\theta}} \ . \tag{1.110}$$

This gives for the scalars

$$\mathcal{L}^{NL}_{\text{scalar}} = -\partial^\mu \varphi^{*i} \left[\frac{\partial^2 K(\varphi^*, \varphi)}{\partial \varphi^{*i} \partial \varphi^j}\right] \partial_\mu \varphi^j \ . \tag{1.111}$$

The metric $g_{ij}(\varphi^*, \varphi)$ obeys the Kähler conditions,

$$\frac{\partial g_{ij}}{\partial \varphi^{*k}} = \frac{\partial g_{kj}}{\partial \varphi^{*i}} \quad , \quad \frac{\partial g_{ij}}{\partial \varphi^k} = \frac{\partial g_{ik}}{\partial \varphi^j} \ . \tag{1.112}$$

The fact that the scalar fields are coordinates of a Kähler manifold is inherent in supersymmetry, so if $G/H$ is a Kähler manifold then no other scalar fields are required to fill the multiplets. Of course, it is always possible to include extra QNGBs to match the QNGF degrees of freedom.

Now, remembering that the superpotential $W(\Phi)$ is holomorphic, i.e. a function of $\Phi$ and not of $\Phi^\dagger$, it is invariant not only under some symmetry $G$ but also its complex extension $\tilde{G}$. The mass condition for the broken degrees of freedom is

$$(M_{QGF})_{i,j}\, \delta_a \langle \phi_j \rangle \equiv \left.\frac{\partial^2 W}{\partial \phi_i \partial \phi_j}\right|_{\phi_i = \langle \phi_i \rangle} \delta_a \langle \phi_j \rangle = 0 \tag{1.113}$$

where $\delta_a$ is the infinitesimal transformation generated by the algebra element $T_a$. Since $\tilde{G} \supset G$, after $G \to H$ there is at least one generator $T_a \in \tilde{G}$, $T_a \notin H$ for which $T_a \langle \phi_i \rangle \neq 0$. So, in general $2n_{QNGF} - n_{NGB} \geq 1$. In the case of equality, one QNGB is

required to fill the open multiplet. This extra boson can be interpreted as the dilaton of the $\tilde{G}$ manifold [35]. We note that since $T_a$ is not hermitian, there can be chiral QNGFs.

In Chapter 3 there is an example $U(6)/[U(4) \times SU(2)]$ coset model, in which the extra QNGB is provided by an additional superfield called the "novino." By the low energy theorem, the soft masses for the first and second generation scalars is set to zero.

## 1.4 Major Aspects of Particle Dark Matter

In this section we discuss some aspects of the phenomenology of particle dark matter, with an emphasis on WIMPs and on aspects of detection that are relevant to later chapters. For reviews, please see for example Refs. [36, 37, 38].

### 1.4.1 Evidence

The first strong evidence for dark matter was the observation of anomalous galaxy rotation velocity curves [39]. Assuming virialized bright and dark galaxy components, the velocity curve should be

$$v(r) = \sqrt{\frac{GM(r)}{r}} \tag{1.114}$$

where $M(r)$ is the mass enclosed at galactic radius $r$. The measured curves are flat going out to large radius, even though there is less and less visible matter, suggesting missing mass. The various mass contributions to the observed velocity at a given radius is shown in Figure 1.3 for a sample galaxy [40]. The dark matter halo component is dominant at large radius. Similar measurements of the velocity dispersion of dwarf spheroidal galaxies in the Local Group show far greater mass than what can be attributed to bright matter [41].

Another method for identifying missing mass is to measure the amount of gravitational lensing of light from background sources. Perhaps the most striking example is the Bullet Cluster, shown in Figure 1.4. The Bullet Cluster is in fact the collision

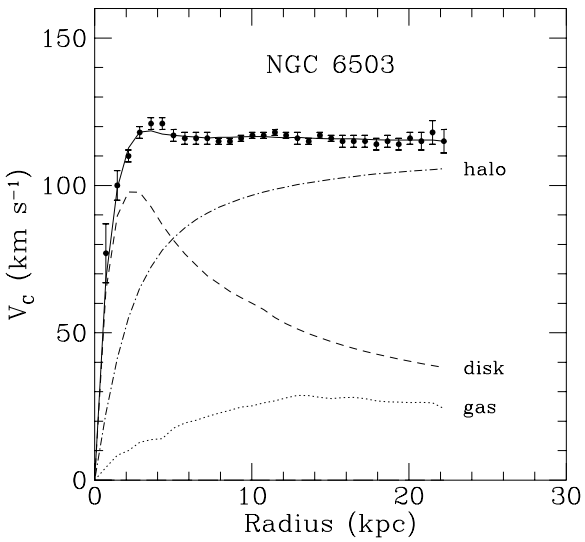


Figure 1.3: The various mass contributions to the observed rotational velocity at a given radius, for a sample galaxy [40]. The dark matter halo component is dominant at large radius.

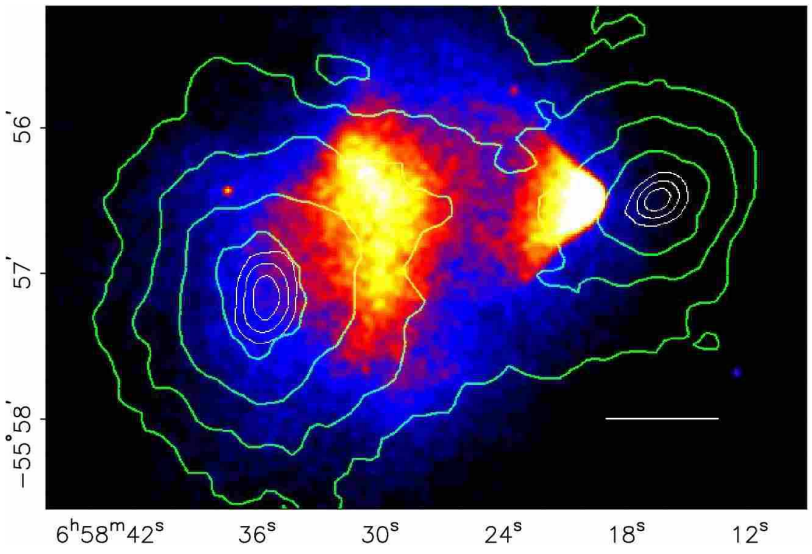


Figure 1.4: Observation of the Bullet Cluster. The green contours show the mass distribution as measured by lensing, and the other colored component shows the distribution of bright matter as measured by X-ray observations [42].

of two galaxy clusters. The green contours show the mass distribution as measured by lensing, and the other colored component shows the distribution of bright matter as measured by X-ray observations. The separation of the shocked bright matter from the region of space creating the lensing effect is highly problematic for modified theories of gravity, but is entirely consistent with the existence of dark matter [42].

At cosmological scales, the dark matter abundance can be inferred by assuming the Big Bang model for universe. The "standard model" for the Big Bang is the Friedmann-Lemaître-Robertson-Walker equation

$$\frac{H^2}{H_0^2} = \Omega_R a^{-4} + \Omega_B a^{-3} + \Omega_{DM} a^{-3} + \Omega_\Lambda \tag{1.115}$$

where $a$ is the scale factor ($a = 1$ today), $H \equiv \dot{a}/a$ is the expansion rate of space, $H_0 = 71 \pm 2.5\ \mathrm{km\,s^{-1}\,Mpc^{-1}}$ is the current expansion rate [25], $\Omega_R$ is the fraction of the critical density $3H_0^2/8\pi G$ composed of radiation, $\Omega_B$ is the fraction of baryonic matter, $\Omega_{DM}$ is the fraction of dark matter, and $\Omega_\Lambda$ is the fraction of dark energy (discussed earlier).

At early times, radiation was dominant and was in thermal equilibrium with the ionized matter in the universe. As space expanded, the radiation component cooled ($\propto a^4$) and decoupled from baryonic matter at around redshift $z = 1090$, when the universe was around 380,000 years old. The surface of last scattering for the photons previously in thermal equilibrium can be seen today as the cosmic microwave background (CMB). The power spectrum of the temperature anisotropies in the CMB contains information on the collective motions of the photon-baryon fluid, called baryon acoustic oscillations. The presence of dark matter, which decoupled at much higher temperatures, offsets the amount of baryonic matter and thus the amplitude of acoustic oscillations. The present-day parameters extracted from the CMB are $\Omega_{DM} = 0.222 \pm 0.026$, $\Omega_B = 0.0448 \pm 0.0028$ and, in combination with supernova observations, $\Omega_\Lambda = 0.734 \pm 0.029$ [25]. At lower redshifts/much later times, the power spectrum of acoustic oscillations is imprinted into the large scale structure (LSS) of matter in the universe. Observations of large scale structure independently give $\Omega_B + \Omega_{DM} = 0.273 \pm 0.025$ [44].

Finally, one more strong piece of evidence for dark matter comes from Big Bang

nucleosynthesis (BBN). Certain light elements were produced very early on in the Big Bang, at MeV scale, but not later in stars. The correct abundances of these light elements is predicted only if the baryon-to-photon ratio is consistent with most of the mass in the universe being dark matter. This approach gives $\Omega_B = 0.044 \pm 0.0026$, again consistent with the CMB parameters.

### 1.4.2 Candidates

Based on what has been presented so far, dark matter likely does not have electromagnetic interactions, otherwise it would conflict with CMB, LSS and BBN measurements. Moreover, dark matter that are too light ($\leq$ 550 eV) would also conflict with LSS and CMB observations because they would be moving too fast at the time of their decoupling, erasing the observed structure [45]; this rules out neutrinos. Then, dark matter must not only be dark, but cold/massive (it turns out, however, that axions are an exception to this rule).

One class of dark matter candidates is the Massive Compact Halo Object (MACHO). These are planet- or star-sized objects composed of exotic matter; baryons are ruled out by BBN. One example of a MACHO is a primordial black hole (PBH), formed during an epoch of the Big Bang with large density fluctuations [46]. During such an epoch, there may be fluctuations that are the size of the horizon, and a sufficient fraction of these may collapse into black holes on order to constitute the observed dark matter abundance. However, the efficiency of this process depends greatly on the details of collisions with nearby fluctuations while forming, their sphericity prior to collapse, etc.

Their mass goes like

$$M_{PBH} \approx M_\odot \left(\frac{T}{100\ \text{MeV}}\right)^{-2} \left(\frac{g_*}{10.75}\right)^{-1/2} \tag{1.116}$$

where $M_\odot$ is the solar mass, $T$ is the temperature at which they form, and $g_*$ is the number relativistic degrees of freedom at this temperature. Black holes from $T < \mathcal{O}(\text{MeV})$ are forbidden because they would interfere with BBN, ruling out much of the intermediate mass ($\mathcal{O}(10^3)M_\odot$) black hole range. MACHOs $10^{-7}M_\odot$ to $\mathcal{O}(10)M_\odot$

are ruled out by microlensing searches in our galaxy [47]. This eliminates QCD-scale PBHs [48], however, electroweak black holes $10^{-8}M_\odot$ [49] evade the bound. Finally, PBHs with mass $\lesssim 10^{-16}M_\odot$ are ruled out because their Hawking radiation would exceed gamma ray diffuse flux limits.

As mentioned previously, axions are also a potential dark matter candidate. After promoting the $\theta$ in the CP-violating QCD coupling to a dynamical field, the action is

$$\mathcal{L}_\theta = \left(\theta + \frac{a}{f_a}\right) \sum_a \epsilon^{\mu\nu\rho\sigma} G^a_{\mu\nu} G^a_{\rho\sigma} \tag{1.117}$$

where $\theta \simeq 10^{-10}$, $a$ is the dynamical field and $f_a$ is the scale of the breaking of the Peccei-Quinn symmetry. The corresponding potential is approximately

$$V \simeq m_\pi^2 f_\pi^2 \left[1 - \cos\left(\theta + \frac{a}{f_a}\right)\right] \tag{1.118}$$

The minimum of the potential is at $a = -\theta f_a$, so the strong CP problem is solved. The mass turns out to be

$$m_a \approx 6\,\mu\text{eV}\,\frac{10^{12}\,\text{GeV}}{f_a}\,. \tag{1.119}$$

Limits on the cooling of stars and supernovae require $f_a \gtrsim 10^{10}$ [1], so the axion is necessarily an extremely light boson. Nonetheless, axions behave like non-relativistic particles at late times. This is because the potential is so flat, the field need not be at the minimum in the early universe. Moreover, coupling to QCD instanton effects dampens the evolution of the field. At late times, when the universe is cold, the axions will have already diluted like normal matter, propagating with very low speeds in the current epoch. This phenomenon is called misalignment production.

Thus, the axion does not destroy structure. On the other hand, to obtain the correct abundance of axions, $f_a \simeq 10^{12}$ is required. This leaves a rather narrow window for axions to be a viable dark matter candidate.

We now turn to the dark matter candidates coming from TeV-scale frameworks such as supersymmetry and extra dimensions. While these frameworks are already well-motivated because they may solve the standard model hierarchy problem(s), they

also provide a viable dark matter candidate. Taking supersymmetry as an example, the LSP, if having only weak charges, may be a plausible dark matter candidate if thermal production gives the correct abundance. This will depend on the LSP's mass and on the availability of other low-lying fields for coannihilation processes. The general class of electroweak-scale dark matter with weak charges is the Weakly Interacting Massive Particle (WIMP).

We can estimate the relic abundance from annihilation using the Boltzmann equation,

$$\frac{dn}{dt} + 3Hn = -\langle\sigma v\rangle \left(n^2 - (n^{eq})^2\right) \tag{1.120}$$

where $\langle\sigma v\rangle$ is the thermal average of the annihilation cross section times the velocity. For a dark matter particle of mass $m$, in the non-relativistic limit the equilibrium distribution is given by the Maxwell-Boltzmann distribution

$$n^{eq} = g\left(\frac{mT}{2\pi}\right)^{3/2} e^{-m/T} \,. \tag{1.121}$$

Changing variables to

$$Y \equiv \frac{n}{s} \quad , \quad Y^{eq} \equiv \frac{n^{eq}}{s} \quad , \quad x \equiv= \frac{m}{T} \tag{1.122}$$

where $s = 2\pi^2 g_* T^3/45$ is the entropy density, and assuming that entropy is preserved in a comoving volume (i.e., $d(sa^3)/dt = 0$), the Boltzmann equation becomes

$$\frac{dY}{dx} = -\frac{\langle\sigma v\rangle\, s}{Hx}\left(Y^2 - (Y^{eq})^2\right) \,. \tag{1.123}$$

Expanding the cross section in the non-relativistic limit as

$$\langle\sigma v\rangle = a + b\left\langle v^2\right\rangle + \mathcal{O}(\left\langle v^4\right\rangle) \approx a + 6b/x \tag{1.124}$$

and integrating from $x = x_F$ to $x = \infty$ we obtain

$$Y_\infty^{-1} = \sqrt{\frac{\pi g_*}{45}} m_{pl}\, m\, x_F^{-1}(a + 3b/x_f) \,. \tag{1.125}$$

Here, $x_F$ is the "freeze-out temperature," the temperature at which the annihilation reaction stops occurring. This can be found iteratively by matching the solutions in

the late-time and early-time regimes of the Boltzmann equation. Then, substituting the current entropy density, the relic density is

$$\Omega_{DM}h^2 \simeq \frac{1.07\times 10^9\,\mathrm{GeV}^{-1}}{m_{pl}}\frac{x_F}{\sqrt{g_*}}\frac{1}{(a+3b/x_F)} \tag{1.126}$$

where $a$ and $b$ are in $\mathrm{GeV}^{-2}$, and $h = H_0/(100\,\mathrm{km\,s^{-1}\,Mpc^{-1}})$ is the so-called Hubble parameter. We also made the substitution

$$H = \left(\frac{\pi^2}{90}\right)^{1/2} g_*^{1/2}\frac{T^2}{m_{pl}} \tag{1.127}$$

which holds in a radiation-dominated universe.

For a WIMP of mass $m \approx 300$ GeV, we put in $a \approx \pi\alpha(m_Z)^2/m^2 \approx 3\times 10^{26}\ \mathrm{cm^3\,s^{-1}}$, $g_* \approx 100$ and $x_F \approx 25$. With these parameters, we obtain $\Omega_{DM} = 0.24$. Thus, for an LSP right near the electroweak scale, annihilation through weak interactions gives precisely the correct dark matter density. This coincidence is known as the "WIMP miracle."

Of course, this "miracle" has some flexibility, as it is the ratio $\langle\sigma v\rangle/m^2$ that matters. For example, if the annihilation is predominantly $p$-wave, then the $b$ portion of the cross section above will dominate, reducing the rate of annihilation at decoupling by an order of magnitude. Similarly, if there is another state heavier by a small amount $\Delta m$, then its density will only be suppressed by the Boltzmann factor $e^{-\Delta m/T}$ compared to the WIMP. Then, the WIMP can coannihilate with that state to give a reduce relic density; if there are two parent particles close to one another in mass, they can coannihilate to give an increased relic density instead. Because of this flexibility, WIMPs can span a mass range from below 100 GeV to nearly 1 TeV. WIMP-like dark matter may be heavier if the strength of interaction is greater, such that the annihilation cross-section is the same. However, then the interaction may no longer be considered weak. The unitarity limit is $m \simeq 110$ TeV [50].

So, WIMPs are well-motivated, because the frameworks in which they reside can solve other problems of the standard model, and because they do not require any contrivance to give the correct dark matter abundance; however, there is still flexibility in WIMP model-building which can entertain other considerations, like new potential

signals. By contrast, the uncertainties in PBH production and the narrow allowed region for axions make them less appealing. There are also many other dark matter candidates (e.g., SuperWIMPs, wimpzillas, Q-balls, etc.), but describing them would be be beyond the scope of this presentation.

### 1.4.3 Detection

Direct detection involves detecting an interaction between a WIMP and a target mass. The velocity of WIMPs in the galactic halo at the radius of our solar system is around $v = 220$ km/s. For a 100 GeV WIMP, this is a kinetic energy of around 50 keV. To see such a small signal against background radiation is quite difficult, more so because the interactions are weak. The event rate is

$$R = n_{DM} v \frac{M}{m_N} \sigma_N \approx \frac{10}{\text{year}} \times \frac{100\,\text{GeV}}{m} \times \frac{M}{100\,\text{kg}} \frac{A}{56} \times \frac{\sigma_N}{10^{-42}\,\text{cm}^2} \tag{1.128}$$

where $n_{DM}$ is the number density of dark matter in the vicinity of the Earth, $M$ is the mass of the detector, $m_N$ is the mass of a nucleon, and $\sigma_N$ is the scattering cross section between the WIMP and the nucleon. The cross section is given by [36]

$$\sigma_N = \frac{4}{\pi} \left( \frac{m m_N}{m + m_N} \right)^2 \left[ (n_p f_p + n_n f_n)^2 + 4 \frac{J+1}{J} (a_p \langle s_p \rangle + a_n \langle s_n \rangle)^2 \right] \tag{1.129}$$

where the first and second terms in the bracket are the spin-independent and the spin-dependent contributions, respectively. The spin-independent WIMP-nucleon coupling for the proton ($p$) and the neutron ($n$)

$$f_{p,n} = \sum f_q \langle p | \bar{q} q | p \rangle_{p,n} \tag{1.130}$$

is an average over the constituent quarks in the nucleon and their couplings to the WIMP. In supersymmetry, the coupling $f_{p,n}$ is dominated by the higgsino-quark Yukawa interaction, since weak squark exchange is suppressed by factor $\sim m_{\tilde{q}}^4$. Thus, for any supersymmetric model in which the WIMP has a significant higgsino contribution, e.g. being in a small $\mu$ region, the detectability will be significantly enhanced. Spin-dependent interactions are also enhanced with higgsino mixing, since $Z$-boson

| Halo model | $\alpha$ | $\beta$ | $\gamma$ | $r_s$ in kpc |
|---|---|---|---|---|
| Cored isothermal [51] | 2 | 2 | 0 | 5 |
| Navarro, Frenk, White [52] | 1 | 3 | 1 | 20 |
| Moore [53] | 1 | 3 | 1.16 | 30 |

exchange becomes more likely. This is the case for one of the model points in Chapter 3. Moreover, an enhancement in the spin-dependent cross-section would increase the capture rate of the WIMP in the sun [54], and thereby enhance the flux of neutrinos from WIMP annihilations from sun.

In addition to the dark matter in the vicinity of the Earth [54, 55], there is the entire Milky Way galactic halo [56], as well as the halos in dwarf spheroidal galaxies [57] and everywhere on cosmological scales. To associate the flux of indirect products (e.g, neutrinos, gamma rays) from dark matter annihilation or decay [58][1] with the nature of the WIMPs, we must understand the halo shapes.

From rotational velocity curves and N-body simulations, halo profiles can be parameterized as

$$\rho(r) = \rho_\odot \left[\frac{r_\odot}{r}\right]^\gamma \left[\frac{1+(r_\odot/r_s)^\alpha}{1+(r/r_s)^\alpha}\right]^{(\beta-\gamma)/\alpha} \tag{1.131}$$

where for the Milky way $\rho_\odot$ is the dark matter density around the sun, $r_\odot$ is the distance from the sun to the galactic center. The parameters are shown in Table 1.4.3. At the galactic core, the flux from annihilations goes like $\rho^2 r^3 \Delta\Omega$, where $\Delta\Omega$ is the solid angle of the region viewed. Then, for the Navarro-Frenk-White (NFW) profile, the flux from successive shells of thickness $dr$ about the galactic center is constant, whereas for the cored isothermal profile it goes like $r^2$, a significant reduction. Thus, it is often advantageous to integrate over a large solid angle to escape uncertainties in the halo shape near the galactic center.

Finally, a recent exciting development in indirect detection is the observation of cosmic-ray $e^\pm$ anomalies by several instruments [59, 60, 61, 62]. Figure 1.5, shows a rising fraction of cosmic ray positrons, and Figure 1.6 shows a hardening in the cosmic-ray $e^\pm$ which cannot be attributed to background. It just so happens that

[1] In supersymmetry, LSP decay can be due to a small violation of R-parity.

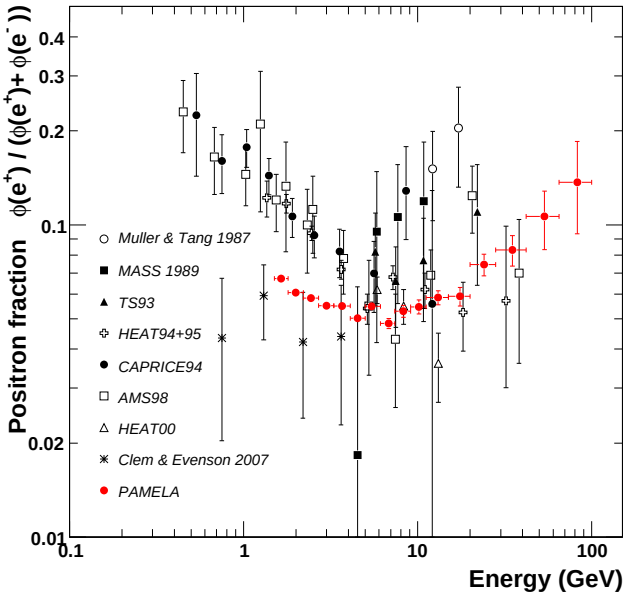


Figure 1.5: Anomalous rise in cosmic-ray positron fraction.

these anomalies are in the mass range of WIMP-like dark matter. If the dark matter annihilates or decays to leptons, it could explain the anomalies.

In the Chapter 2, we use observations of gamma rays and neutrinos to constrain the dark matter interpretation of these anomalies. In particular, we discuss the propagation of cosmic-ray $e^{\pm}$, the contributions to signal, characterization of backgrounds, and techniques for reducing systematic errors, such as that due to the choice of dark matter halo profile.

In Chapter 3, we examine model points from different parameters regions, and these have different dark matter candidates. In one region, the small $\mu$ character of the point gives a large higgsino component to the LSP. This enhances the direct detection cross-section, while also enhancing the annihilation rate. With further analysis, this could explain the anomalous rise in the positron fraction. Conversely, at the other model points the LSPs are almost entirely "bino," which is Majorana. Due to the Pauli principle, their annihilation is is $p$-wave and therefore suppressed by $v$, which

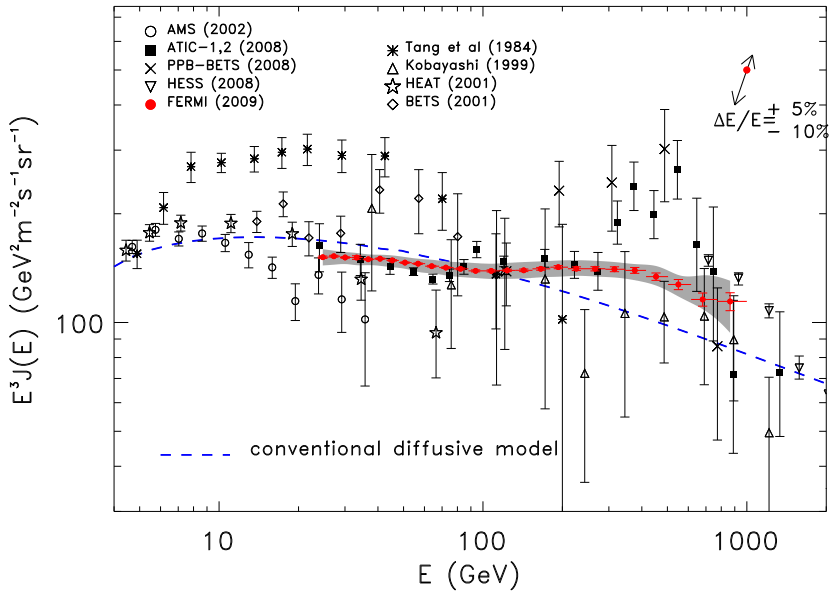


Figure 1.6: Anomalous hardening of cosmic-ray $e^{\pm}$ spectrum.

is only $0.001c$ in the present epoch — these cannot be seen by the current generation of instruments.

# Chapter 2

# Novel Astrophysical Constraints on Particle Dark Matter

## 2.1 Introduction

The existence of dark matter has been established by numerous observations. Although it constitutes most of the matter in the universe [24], the nature of dark matter remains largely unknown. One widely held possibility is that it is a new fundamental particle produced in the early universe and present today as a thermal relic. Among the best motivated of these are the so-called weakly interacting massive particles, or "WIMPs" (for reviews, see Refs. [36, 37]) which are predicted to be undergoing annihilations [54, 55, 56, 57] and possibly decays [58] in the current epoch.

Recently, the instruments PAMELA [59], ATIC [60], PPB-BETS [61], and Fermi [62] have observed features in the cosmic-ray $e^{\pm}$ spectrum and a positron fraction that are inconsistent with known backgrounds. While these anomalies may be due to unidentified astrophysical sources [63], one exciting possibility is that they are due to the decay [64, 65, 66, 67, 68, 69, 70] or annihilation [71, 72, 73, 74, 75, 79] of dark matter particles into standard model states. Even in the case that anomalies are not caused by new physics in the dark sector, the constraints are generally applicable to dark matter models.

In order for dark matter to explain the anomalies, the products of decay or

annihilation must be primarily leptonic. In either case, the Fermi observation gives the most precise preferred region in mass and lifetime/cross-section; for decays, only $\mu^+\mu^-$ and $\tau^+\tau^-$ final states fit the data, while for annihilations a small region of $e^+e^-$ is also permitted [76]. For the allowed parameter space, decays or annihilations into hadrons and weak and Higgs bosons are severely limited. Decays are constrained by the Fermi observation of the isotropic diffuse gamma-ray flux [77], and annihilations are constrained by the production of antiprotons [78].

Explaining the anomalies with annihilations has an additional challenge. In order to match the observed rates, the cross-section required is $10^3$–$10^4$ times that expected for thermal production of the dark matter in the early universe. This necessitates nonthermal production mechanisms or low-velocity enhancements to the cross-section, such as the Sommerfeld enhancement [74, 79] or the Breit-Wigner enhancement [80, 81]. Moreover, high cross section annihilations to leptonic states are tightly constrained by synchrotron radio emissions from the galactic center, although this constraint can be evaded if the true galactic dark matter halo profile is much less steep at the galactic center than benchmark profiles [82, 76]. Thus, the leptophilic decaying DM scenario has recently gained momentum.

In this chapter, we develop the constraint from gamma-rays for decaying dark matter, then propose enhancements to these constraints, as well as the constraints to dark matter annihilations, using future neutrino detectors.

## 2.2 Gamma-ray Constraints on Decaying Dark Matter

Although the existence of dark matter (DM) has been firmly established by numerous observations, the nature of DM mostly remains unknown. In particular, it is not known whether DM is absolutely stable or not. If DM is unstable, it will eventually decay into lighter particles which may be observed as an excess in the cosmic-ray spectrum.

If DM is related to new physics which appears at the weak scale, it is natural

to expect that the DM mass is in the range $\mathcal{O}(100)\,\mathrm{GeV}$–$\mathcal{O}(10)\,\mathrm{TeV}$. However, the longevity of DM whose mass is of the weak scale is a puzzle and calls for some explanation. The (quasi)stability may be the result of a discrete symmetry or extremely weak interactions. For instance, in a supersymmetric (SUSY) theory, the lightest SUSY particle (LSP) is stable and therefore a candidate for DM if R-parity is an exact symmetry. However, R-parity violation may be a common phenomenon in the string landscape [83], in which case the LSP DM is unstable and eventually decays into standard model (SM) particles. On the other hand, if DM is in a hidden sector which has extremely suppressed interactions with the SM sector, the only way to probe DM may be to look in the cosmic rays for signatures of its decay products.

Leptophilic decaying DM models can be broadly divided into two categories. One is such that DM first decays into additional light particles, which subsequently decay into muons or electrons, while the decays into hadrons are forbidden by kinematics [84]. The other is such that the DM particle couples mainly to leptons due to symmetry [65] or geometric setup [85]. While the hadronic activities are absent in the former case, it is model-dependent to what extent the DM is leptophilic in the latter case. One example is the hidden gauge boson decaying into the SM particles through a mixing with a $\mathrm{U}(1)_{B-L}$ gauge boson [64]; the DM is certainly leptophilic in the sense that it mainly decays into leptons, but a certain amount of quarks are also produced.

In this section we study the current constraints on the hadronic and leptonic decay of DM. The anti-proton flux is known to provide a tight constraint on the hadronic activities, but there are large uncertainties in the propagation [86]. The other constraint comes from gamma-ray observation. In contrast to charged cosmic-ray particles, gamma-rays travel undeflected and there is no uncertainty in the propagation; the main uncertainty is the dark matter profile. Furthermore, the Fermi satellite has been measuring gamma-rays with both unprecedented precision and statistics, and we can expect a significant improvement over EGRET data [87, 88]. In this section we will derive constraints on the partial decay rates of DM into $WW$, $ZZ$, $hh$, $q\bar{q}$ and $gg$ as well as $e^+e^-$, $\mu^+\mu^-$ and $\tau^+\tau^-$ using the Fermi [89, 90] and HESS [91] data. The bounds obtained in this section are not only generic but also can be used to

know what branching ratios are allowed in decaying DM models which account for the PAMELA/Fermi cosmic-ray electron/positron excess.

### 2.2.1 Analysis

There are several contributions to the gamma-ray spectrum when DM decays into SM particles. Photons from fragmentation are generated by the decay of mesons, especially $\pi^0$, and final-state radiation (FSR) is always produced when the DM decays into charged particles. The electrons and positrons produced by the DM decay will lose energy by emitting synchrotron radiation in the galactic magnetic field and through inverse Compton (IC) scattering off ambient photons (star light, dust re-emission, and CMB). In this section we summarize the calculation of these contributions and how we derive constraints.

#### Local contributions

First, we use `PYTHIA 6.4.21` [92] to simulate the fragmentation of the various final states at a range of DM masses, and for charged final states we use the expression in Ref. [93] for the photon multiplicity from final-state radiation. Since these contributions are local to the site of DM decay, and because gamma-rays travel undeflected, the differential flux from our galactic DM halo is given by flux conservation:

$$\left(\frac{d\Phi_\gamma}{dEd\Omega}\right)^{(\mathrm{gal.})}_{\mathrm{local}} = \frac{1}{4\pi}(r_\odot\rho_\odot)\frac{1}{m_{\mathrm{DM}}\tau}\left(\frac{dN_\gamma^{(\mathrm{frag.})}}{dE}+\frac{dN_\gamma^{(\mathrm{FSR})}}{dE}\right)J(\Delta\Omega) \tag{2.1}$$

where $r_\odot = 8.5\,\mathrm{kpc}$ is the solar distance from the galactic center [94], $\rho_\odot = 0.3\,\mathrm{GeV\,cm^{-3}}$ is the density of the DM halo at this distance, $\tau$ is the DM lifetime, and

$$J(\Delta\Omega) = \frac{1}{\Delta\Omega}\int_{\Delta\Omega} d\Omega \int_{\mathrm{l.o.s.}} \frac{ds}{r_\odot}\left(\frac{\rho_{\mathrm{DM}}(\vec{x})}{\rho_\odot}\right) \tag{2.2}$$

is the line-of-sight integral, in which $\Delta\Omega$ is the region of sky observed by a given experiment and $\rho_{\mathrm{DM}}(\vec{x})$ is the halo profile. In this analysis we use the NFW halo profile [52].

There is also an isotropic, diffuse extragalactic contribution on cosmological scales from DM residing in our past light cone. We find that this contribution to the

differential flux is given by

$$\left(\frac{d\Phi_\gamma}{dEd\Omega}\right)^{(\mathrm{ex.})}_{\mathrm{local}} = \frac{c}{4\pi}\frac{\Omega_{\mathrm{DM}}\rho_c}{H_0\Omega_{\mathrm{M}}^{1/2}}\frac{1}{m_{\mathrm{DM}}\tau} \times \int_1^\infty dy \frac{y^{-3/2}}{\sqrt{1+\Omega_\Lambda/\Omega_{\mathrm{M}}y^{-3}}}\left(\frac{dN_\gamma^{(\mathrm{frag.})}}{d(Ey)} + \frac{dN_\gamma^{(\mathrm{FSR})}}{d(Ey)}\right) \tag{2.3}$$

where $y \equiv 1+z$ and the cosmological parameters are given by Ref. [24]; the density of radiation is taken to be negligible. This expression duplicates the result of Ref. [95].

**Contributions from propagating electrons and positrons**

Electrons and positrons as final states of DM decay, as well as those from the fragmentation of other final states, will lose energy via synchrotron radiation and IC scattering off ambient photons. Here we describe the calculation of these effects and the resulting contribution to the gamma-ray flux; our analysis parallels that of Ref. [96].

First, let us consider the galactic contribution. The diffusion of $e^\pm$ is governed by the equation

$$K(E)\nabla^2 f_e(E,\vec{x}) + \frac{\partial}{\partial E}\left[b(E,\vec{x})f_e(E,\vec{x})\right] + Q(E,\vec{x}) = 0 \tag{2.4}$$

where $K(E)$ is the diffusion coefficient, $f_e(E,\vec{x})$ is the $e^\pm$ phase space distribution, $b(E,\vec{x}) = b_{\mathrm{syn}}(E,\vec{x}) + b_{\mathrm{IC}}(E,\vec{x})$ is the energy loss rate, and $Q(E,\vec{x})$ is the $e^\pm$ source term. For this analysis we adopt the MED propagation model [97] to set $K(E)$ and the geometric boundary of diffusion. Under this model the propagation length for $e^\pm$ with $E \gtrsim 100\,\mathrm{GeV}$ is $\mathcal{O}(0.1)\,\mathrm{kpc}$ before losing its most of the energy. In the limit that this length is small compared to the distance traveled, $f_e(E,\vec{x})$ is well-approximated by

$$f_e(E,\vec{x}) = \frac{1}{b(E,\vec{x})}\frac{\rho_{\mathrm{DM}}(\vec{x})}{m_{\mathrm{DM}}\tau}\int_E^\infty dE'\,\frac{dN_e}{dE'}\,. \tag{2.5}$$

The energy loss rate due to synchrotron radiation is given by

$$b_{\mathrm{syn}}(E) = \frac{4}{3}\sigma_T\left(\frac{E}{m_e}\right)^2\left(\frac{B^2}{2}\right) \tag{2.6}$$

where $\sigma_T$ is the Thomson cross-section and $B \approx 3\mu$G is taken as the strength of the galactic magnetic field.[1] The energy loss rate due to IC scattering is given by

$$b_{\rm IC}(E,\vec{x}) = \int dE_\gamma dE_{\gamma_{\rm BG}} (E_\gamma - E_{\gamma_{\rm BG}}) \frac{d\sigma_{\rm IC}}{dE_\gamma} f_{\gamma_{\rm BG}}(E_{\gamma_{\rm BG}}, \vec{x}) \tag{2.7}$$

where $d\sigma_{\rm IC}/dE_\gamma$ is the IC differential cross-section as given in Ref. [98], and $f_{\gamma_{\rm BG}}(E_{\gamma_{\rm BG}}, \vec{x})$ is the sum of the CMB radiation field and the galactic radiation field (star light and dust re-emission). In our calculation we use the interstellar radiation field (ISRF) furnished by the GALPROP collaboration [99].

Because the magnetic field is so weak, synchrotron emissions would only be in the radio and is thus only relevant in this calculation as an energy-loss mechanism. On the other hand, IC processes for $e^\pm$ of $E \sim \mathcal{O}(100)\,$GeV would produce gamma-rays of $E \sim \mathcal{O}(1)\,$GeV which is in the range of the Fermi observations. Therefore, the differential gamma-ray flux is given by

$$\left(\frac{d\Phi_\gamma}{dE d\Omega}\right)^{\rm (gal.)}_{\rm prop.} = \frac{1}{4\pi}\frac{1}{\Delta\Omega}\int_{\Delta\Omega} d\Omega \int_{\rm l.o.s.} ds \int dE_e dE_{\gamma_{\rm BG}}\, \frac{d\sigma_{\rm IC}}{dE} f_{\gamma_{\rm BG}}(E_{\gamma_{\rm BG}}, \vec{x}) f_e(E_e, \vec{x}) \tag{2.8}$$

Now let us turn to the extragalactic contribution. On cosmological distances, there is no interstellar radiation field, only the CMB, and negligibly small magnetic fields. Thus, the only energy-loss mechanism is IC scattering of CMB photons. Moreover, assuming the universe is indeed isotropic and homogeneous, the distributions of CMB photons and DM are spatially invariant. Then the diffusion equation becomes

$$\frac{\partial}{\partial E}\left[b(t,E) f_e(t,E)\right] + Q(t,E) + H\, E\, \frac{\partial f_e(t,E)}{\partial E} = \frac{\partial f_e(t,E)}{\partial t} \tag{2.9}$$

where $H$ is the Hubble parameter. Since the CMB photon energy is so low the $e^\pm$ are non-relativistic in the center-of-momentum frame, the energy loss rate due to IC scattering is given by the Thomson limit

$$b_{\rm cosm}(y,E) = \frac{4}{3}\left(\frac{E}{m_e}\right)^2 \sigma_T\, \left(\rho_{\rm CMB}\, y^4\right) \tag{2.10}$$

where $\rho_{\rm CMB} \simeq 0.26\,{\rm eV\,cm^{-3}}$ is the present-day CMB energy density and $y \equiv 1+z$ as before. The timescale of energy-loss $E/b_{\rm cosm} \lesssim \mathcal{O}(10^{14})\,$sec is much less than the

[1] The value of the magnetic field strength may be different close to the galactic center.

Hubble time, so the term $\mathcal{O}(H)$ in the diffusion equation can be ignored. This gives for the $e^{\pm}$ spectrum

$$f_e(y,E) = \frac{1}{b_{\rm cosm}(y,E)} \, \frac{1}{m_{\rm DM}\tau} \, \left(\rho_{\rm DM}\, y^3\right) \int_E^\infty dE' \, \frac{dN_e}{dE'} \, . \tag{2.11}$$

Finally, we find for the differential flux

$$\left(\frac{d\Phi_\gamma}{dE d\Omega}\right)^{\rm (ex.)}_{\rm prop.} = \frac{c}{4\pi} \frac{1}{H_0 \Omega_{\rm M}^{1/2}} \int_1^\infty dy \frac{y^{-9/2}}{\sqrt{1+\Omega_\Lambda/\Omega_{\rm M} y^{-3}}} A(y,E) \tag{2.12}$$

where

$$A(y,E) \equiv \int dE_e \, dE_{\gamma_{\rm BG}} \, \frac{d\sigma_{\rm IC}}{d(Ey)} \, f_{\gamma_{\rm BG}}(y, E_{\gamma_{\rm BG}}) \, f_e(y,E_e) \tag{2.13}$$

and $f_{\gamma_{\rm BG}}(y, E_{\gamma_{\rm BG}})$ is the CMB spectrum at redshift $z = y-1$. Comparable expressions for annihilating dark matter may be found in Refs. [100, 101].

**Derivation of constraints from data sets**

We derive constraints using three data sets: observation of gamma-rays from the galactic center (within 0.1°) by the HESS telescope [91], observation of the galactic mid-latitude ($10° \leq |b| \leq 20°$) diffuse gamma-ray flux by the Fermi LAT [89], and preliminary data for the isotropic diffuse flux ($|b| \geq 10°$) also by the Fermi LAT [90].

We do not use the HESS observation of the galactic center ridge [102] because it requires a subtraction of nearby flux levels.[2] The result of this procedure is highly profile dependent: we find that for the NFW profile this procedure weakens the constraint by a factor 5, and for the less-cuspy isothermal profile the constraint would be weakened by a factor 200. Before the procedure our result is comparable to that of Ref. [76].

For various DM masses and lifetimes, we calculate and sum the various contributions to the gamma-ray flux for each of the energy bins of each data set, with two exceptions due to limited computational power:

[2] We are grateful to J. F. Beacom [103] for pointing this out.

- We use only the two highest bins of the Fermi mid-latitude data (energy $\sim \mathcal{O}(10)\,\mathrm{GeV}$) when calculating the constraints for weak boson and colored channels. Since the spectra from DM decay are harder than the observed spectra, any excess will be dominated by the highest energy bins anyway.

- We include galactic ICS for comparison to the HESS galactic center data only for the leptonic final states, because they copiously produce hard $e^{\pm}$. Also, since we cannot know at this time how much galactic contribution (namely, galactic ICS and galactic halo contributions) is present in the isotropic flux reported by Fermi, we give this constraint both with and without galactic contribution added in. For the Fermi mid-latitude data we include galactic ICS for all channels.

Then, we compute how many standard deviations the calculated flux exceeds the data for these bins and take the largest of these, as in Ref. [76]. Again because the spectra from DM decay are harder than the observed spectra, this statistic is little different than reduced-$\chi^2$, but without the aliasing errors due to the number of effective degrees of freedom changing near a contour. The $3\sigma$ contours are shown on Figures 2.1, 2.2, and 2.3 for weak and Higgs boson, colored and leptonic channels, respectively. The lower dotted blue line is the constraint from Fermi isotropic diffuse flux without galactic contribution, and the upper dotted-dashed blue line is the the constraint with galactic contribution.

**Uncertainties**

Finally, let us consider the uncertainties in these calculations:

- *DM halo profile:* We use the NFW profile for the galactic dark matter halo. If we were to use instead the isothermal profile, the calculated flux of fragmentation and FSR photons from the galactic center would be reduced by a factor 4, weakening the constraint from the HESS observation. By contrast, because the Fermi observations cover a much larger portion of the sky looking away from the galactic center, switching to the isothermal profile would hardly change these constraints.

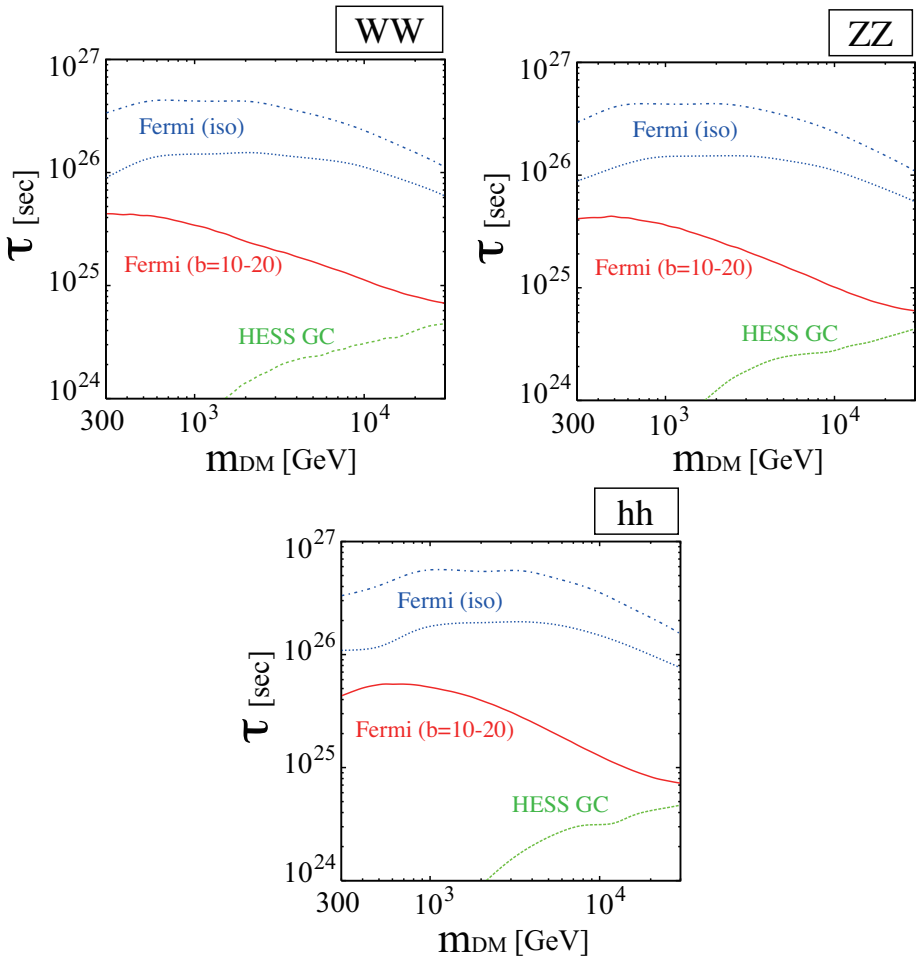


Figure 2.1: $3\sigma$ constraints for $WW$, $ZZ$ and $hh$ final states. The dotted green line ("HESS GC") is the constraint from HESS gamma-ray observations of the galactic center; the solid red line ("Fermi (b=10-20)") is the constraint from Fermi gamma-ray observations of the galaxy at mid-latitudes, $b = 10 - 20$. The lower dotted blue line is the constraint from Fermi isotropic diffuse flux without galactic contribution, and the upper dotted-dashed blue line is the the constraint with galactic contribution ("Fermi (iso)").

- *Local DM density:* We use the conservative, standard value $\rho_\odot = 0.3\,\mathrm{GeV\,cm^{-3}}$ for the DM halo density at the radius of our solar system, though a wide range is accepted [104]. A recent analysis gives the value $\rho_\odot = 0.39\,\mathrm{GeV\,cm^{-3}}$ within 10% [94].

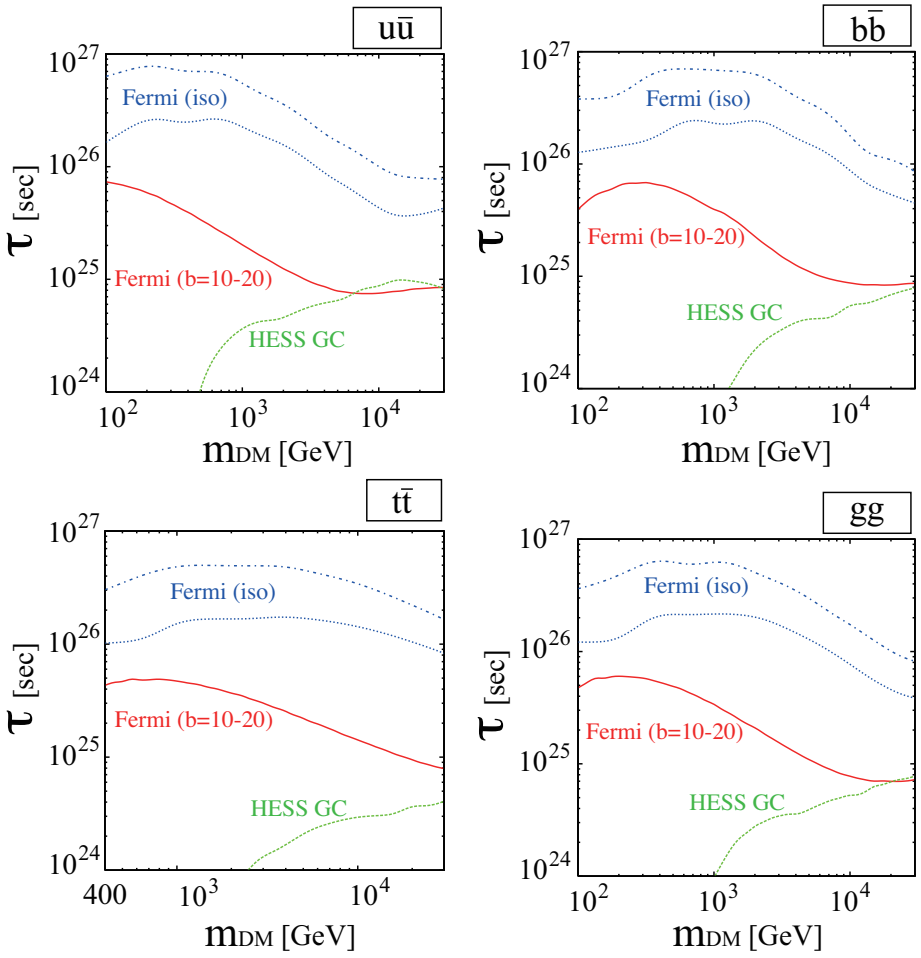


Figure 2.2: $3\sigma$ constraints for colored final states.

- *ICS calculation:* There are uncertainties associated with parameters such as the galactic magnetic field and interstellar radiation field, as well as the choice of the diffusion model and the approximation of dropping the diffusion effect in calculating the $e^{\pm}$ phase space distribution. Ref. [105] found that the same calculation with a slightly different setup matched the numerical results of GALPROP, and Ref. [76] estimates that the no-diffusion approximation can change photon flux by a factor of 2. Consequently, we estimate that the uncertainty in our calculation of ICS is $\mathcal{O}(1)$.

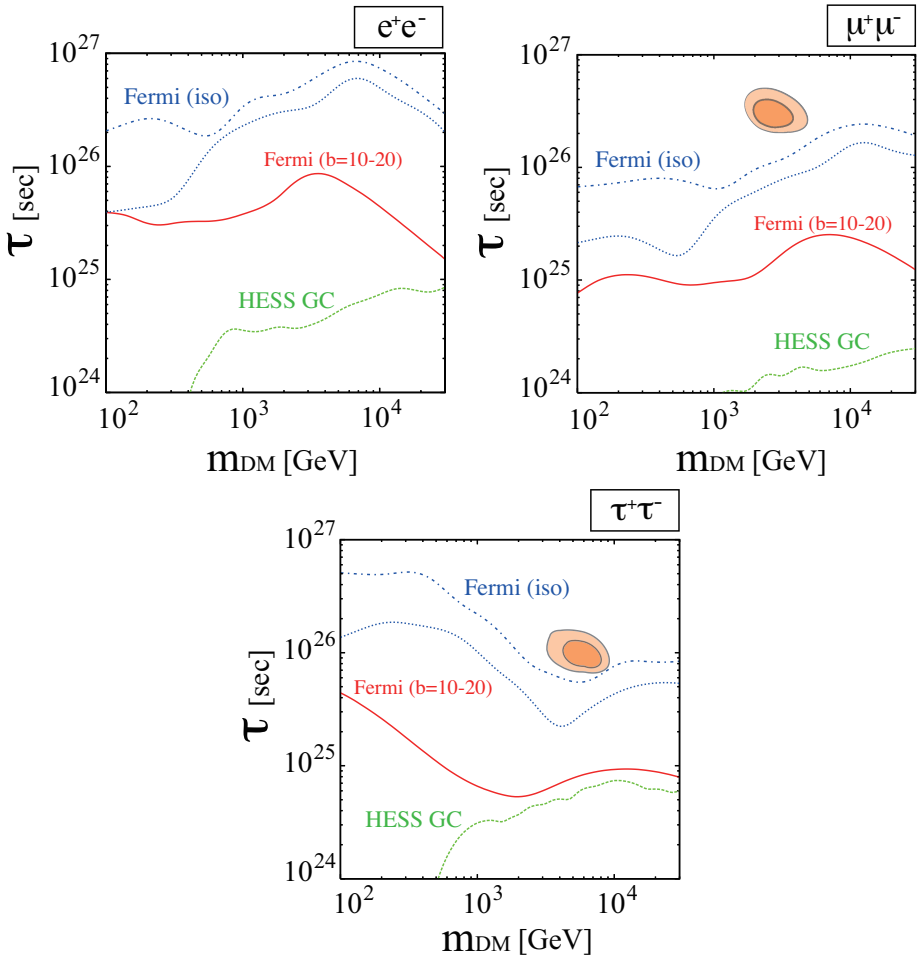


Figure 2.3: $3\sigma$ constraints for leptonic final states. The orange ellipse represents the region favored by the PAMELA/Fermi excess [76].

### 2.2.2 Discussion

For a whole range of DM masses, it is the Fermi isotropic diffuse flux that places most stringent constraints on the lifetime, followed by the Fermi galactic mid-latitude data and then by the HESS galactic center data. We can also see that for the hadronic channels shown in Figs. 2.1 and 2.2, as well as for the $\tau^+\tau^-$ channel shown in Fig. 2.3, the constraints derived from the Fermi mid-latitude data becomes weaker at heavier DM masses. This feature can be understood as follows. The gamma-ray energy spectrum from decaying DM is dominated by fragmentation and final-state radiation

at energies near the threshold $\sim m_{\rm DM}/2$, while the up-scattered photons through IC process dominate at low energies. Since the Fermi mid-latitude data is available up to $\mathcal{O}(10)\,\mathrm{GeV}$, it depends on the DM mass which contribution becomes important. The up-scattered photons tend to be dominant at $E \simeq \mathcal{O}(10)\,\mathrm{GeV}$ for a DM mass above $\mathcal{O}(1)\,\mathrm{TeV}$. That is why the constraints become flatter above $\mathcal{O}(1)\,\mathrm{TeV}$. The constraints from the Fermi isotropic data, which also goes up to $\mathcal{O}(10)\,\mathrm{GeV}$, show a similar flattening for $u\bar{u}$, $b\bar{b}$, $gg$ and $\tau^+\tau^-$ final states, which fragment into hard mesons. It is interesting to note that the IC scattering is important for the hadronic and $\tau^+\tau^-$ modes if the DM mass is heavier than several TeV.

From Fig. 2.3 one can see that the decay into $e^+e^-$ and $\tau^+\tau^-$ are more tightly constrained than that into $\mu^+\mu^-$. This is because the direct production of energetic electron/positron enhances the gamma-ray flux through final-state radiation and IC scattering, and because the decay of $\tau$ is accompanied by the fragmentation photons. The DM lifetime should be $\mathcal{O}(10^{26})$ sec in order to explain the PAMELA/Fermi excess in cosmic-ray electrons/positrons (shown by the orange ellipses in the figure). Therefore, in order to simultaneously satisfy the gamma-ray constraints and as well as account for the PAMELA and Fermi excess, DM must decay primarily into either muons or taus.

Suppose that the DM mainly decays into $\mu^+\mu^-$ at a lifetime of $\mathcal{O}(10^{26})$ sec. The allowed hadronic branching ratio is about $\mathcal{O}(10)\%$ from the figure. Of course the precise value depends on DM models. In next section we consider a DM model in which a hidden gauge boson decays into quarks and leptons through a mixing with an $\mathrm{U}(1)_{B-L}$ gauge boson. The allowed hadronic branching ratio in this DM model is about 30% at a reference point, $m_{\rm DM} = 2\,\mathrm{TeV}$ and $\tau = 1.5 \times 10^{26}$ sec.

We may, however, compare these generic gamma-ray constraints with the generic constraints from neutrinos. Bounds on leptonic final states from upward-going muons due to neutrinos interacting with the Earth [106] are 10–100 times weaker than those presented here, though the direct neutrino bounds from IceCube+DeepCore will surpass present-day gamma-ray constraints after a few years of running [107].

In the above analysis we required that the the DM contribution should not exceed the Fermi/HESS data points at more than $3\sigma$. If a fraction $f$ of the observed flux is

due to the astrophysical gamma-ray sources, the constraint on the DM lifetime will be improved by about $1/f$. For instance, Ref. [108] proposed a model of blazars and estimate its contribution to the diffuse isotropic gamma-ray flux. Although there is uncertainty in the blazar model, their estimate agrees well with the preliminary Fermi data. As the astrophysical understanding of the origin of the observed gamma-rays flux is improved, the constraint on the DM property gets stronger.

### 2.2.3 Constraints on a dark matter model

Using the constraints derived in the previous section, we should be able to check whether a specific DM model is allowed by the current gamma-ray observation. As an example, we take up a model which was proposed in Ref. [109] to account for the PAMELA and Fermi excess.

First, let us briefly review the model (see the original reference for details). The lifetime needed to account for the excess is of $\mathcal{O}(10^{26})$ seconds, and such a longevity calls for some explanation. To this end we introduce an extra dimension, which is assumed to be compactified on $S^1/Z_2$ with two distinct boundaries. Suppose that a hidden $\mathrm{U(1)_H}$ gauge field is confined on one boundary and the SM particles on the other. In such a set-up, direct interactions between the two sectors are suppressed by a factor of $\exp(-M_* L)$, where $M_*$ is the five-dimensional Planck scale and $L$ denotes the size of the extra dimension. For e.g. $M_* L \sim 10^2$, the direct couplings are so suppressed that the hidden gauge boson will be practically stable in a cosmological time scale [109]. Assuming that the hidden $\mathrm{U(1)_H}$ gauge symmetry is spontaneously broken, the hidden gauge boson, $A_H$, can be therefore a candidate for DM.

Let us introduce an $\mathrm{U(1)_{B-L}}$ in the bulk. Through a kinematic mixing between the $\mathrm{U(1)_H}$ and $\mathrm{U(1)_{B-L}}$, which is generically present, the $A_H$ will then decay into the SM quarks and leptons at a rate determined by their $B - L$ quantum number. After integrating out the heavy $\mathrm{U(1)_{B-L}}$ gauge boson[3], the effective couplings between the hidden gauge boson $A_H$ and the SM fermion $\psi_i$ can be extracted from the $\mathrm{U(1)_{B-L}}$

[3]We expect that the $\mathrm{U(1)_{B-L}}$ gauge symmetry is spontaneously broken around the grand unification theory (GUT) scale of about $10^{15}$ GeV, since the seesaw mechanism [110] for neutrino mass generation suggests the right-handed neutrinos of a mass about $10^{15}$ GeV.

gauge interactions

$$\mathcal{L}_{\rm int} \;=\; -\lambda\, q_i \frac{m^2}{M^2} A_H^\mu\, \bar{\psi}_i \gamma_\mu \psi_i, \tag{2.14}$$

where $\lambda$ is a coefficient of the kinetic mixing, $q_i$ denotes the $B-L$ charge of the fermion $\psi_i$, and $m$ and $M$ are the masses of the hidden gauge boson $A_H$ and the $\mathrm{U(1)_{B-L}}$ gauge boson, respectively. The lifetime of $A_H$ is therefore given as

$$\tau \;\simeq\; 1\times 10^{25}\,\mathrm{sec}\left(\sum_i N_i q_i^2\right)^{-1}\left(\frac{\lambda}{0.01}\right)^{-2}\left(\frac{m}{2\,\mathrm{TeV}}\right)^{-5}\left(\frac{M}{10^{15}\mathrm{GeV}}\right)^{4}, \tag{2.15}$$

where $N_i$ is the color factor (3 for quarks and 1 for leptons), the sum is taken over the SM fermions, and we have neglected the fermion masses. The introduction of the $\mathrm{U(1)_{B-L}}$ has two merits. One is that, for a natural choice of the $B-L$ breaking scale, the lifetime of DM falls in a desired range of $\mathcal{O}(10^{26})$ seconds. The other is that the DM decay mode is leptophilic and the branching ratios simply reflect the $B-L$ charge assignment, which makes the model very predictive; the branching ratio into a quark pair is given by 2/39, while that into a charged lepton pair is 2/13.

In a similar way as we did in the previous section, we have derived constraints on the lifetime of $A_H$ from the gamma-ray data. See Fig. 2.4. The Fermi galactic mid-latitude data plays an important role in constraining the model at low side of DM masses, while the HESS galactic center data takes over for the high side. For example, the lifetime of the $A_H$ of mass 500 GeV (2 TeV) should be longer than about $2\times 10^{25}$ ($2.7\times 10^{25}$) seconds. We take the reference point $m_{\rm DM} = 2\,\mathrm{TeV}$ and the lifetime $\tau = 1.5\times 10^{26}\,\mathrm{sec}$ shown as a star in Fig. 2.4 which can explain both the Fermi and PAMELA excess. The antiproton flux was calculated for the reference point and we found that it is consistent with the current PAMELA [78] and other observational data on the cosmic-ray antiproton. On the other hand, as one can see from Fig. 2.4, the reference point is marginally excluded by the bound obtained from the Fermi isotropic diffuse data. Since the gamma-ray flux calculation is more robust over the antiproton flux[4], we conclude that the hidden gauge boson DM model, which

[4] The flux of the antiproton produced by DM annihilation/decay is very sensitive to the diffusion model and it varies by about two orders of magnitude for different diffusion models.[86]

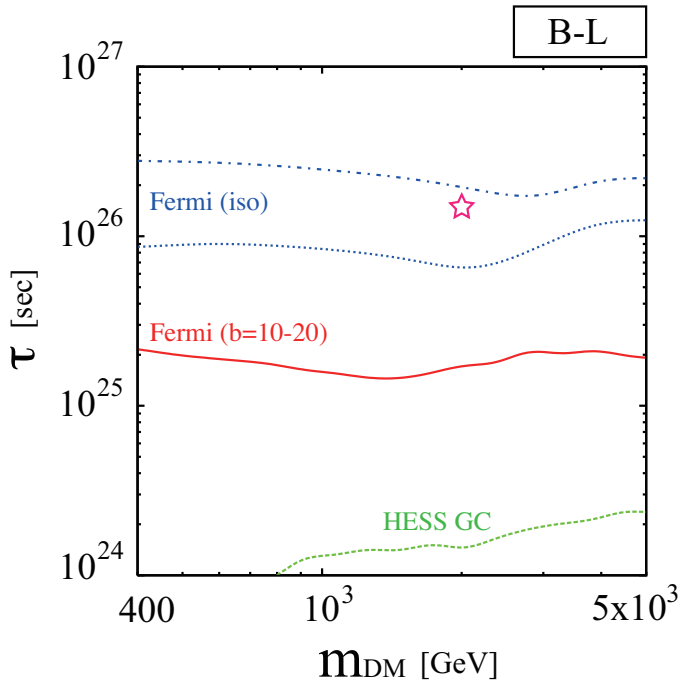


Figure 2.4: $3\sigma$ constraints for $\mathrm{U(1)_{B-L}}$ model with a star representing the reference point, $m_{\mathrm{DM}} = 2\,\mathrm{TeV}$ and $\tau = 1.5 \times 10^{26}$ sec, which accounts for both PAMELA and Fermi excess.

can account for both the PAMELA and Fermi excess while satisfying the antiproton flux constraint, is now marginally excluded by the Fermi isotropic diffuse gamma-ray data.

### 2.2.4 Conclusions

In this section we have derived constraints on the partial decay rates of DM into $WW$, $ZZ$, $hh$ and $q\bar{q}$ as well as $e^+e^-$, $\mu^+\mu^-$ and $\tau^+\tau^-$ using the gamma-ray data observed by the Fermi LAT and HESS. One of the merits of using gamma-ray is that the predicted flux does not depend on the diffusion model in the Galaxy, in contrast to charged cosmic-rays. The constraints derived in this section provide implications for DM model-building attempting to account for the PAMELA/Fermi excess. According to our results, the allowed hadronic branching ratio is of $\mathcal{O}(10)$ %. We have applied

the result to a DM model based on the hidden gauge boson decaying through a mixing with the $U(1)_{B-L}$, and found that the model is now marginally excluded by the Fermi gamma-ray observation. The allowed hadronic branching ratio is about 30% at the reference point shown as a star in Fig. 2.4.

Gamma-ray observations have the power to constrain the properties of DM. Thanks especially to the Fermi LAT data, which provides greater accuracy and statistics over the experiments in the past, the gamma-ray constraint has become as tight as or even tighter than current neutrino and antiproton constraints. However, neutrino constraints may surpass gamma-ray constraints in the future.

## 2.3 Future Neutrino Constraints on Dark Matter Decay and Annihilation

For either decays or annihilations, neutrino observations may provide the strongest constraints — or the most promising corroborating signatures — for dark matter to be the source of the anomalies. With the exception of the disfavored $e^+e^-$ channel, the required leptonic final states decay into neutrinos. These travel undeflected from their sources, eliminating any uncertainties in modeling their propagation. Moreover, astrophysical sources that may explain the anomalies are not expected to produce a large flux of neutrinos. Pulsars, for example, would generate at most $\mathcal{O}(1)$ events/year at a full km-scale detector, and only at energies greater than 10 TeV [111].

There are, however, challenges to constraining dark matter models with neutrinos. As they are observed only by collecting Cherenkov light from induced particle showers or from secondary muons, angular resolution is poor compared to gamma-ray observatories. Also, there are significant backgrounds from atmospheric muon and neutrino fluxes. However, if these backgrounds can be controlled, the poor angular resolution need not be a barrier; indeed by integrating the flux over a large area of the sky, the resulting constraint is much less sensitive to the choice of dark matter profile [112, 113]. Moreover, by observing the galactic and extragalactic diffuse dark matter, rather than any that may have been captured by the Sun or the Earth, any

constraints will be independent of the dark matter-nucleon cross sections, which are related to final states in a model-specific way [114].

Recent analyses show the power of neutrino constraints, using various strategies to reduce the effect of atmospheric backgrounds. The Super-Kamiokande observatory resides in the northern hemisphere, facing away from the galactic center, minimizing atmospheric backgrounds. Measurements of upward-going muons place a limit on the flux of galactic $\nu_\mu$, providing a robust constraint that eliminates annihilations to $\tau^+\tau^-$ as a source of the $e^\pm$ anomalies [106, 76]. The IceCube observatory, on the other hand, resides at the South Pole where down-going atmospheric fluxes are coincident with the neutrinos from the galactic center. The overwhelming background of atmospheric muons can be suppressed by event selection to establish an isotropic diffuse flux limit [115, 116, 117], but this limit only starts at a high energy threshold $\mathcal{O}(10\text{ TeV})$, and yields a relatively weak constraint as we will show.

Currently under construction is DeepCore [118], an in-fill of the IceCube detector which will use the outer instrumented volume as a veto on downward-going muons to a level of one part in $10^6$ [119]. This will allow the galactic neutrino flux to be measured and compared against the atmospheric neutrino flux, providing a constraint on dark matter decays and annihilations. Recent work [120, 121] by some of the authors shows that IceCube+DeepCore will be able to significantly constrain the parameter space of decays to $\mu^+\mu^-$, and rule out decays to $\tau^+\tau^-$ and annihilation to $\mu^+\mu^-$ as possible sources of the anomalies in less than five years of running.

Recently, IceCube+DeepCore has demonstrated in simulations the ability to distinguish between track-like events, which are due to the charged-current interactions of $\nu_\mu$, and cascade events, which are induced by $\nu_{e,\tau}$ through charged-current interactions and by all neutrino flavors through neutral-current interactions [122, 123]. This is very useful for constraining dark matter neutrino fluxes because $\nu_\mu$ is the dominant flavor of atmospheric neutrinos above 40 GeV [124, 125]. The neutrino-nucleon cross sections are the same for all flavors, so signal would be considerably enhanced, while background would be reduced because $\nu_\mu$ only creates cascade events through the neutral-current interaction, which is lower in cross section than the charged-current interaction [126, 127, 112] (see Fig. 2.5). Moreover, cascade events are easy to distin-

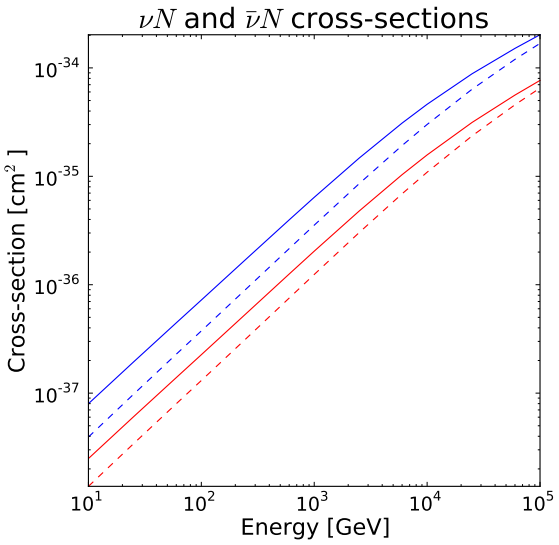


Figure 2.5: Cross sections for (anti)neutrino-nucleon interactions, given by Ref. [126]. The blue lines are for charged-current interactions, and the red lines are for neutral-current interactions. Solid lines are for neutrinos and dashed lines are for antineutrinos.

guish from the tracks caused by any atmospheric muons that are not vetoed by the outer volume.

In this section we show that observation of cascade events at IceCube+DeepCore can enhance the neutrino constraints on dark matter, and rule out (or corroborate) dark matter decays to $\mu^+\mu^-$ or $\tau^+\tau^-$ and annihilation to $\mu^+\mu^-$ as sources of the observed $e^\pm$ cosmic-ray anomalies in a much shorter time compared to searches that rely solely on track-like events.

### 2.3.1 Analysis

For brevity, in the expressions below we write only the terms for neutrinos and not the terms for antineutrinos. The terms are identical, except replacing "$\nu$" by "$\bar{\nu}$".

**Galactic flux signal and background**

The flux of neutrinos from the galactic dark matter halo is given by

$$\frac{d\Phi_{\nu_i}}{dEd\Omega} = \frac{1}{4\pi}(r_\odot \rho_\odot)\frac{1}{m\tau}\frac{dN_{\nu_i}}{dE}J_1(\Delta\Omega) \tag{2.16}$$

for decays and by

$$\frac{d\Phi_{\nu_i}}{dEd\Omega} = \frac{1}{8\pi}(r_\odot \rho_\odot^2)\frac{1}{m^2}\left\langle\sigma v\right\rangle\frac{dN_{\nu_i}}{dE}J_2(\Delta\Omega) \tag{2.17}$$

for annihilations, where $r_\odot = 8.5$ kpc is the distance from the Sun to the galactic center [94], $\rho_\odot = 0.3\ \mathrm{GeV\,cm^{-3}}$ is the dark matter density in the solar neighborhood, $m$ is the dark matter mass, and $\tau$ and $\langle\sigma v\rangle$ are the dark matter lifetime and thermally averaged cross section respectively. $J_n$ is the line-of-sight (los) integral through the halo profile:

$$J_n(\Delta\Omega) = \frac{1}{\Delta\Omega}\int_{\Delta\Omega} d\Omega \int_{\text{l.o.s.}} \frac{ds}{r_\odot}\left(\frac{\rho}{\rho_\odot}\right)^n \tag{2.18}$$

where $\Delta\Omega$ is the region of sky observed. In this analysis we use the Navarro-Frenk-White (NFW) halo profile [52]

$$\rho(r) = \rho_\odot\left(\frac{r_\odot}{r}\right)\left(\frac{1+r_\odot/r_s}{1+r/r_s}\right)^2 \tag{2.19}$$

with $r_s = 20$ kpc.

The neutrino source spectra $dN_{\nu_i}/dE$ for flavors $i$ are given by `PYTHIA` [92] simulation. Assuming $\sin^2 2\theta_{12} : \sin^2 2\theta_{13} : \sin^2 2\theta_{23} \approx 1 : 1 : 0$, the flavor distribution will be $1 : 1 : 1$ as the neutrinos reach the Earth, having traveled a variety of long distances across the galaxy and being well mixed through vacuum oscillations.

As discussed in the Introduction, the only background to cascade events is atmospheric neutrinos after the veto suppresses the background of atmospheric muons to one part in $10^6$ and event selection is used to eliminate the rest. The $\nu_\mu$ and $\nu_e$ fluxes are given by Ref. [124], where the $\nu_\mu$ flux agrees well with AMANDA observation [130]. At low zenith angles, the flux of background $\nu_\mu$ is $\sim 20$ times greater than the flux of $\nu_e$ from 40 GeV to 100 TeV; it is $\sim 1000$ times greater than the flux of $\nu_\tau$ (see Ref. [125]). However, below 40 GeV, especially at high zenith angles, the atmospheric fluxes of the three flavors only differ by $\mathcal{O}(1)$ due to flavor mixing. Since

modeling the background (and signal) below 40 GeV would require simulating flavor mixing as the neutrinos propagate through the limb of the Earth, for this analysis we simply set an energy cutoff of $E_{\rm thresh} = 40$ GeV.

To obtain the event rates due to the galactic and background fluxes, we first set energy bins for dark matter of mass $m$ to be $[\max(E_{\rm thresh}, m/10), m/2]$ for decays and $[\max(E_{\rm thresh}, m/5), m]$ for annihilations. Note that the bin width is much greater than the energy resolution, $\log_{10}(E_{\rm max}/E_{\rm min}) \simeq 0.4$ for track-like events and $\log_{10}(E_{\rm max}/E_{\rm min}) \simeq 0.18$ for cascade events [119]. We then integrate the flux times the effective area over the energy for each bin.

For track-like events due to $\nu_\mu$, the event rate is

$$\Gamma_{\rm tr.} = \int d\Omega \int_{E_{\rm min}}^{E_{\rm max}} dE\ \rho_{\rm ice} N_A V_{\rm tr.} \left( [\sigma_{\nu N}(E)]_{\rm CC} \frac{d\Phi_{\nu_\mu}}{dE d\Omega} \right) \tag{2.20}$$

where $\rho_{\rm ice} = 0.9\ {\rm g\,cm^{-3}}$ is the density of ice, $N_A = 6.022 \times 10^{23}\ {\rm g^{-1}}$ is Avogadro's number (to convert mass to number of nucleons), $[\sigma_{\nu N}(E)]_{\rm CC}$ is the neutrino-nucleon cross section for the charged-current interaction, and $V_{\rm tr.} \approx 0.04\ {\rm km^3}$ is the effective volume of the detector for track-like events [119]. Note that we do not add the residual atmospheric muon background to the background of track-like events due to the uncertainty in its value.

For cascade events we use the instrumented volume $V_{\rm casc} \approx 0.02\ {\rm km^3}$ [119, 129], the charged-current interaction for $\nu_{e,\tau}$, and the neutral-current interaction for all flavors to obtain

$$\Gamma_{\rm casc.} = \int d\Omega \int_{E_{\rm min}}^{E_{\rm max}} dE\ \rho_{\rm ice} N_A V_{\rm casc.} \left( [\sigma_{\nu N}(E)]_{\rm CC} \frac{d\Phi_{\nu_{e,\tau}}}{dE d\Omega} + [\sigma_{\nu N}(E)]_{\rm NC} \frac{d\Phi_{\nu_{e,\mu,\tau}}}{dE d\Omega} \right) . \tag{2.21}$$

Unlike track-like events, cascade events are well contained, so the effective volume for their detection will vary little with energy. Also, we assume that in neutral-current interactions all the energy of the neutrino goes into the cascade. Taking partial energy transfer into account would yield a modest improvement in significance, since most of the signal is from $\nu_{e,\tau}$ charged-current interactions but most of the background is from $\nu_\mu$ neutral-current interactions.[5]

[5]Inelasticity curves are given in Ref. [128], but only for energies 10 TeV and higher.

Finally, because the pointing capability for cascades is approximately 50° [119, 122] and the pointing capability for track-like events has yet to be established, we integrate over the $2\pi$ field of view around the galactic center. As mentioned before, this should provide a constraint which is robust to changes in dark matter halo profile. Specifically, the fractional change between the NFW profile used here and the much less steep isothermal profile for $J_1(2\pi)$ is $\mathcal{O}(10^{-3})$, and for $J_2(2\pi)$ is $\mathcal{O}(0.1)$.

**Extragalactic isotropic diffuse flux**

For comparison to the DeepCore constraints from down-going fluxes, we calculate the constraint from the isotropic diffuse flux limit for AMANDA-II from track-like events [116] and the projected limit for IceCube from cascade events [117].

The main contribution from dark matter decay to the isotropic diffuse flux is that from extragalactic dark matter residing on cosmological scales. The flux from the decay of cosmological dark matter is given by the previously derived formula [95, 77]

$$\left(\frac{d\Phi_{\nu_i}}{dEd\Omega}\right)^{(\mathrm{ex.})} = \frac{c}{4\pi}\frac{\Omega_{\mathrm{DM}}\rho_c}{H_0\Omega_{\mathrm{M}}^{1/2}}\frac{1}{m\tau}\int_1^\infty dy \frac{y^{-3/2}}{\sqrt{1+\Omega_\Lambda/\Omega_{\mathrm{M}}y^{-3}}}\left(\frac{dN_{\nu_i}}{d(Ey)}\right) \tag{2.22}$$

where $y \equiv 1+z$, with $z$ being the redshift, $H_0 = 71.9\ \mathrm{km\,s^{-1}\,Mpc^{-1}}$ is the Hubble constant, $\rho_c = 3H_0^2/(8\pi G_N)$ is the critical density, $\Omega_{\mathrm{M}} = 0.258$, $\Omega_{\mathrm{DM}} = 0.214$, and $\Omega_\Lambda = 0.721$ are, respectively, the total matter, dark matter, and dark energy densities divided by the critical density [24]. The isotropic diffuse flux from the annihilations of cosmological dark matter is too small to be relevant, since the density of dark matter on cosmological scales is very low, and the flux is suppressed by another power of $\rho_c/m$.

Because of the loss of signal due to event selection and the presence of background fluxes, both the AMANDA-II limit and the projected IceCube limit are only valid at energies greater than $\sim 20$ TeV. Below these thresholds we add the atmospheric background flux to these limits, and use these total fluxes to calculate the constraints on the dark matter lifetime.

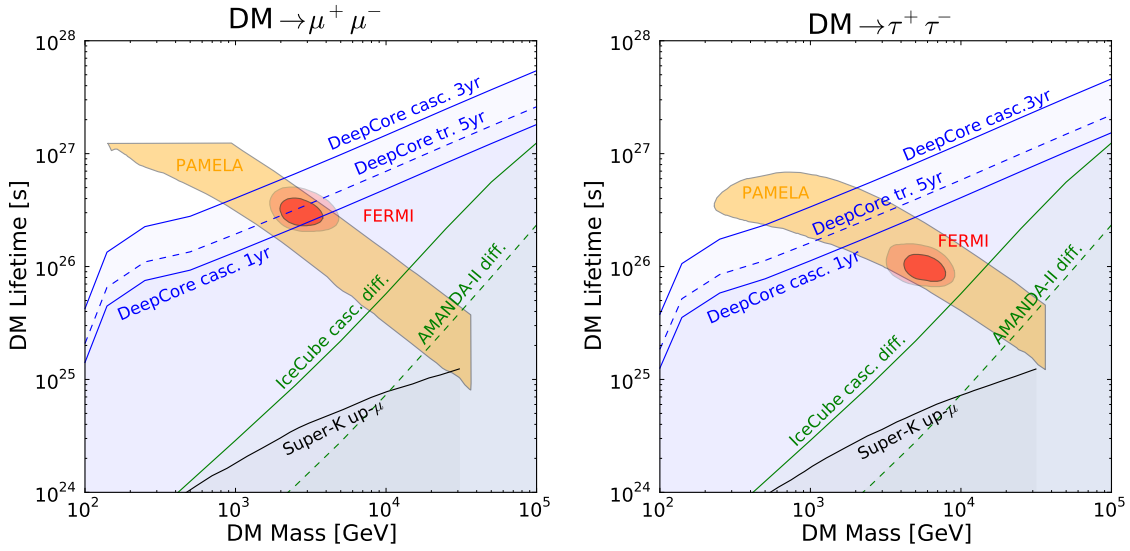


Figure 2.6: Constraints for decay to $\mu^+\mu^-$ (left) and $\tau^+\tau^-$ (right); the regions below the contours are excluded. The black contour ("Super-K up-$\mu$") is the Super-Kamiokande limit to $3\sigma$ from up-going muons, the orange band is the PAMELA-preferred region, and the red ellipses are the Fermi-preferred region; these three are given by Ref. [76]. The dashed green line ("AMANDA-II diff.") is the constraint to 90% confidence from the AMANDA-II limit on the isotropic diffuse flux of $\nu_\mu$, and the solid green line ("IceCube casc. diff.") is the constraint to 90% confidence from the projected IceCube limit on the isotropic diffuse flux using cascade events. The dashed blue line ("DeepCore tr. 5yr") is the constraint to $2\sigma$ from IceCube+DeepCore for $\nu_\mu$ track-like events after five years of running, and the solid blue lines are the constraints to $2\sigma$ for all-flavor cascade events after one year ("DeepCore casc. 1yr") and three years ("DeepCore casc. 3yr") of running.

### 2.3.2 Results

The results for dark matter decays are shown in Fig. 2.6; the regions below the contours are excluded. The black contour ("Super-K up-$\mu$") is the Super-Kamiokande limit to $3\sigma$ from up-going muons discussed in the Introduction. The orange band is the preferred region to fit the PAMELA $e^\pm$ anomaly, and the red ellipses are the preferred region to fit the Fermi $e^\pm$ anomaly. These three regions are given by Ref. [76] up to mass 30 TeV and lifetime $10^{27}$ s.

The dashed green line ("AMANDA-II diff.") is the constraint to 90% confidence

from the AMANDA-II limit on the isotropic diffuse flux of $\nu_\mu$, and the solid green line ("IceCube casc. diff.") is the constraint to 90% confidence from the projected IceCube limit on the isotropic diffuse flux using cascade events. Since the flux from cosmological dark matter is weak to begin with, contributing only 1% of the total flux over the $2\pi$ facing the galactic center, we see that it is quickly overwhelmed by the atmospheric flux below $\sim 40$ TeV. Nonetheless, due to the lower background of atmospheric $\nu_e$ compared to $\nu_\mu$ at these high energies, using cascade events improves the constraint by a factor of $\sim 5$.

The dashed blue line ("DeepCore tr. 5yr") is the constraint to $2\sigma$ from IceCube+DeepCore for track-like events after five years of running, and the solid blue lines are the constraints to $2\sigma$ for cascade events after one year ("DeepCore casc. 1yr") and three years ("DeepCore casc. 3yr") of running. We see that for the $\mu^+\mu^-$ final state, while track-like events can only reduce the available Fermi-preferred parameter space in five years, cascade events can rule it out altogether in only three years. Similarly for the $\tau^+\tau^-$ final state, track-like events can rule out the parameter space in less than five years, but with cascade events it will only take one year. Note the weakening of the constraints below $m = 250$ GeV, where the energy per final-state particle is less than 125 GeV. This is caused by the energy cutoff at 40 GeV.

The results for annihilation are shown in Fig. 2.7; the regions above the contours are excluded. The plots show the same constraints as for decay, except that no isotropic limits are shown because they are weaker than the Super-Kamiokande limit by a factor $\sim 10^5$ due to the low density of dark matter on cosmological scales. As with decays, cascade events greatly accelerate the development of a useful constraint. For the $\mu^+\mu^-$ final state the region by the Fermi data can be eliminated in only one year.

The exclusion plot for annihilations to $\tau^+\tau^-$ is shown only for completeness, as the Fermi-preferred region has already been eliminated by the Super-Kamiokande observation of upward-going muons. However, it may provide a useful generic constraint on all dark matter models irrespective of the $e^\pm$ anomalies.

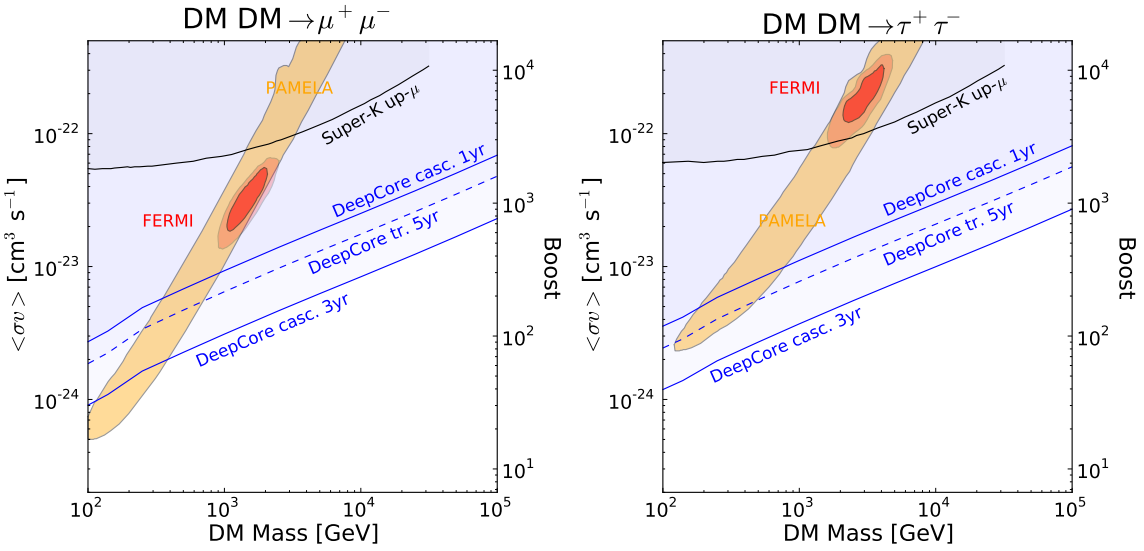


Figure 2.7: Constraints for annihilation to $\mu^+\mu^-$ (left) and $\tau^+\tau^-$ (right); the regions above the contours are excluded. The black contour ("Super-K up-$\mu$") is the Super-Kamiokande limit to $3\sigma$ from up-going muons, the orange band is the PAMELA-preferred region, and the red ellipses are the Fermi-preferred region; these three are given by Ref. [76]. The dashed blue line ("DeepCore tr. 5yr") is the constraint to $2\sigma$ from IceCube+DeepCore for $\nu_\mu$ track-like events after five years of running, and the solid blue lines are the constraints to $2\sigma$ for all-flavor cascade events after one year ("DeepCore casc. 1yr") and three years ("DeepCore casc. 3yr") of running.

### 2.3.3 Conclusions

We have shown that, by using cascade events, IceCube+DeepCore can more quickly establish constraints on dark matter models that would explain the reported $e^\pm$ anomalies, and over time establish stronger constraints than from track-like events. Specifically, track-like events will be able to significantly constrain the parameter space of decays to $\mu^+\mu^-$, and rule out decays to $\tau^+\tau^-$ and annihilations to $\mu^+\mu^-$ in less than five years of running. In comparison, cascade events can rule out decays to $\mu^+\mu^-$ in only three years, and rule out decays to $\tau^+\tau^-$ and annihilation to $\mu^+\mu^-$ after only one year. Moreover, these constraints are highly robust to the choice of dark matter halo profile and independent of dark matter-nucleon cross section.

In closing, we note two interesting possibilities for future work. First, if the

pointing accuracy for track-like events at IceCube+DeepCore is established to be less than 10°, the signal-to-noise for annihilations may be significantly enhanced by observing a smaller region around the galactic center, possibly out-performing cascade searches (albeit with greater dependence on the choice of dark matter halo profile). This would strengthen the discovery potential for dark matter because the galactic center could be identified as a localized source of excess neutrinos. Second, because the $\nu_\tau$ atmospheric background is so low at energies above 40 GeV and at low zenith angles, if IceCube+DeepCore can demonstrate efficient $\nu_\tau$ discrimination [123], signal to noise could be increased by a factor $\sim 100$. This would put leptophilic dark matter to a severe test.

# Chapter 3

# Quarks and Leptons as quasi-Nambu-Goldstone Fermions

## 3.1 Introduction

One of the fundamental problems in particle physics is to explain the hierarchy in the Yukawa couplings of the quarks and leptons. This is a long-standing problem, and in fact many models have been proposed to account for the smallness of the Yukawa couplings of the first and second generations relative to those of the third. In supersymmetric (SUSY) theories, there arises an intriguing possibility that the quarks and leptons are nothing but SUSY partners of Nambu-Goldstone (NG) bosons [131, 132], where the Yukawa couplings are forbidden by the celebrated low-energy theorem [21]. Thus, the small Yukawa couplings for the first and second generations are regarded as small breakings of postulated symmetries.

If that is indeed the case, then squarks and sleptons in the first and second generations are approximately massless at some cut-off scale $\Lambda$ of the theory and they acquire masses from radiative corrections. If the corrections are dominated by the standard model gauge interactions, then they each have nearly flavor-independent masses, solving the SUSY flavor-changing neutral current problem. This hypothesis predicts a remarkable spectrum for SUSY particles at the electroweak scale. The purpose of this chapter is to examine the low-energy implications of the Nambu-

Goldstone hypothesis.

It is very important to note here that if the Kähler manifold parameterized by the NG bosons is a compact manifold such as $\mathbf{CP^n}$, the symmetry is explicitly broken by a constant term $\mathcal{O}(m_{3/2})$ in the superpotential [133][1]. As a consequence of the explicit breaking, the NG bosons have masses of $\mathcal{O}(m_{3/2})$, and it will be not easy to test the NG hypothesis at the Large Hadron Collider (LHC). Thus, we consider in this chapter some non-compact complex manifold (non-linear sigma model) accommodating squarks and sleptons in the first and second generations as massless NG bosons, which will yield dramatic signatures at the LHC. (The results in this chapter do not depend on the explicit model for the non-compact complex manifold. We show it for the existence proof of a model.) We treat quark and lepton chiral multiplets in the third generation and Higgs chiral multiplets as just matter fields and hence their scalar bosons have soft SUSY-breaking masses of order of the gravitino mass, $m_{3/2}$, at the cut-off scale $\Lambda$ [2].

Finally, this class of models has a lightest supersymmetric particle (LSP) which is a promising dark matter candidate. Depending on the parameter region, the LSP may evade all current detection efforts or give interesting signals in direct detection and cosmic rays.

---

[1]It is very interesting that two light generations in an $SO(10)$ GUT are naturally accommodated in $E_7/SO(10)\times U(1)^2$. It has been shown that if one eliminates the $U(1)^2$ in the unbroken subgroup one can couple the non-linear sigma model to supergravity without any explicit breaking of the $E_7$ [134].

[2]The boundary condition of SUSY-breaking masses in the this chapter may be also realized in a brane world. That is, one assumes that quark and lepton multiplets in the first and second generation are confined on one brane separated from the other brane on which the third-generation quark and lepton, Higgs and hidden-sector multiplets ride. The gauge multiplets are in the bulk. This model may generate a partially realized Higgs-exempt [135] no-scale type supergravity model [136] where squarks and sleptons in the first and second generation have very small SUSY-breaking masses, while those in the third generation have masses of order the gravitino mass $m_{3/2}$.

## 3.2 An example of a non-compact manifold for the first and second generations

Let us first consider a non-compact complex manifold that accommodates one generation of left-handed quark and lepton multiplets. In particular, take a SUSY $U(6)/[U(4) \times SU(2)]$ non-linear sigma model which consists of $(4 \times 2 + 1)$ NG chiral multiplets, $\phi_i^a$ and $\varphi$, where $a = 1, \ldots, 4$ and $i = 1, 2$. The former superfield contains the left-handed quarks and leptons,

$$\phi_i^a = \begin{pmatrix} u_L^\xi & \nu_L \\ d_L^\xi & e_L^- \end{pmatrix} \sim (\mathbf{4}, \mathbf{2}) \tag{3.1}$$

where $\xi = 1, 2, 3$ is the color index. The latter is a non-standard-model field known as the "novino" [132]. All the bosons in $\phi_i^a$ and one real boson in $\varphi$ are NG-boson coordinates of the $U(6)/[U(4) \times SU(2)]$ manifold. The other extra real boson in the novino superfield, $\varphi$, is necessary to construct the SUSY $U(6)/[U(4) \times SU(2)]$ non-linear sigma model [35]. Then, we have a complex manifold which consists of all 18 bosons.

We arrange these into a matrix,

$$\Psi = \begin{pmatrix} e^{\kappa\varphi/v}\mathbf{1}_2 \\ \phi_i^a/v \end{pmatrix}, \tag{3.2}$$

which has 12 components $\Psi_i^\alpha$, $\alpha = 1, \ldots, 6$. The general form of the Kähler potential of the SUSY $U(6)/[U(4) \times SU(2)]$ non-linear sigma model is then given by [137]

$$K = v^2 F(\det[\Psi_\alpha^\dagger \Psi^\alpha]), \tag{3.3}$$

where the dimension-one constant $v$ is determined, together with the constant $\kappa$, by normalization conditions for the NG chiral multiplets as

$$v^2 \frac{\partial^2 F}{\partial \phi_a^{\dagger i} \partial \phi_j^b}\bigg|_{\phi_i^a = \varphi = 0} = \delta_b^a \delta_i^j \tag{3.4}$$

$$(\kappa v)^2 \frac{\partial^2 F}{\partial \varphi^\dagger \partial \varphi}\bigg|_{\phi_i^a = \varphi = 0} = 1. \tag{3.5}$$

The parameter $v$ corresponds to the energy scale of the $U(6)$ breaking. Here, notice that the function $F(x)$ is an arbitrary function satisfying (3.4) and (3.5). This freedom originates from the presence of one extra (non-NG) boson in the novino superfield, $\varphi$ [132, 138].

The above Kähler potential is invariant under the $U(6)_{\rm global} \times SU(2)_{\rm local}$ symmetry

$$\Psi \to g\Psi h^{-1}(x,\theta), \tag{3.6}$$

where $g$ is a parameter of the global $U(6)$ transformation and $h(x,\theta)$ is a chiral superfield parameter of the hidden local $SU(2)$ transformation. The form in (3.3) is maintained by using the local $SU(2)$ transformation. Thus, the global $U(6)$ symmetry is non-linearly realized by the NG chiral multiplets, $\phi_i^a$ and $\varphi$.

Let us now couple the above model to supergravity. The Lagrangian is given by

$$\mathcal{L} = 3\int d^2\theta d^2\bar{\theta}\mathcal{E}\exp\Big(\frac{1}{3}K(\phi_i^a,\varphi,\phi_a^{\dagger i},\varphi^\dagger)\Big). \tag{3.7}$$

Here, $\mathcal{E}$ is the supervierbein determinant. It should be stressed here that the supergravity Lagrangian is completely invariant under the global $U(6)$ symmetry.

It is straightforward to introduce the hidden sector responsible for the SUSY breaking. For simplicity, we introduce a single singlet field, $Z$, for this purpose. Then, the total Kähler potential is

$$K = K(\phi_i^a,\varphi,\phi_a^{\dagger i},\varphi^\dagger) + Z^\dagger Z + .... \tag{3.8}$$

The introduction of this SUSY-breaking sector preserves the global $U(6)$ symmetry and, therefore, leaves our NG bosons massless. However, there is a real scalar in $\varphi$ that is not a NG boson, and it acquires a soft mass of $\mathcal{O}(m_{3/2})$. This fact is shown by an explicit calculation [139].

So far, only the left-handed quarks and leptons have been introduced in our non-linear sigma model. It is straightforward to accommodate the right-handed quarks and leptons in another $U(6)/[U(4)\times SU(2)]$ manifold. The NG chiral multiplets are

$$\widetilde{\Psi} = \begin{pmatrix} e^{\kappa\widetilde{\varphi}/v}\mathbf{1}_2 \\ \widetilde{\phi}_a^i/v \end{pmatrix}, \tag{3.9}$$

where the $\widetilde{\phi}_a^i$ are the chiral multiplets for the right-handed quarks and leptons and the $\widetilde{\varphi}$ is another novino. The total manifold is now $(U(6)/[U(4)\times SU(2)])^2$. The SM gauge group is a subgroup of the unbroken $(U(4)\times SU(2))^2$. If one gauges the $SU(2)\times SU(2)$ and a diagonal $SU(4)$ subgroup of the $U(4)\times U(4)$ in the unbroken symmetry, one obtains the Pati-Salam gauge model with one generation.

It is now clear how to extend the model to accommodate the second generation of quarks and leptons. That is, we consider a manifold $(U(10)/[U(8)\times SU(2)])^2$, such that the left and right multiplets are

$$(\phi_i^a)_L = \begin{pmatrix} u_L^\xi & \nu_{eL} & c_L^\xi & \nu_{\mu L} \\ d_L^\xi & e_L^- & s_L^\xi & \mu_L^- \end{pmatrix} \sim (\mathbf{8},\mathbf{2}) \tag{3.10}$$

$$(\phi_i^a)_R = \begin{pmatrix} u_R^\xi & \nu_{eR} & c_R^\xi & \nu_{\mu R} \\ d_R^\xi & e_R^- & s_R^\xi & \mu_R^- \end{pmatrix} \sim (\mathbf{8},\mathbf{2})\ . \tag{3.11}$$

Gauging suitable subgroups properly we obtain the supersymmetric standard model (SSM) with three generations, where the first two generations are Nambu-Goldstone bosons in the coset space and the third generation is fundamental. After SUSY breaking, according to the low-energy theorem we have massless squarks and sleptons in the first two generations. On the other hand, the Higgs and the squarks and sleptons in the third generation may have soft-SUSY breaking masses of $\mathcal{O}(m_{3/2})$, since they are just matter fields.

The masslessness of squarks and sleptons in the first and second generations is guaranteed when the global $U(10)\times U(10)$ symmetry is exact. However, once we introduce the SSM gauge interactions and necessary Yukawa interactions, the global symmetry is explicitly broken and the squarks and sleptons are no longer true NG bosons. Therefore, the radiative corrections from the gauge and Yukawa interactions induce masses for the squarks and sleptons. The induced masses are logarithmically divergent and hence we need counter terms in the Kähler potential. In principle, we cannot determine the counter terms, but we expect those terms to vanish at some cut-off scale $\Lambda$ where the present non-linear sigma model is realized. In this chapter, we simply assume the GUT scale $\simeq 2\times 10^{16}$ GeV to be the cut-off scale. In other words, we choose a boundary condition such that squarks and sleptons in the first and second

generations are massless at the GUT scale. We easily see that squarks and sleptons in the first two generations have almost flavor-independent masses, since the SM gauge interactions are flavor blind and the Yukawa couplings are negligible compared with the gauge interactions. Thus, we do not have the serious flavor-changing neutral current problem.

However, this model does likely suffer from a gravitino problem [140] since $m_{3/2}$ is of $\mathcal{O}(1$ TeV). The problem of late-decaying, non-LSP gravitinos can be solved through a dilution process with a sufficiently low reheating temperature [141], but such a discussion is beyond the scope of this study. Similarly, although the novino may have interesting phenomenology because its mass is of $\mathcal{O}(m_{3/2})$, making numerical predictions would require an explicit model which we do not provide here.

The results that follow do not rely on any particular model. We assume that non-MSSM fields, including those of the GUT and the novino, are efficiently decoupled. Our results then follow from a set of SUSY-breaking parameters specified at the cut-off scale which are generic to the NG hypothesis on non-compact manifolds.

## 3.3 Low-energy spectrum for SUSY particles

Consistent with the NG hypothesis on non-compact manifolds, we consider the subspace of mSUGRA [142] models with the SUSY-breaking parameters

$$m_{1/2} = 300 \text{ GeV}, \quad \tan\beta = 10, \quad \mu > 0, \quad \mathrm{A}_0 = 0 \tag{3.12}$$

while setting $m_0 = 0$ for the first and second generation of scalars and $m_0 = 1$ TeV for the third generation scalars. Using the `SOFTSUSY` SUSY spectrum calculator (version 3.0.7) [143] and the `DarkSUSY` suite (version 5.0.5) [144, 145, 146, 147] we scan the $(M_{H_u}, M_{H_d})$ parameter space where $M_{H_u} \sim M_{H_d} \sim \mathcal{O}(m_{3/2})$ to find the region which gives the correct dark matter relic density while also evading other phenomenological constraints. We set the top mass to $m_t = 175$ GeV and let `SOFTSUSY` solve for the GUT scale, which is always $\simeq 2 \times 10^{16}$ GeV. Results for the most relevant bounds are shown in Figure 3.1. The colored regions are as follows:

- **red:** $3\sigma$-allowed dark matter relic density given by the seven-year WMAP data [25].
- **gray:** Charged LSP.
- **magenta:** Excluded by `DarkSUSY` limits on $b \to s\gamma$.
- **yellow:** Excluded by `DarkSUSY` Higgs mass bounds.
- **blue:** Excluded by 90% limit on spin-independent WIMP-nucleon cross sections in direct detection experiments [148]. For any given bin the more stringent limit among the proton or neutron cross sections is chosen.
- **green:** Same as the blue region, but for spin-dependent limits.

The allowed parameter space in Figure 3.1 shows some interesting properties. First, significantly different combinations of $(M_{H_u}, M_{H_d})$ can give the correct relic density. The upper and lower branches with a large difference between the two soft masses compose a "bulk region" where coannihilation with $\tilde{e}$, $\tilde{\mu}$ or $\tilde{\nu}_{e,\mu}$ yields the required abundance. The "bridge" at $M_{H_u} \approx M_{H_d} \approx 1100$ GeV is a small-$\mu$ region where annihilation though $\tilde{h}$ contributes to the correct abundance for a relatively light neutralino [149]. Due to the large higgsino component in $\tilde{\chi}_1^0$, this bridge branch is near the region excluded by direct detection experiments (see, for example, Ref. [150]). For the upper, lower and bridge branches we have chosen benchmark points for further study, marked by black stars. (These benchmark points give dark matter relic densities within $1\sigma$ of the WMAP7 value.)

Second, the regions giving the correct relic density are far from those excluded by bounds from $b \to s\gamma$ and Higgs mass. The former is not surprising since we have chosen small $\tan\beta$, $\mu > 0$ and a gaugino soft mass that is not too light, but heavy $\tilde{t}$ and $\tilde{b}$ also suppress the relevant diagrams. If $\tilde{t}$ and $\tilde{b}$ were nearly as light as the squarks of the first and second generation, the $b \to s\gamma$ limit would be exceeded for nearly all of the $(M_{H_u}, M_{H_d})$ plane. Similarly, the Higgs mass bound is also avoided rather easily because $\tilde{t}$ is heavy, enhancing the contribution of the $y_t$ term in the MSSM running of the $h_0$ mass, although the relationship to $(M_{H_u}, M_{H_d})$ is more intricate.

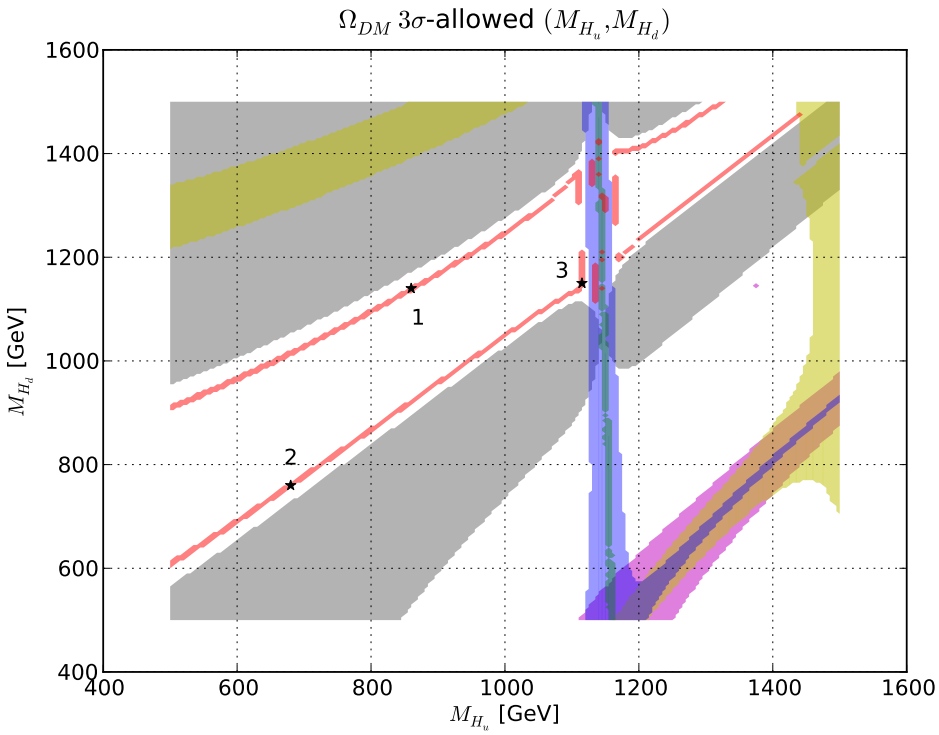


Figure 3.1: Scan in $(M_{H_u}, M_{H_d})$ for the mSUGRA subspace $m_{1/2} = 300$ GeV, $\tan\beta = 10$, $\mu > 0$ and $A_0 = 0$, with $m_0 = 0$ for the first and second generation scalars and $m_0 = 1$ TeV for the third generation scalars. The regions shown are: $3\sigma$-allowed dark matter relic density given by the seven-year WMAP data (red), charged LSP (gray), excluded by `DarkSUSY` limits on $b \to s\gamma$ (magenta), excluded by `DarkSUSY` Higgs mass bounds (yellow), excluded by 90% limit on spin-independent WIMP-nucleon cross sections in direct detection experiments (blue), excluded by 90% limit on spin-dependent WIMP-nucleon cross sections in direct detection experiments (green). Benchmark points chosen for further study are denoted by the black stars (see text for details).

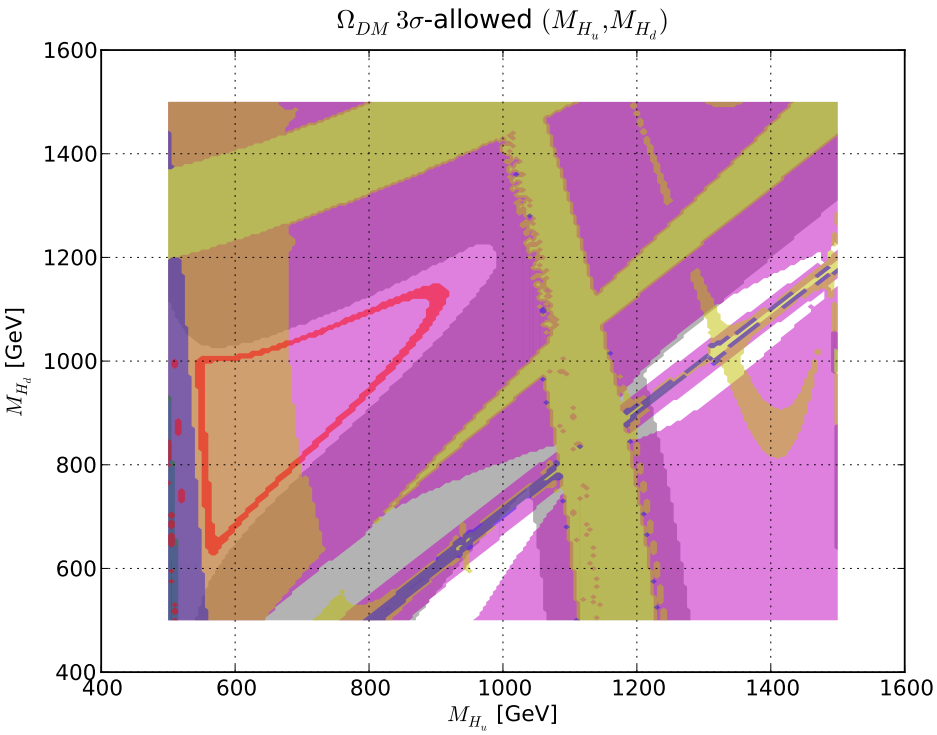


Figure 3.2: Same as Figure 3.1, except with $m_0 = 0$ for the third generation scalars as well.

For comparison, see Figure 3.2, which has the same parameters as Figure 3.1 except that $m_0 = 0$ for the third generation scalars as well.

Finally, we note that at small $m_0$ a gaugino soft mass $m_{1/2} \simeq 300$ has some phenomenological support, as it gives $\tilde{\chi}^0_{1,2}$ and $\tilde{\chi}^{\pm}_{1,2}$ masses favored by muon $g-2$ [151]. Also, although a small $m_0$ usually gives dangerously small $\tilde{\tau}$ masses [151], this is not the case if it is only for the first and second generations. This accounts for the difference between the gray regions of Figures 3.1 and 3.2.

Altogether, these properties show that for the choices $\tan\beta = 10$, $\mu > 0$ and $A_0 = 0$, the NG hypothesis meets the relevant SUSY phenomenological requirements rather generically: several different regions of $(M_{H_u}, M_{H_d})$ at the correct mass scale can give the required relic density, and only a small portion of these regions is subject to other phenomenological constraints. We now consider how this scenario can be

| Benchmark point | $M_{H_u}$ | $M_{H_d}$ |
|---|---|---|
| BP 1 | 860 | 1140 |
| BP 2 | 680 | 760 |
| BP 3 | 1115 | 1150 |

Table 3.1: Higgs soft masses for benchmark points, in GeV.

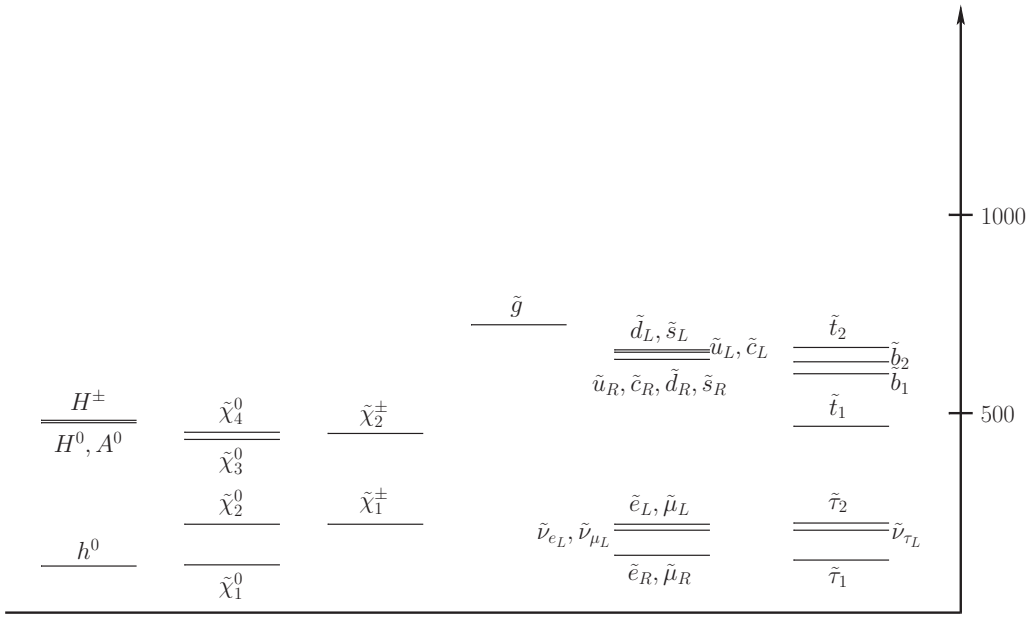


Figure 3.3: Spectrum for comparison point (CP), in GeV.

distinguished from conventional mSUGRA by examining the spectra of the benchmark points, whose $(M_{H_u}, M_{H_d})$ are shown in Table 3.1.

First, we choose a conventional mSUGRA point with similar soft masses for comparison:

$$m_0 = 75 \text{ GeV},\ \mathrm{m}_{1/2} = 300 \text{ GeV},\ \tan\beta = 10,\ \mu > 0,\ \mathrm{A}_0 = -200 \text{ GeV} . \qquad (3.13)$$

This point, denoted CP, gives roughly the correct $\tilde{\chi}_1^0$ relic density through $\tilde{\tau}$ coannihilation and exhibits a small $\tilde{l}_R$-$\tilde{\chi}_1^0$ mass splitting. The choice of $A_0 = -200$ GeV is to avoid Higgs mass bounds. The resulting spectrum is shown in Figure 3.3.

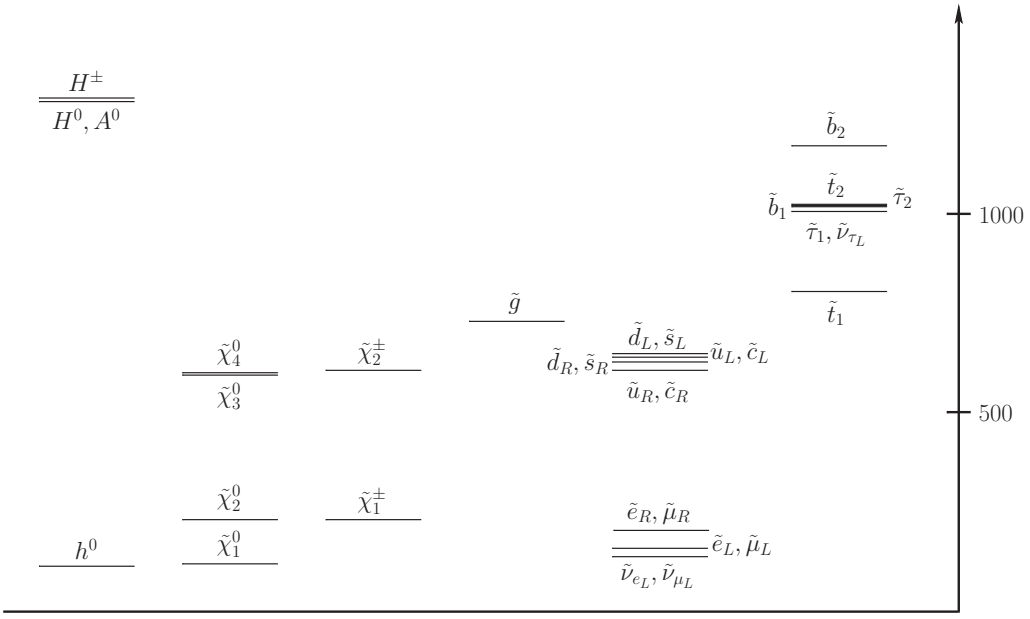


Figure 3.4: Spectrum for benchmark point 1 (BP 1), in GeV.

Let us consider benchmark point 1 (BP 1) shown in Figure 3.4. As expected, compared to CP, the third generation scalars are very heavy, as are the heavy Higgs bosons due to the large values of $M_{H_u}$ and $M_{H_d}$. Also, like CP, there is a small splitting between the lightest slepton and $\tilde{\chi}_1^0$. However, the expected hierarchy of sleptons is "inverted," i.e. $\tilde{\nu}_{e,\mu}$ and $\tilde{e}_L$ are lighter than $\tilde{l}_R$. This is due to the $S$ term in the running of the scalar masses (see, for example, Ref. [32]),

$$16\pi^2 \frac{d}{dt} m_{\phi_i}^2 = -\sum_a 8C_a(i) g_a^2 \left|M_a\right|^2 + \frac{6}{5} Y_i g_1^2 S \tag{3.14}$$

where

$$S \equiv \mathrm{Tr}\left[Y_j m_{\phi_j}^2\right] = M_{H_u}^2 - M_{H_d}^2 + \mathrm{Tr}\left[\mathbf{m_Q^2} - \mathbf{m_L^2} - 2\mathbf{m_{\bar{u}}^2} + \mathbf{m_{\bar{d}}^2} + \mathbf{m_{\bar{e}}^2}\right] . \tag{3.15}$$

In (3.15), the rightmost trace is zero for our case since $m_0$ is universal across all the scalars in a given generation, so $S = (M_{H_u}^2 - M_{H_d}^2)$. Since $\tilde{l}_R$ has hypercharge of $Y = -1$, but $\tilde{l}_L$ and $\tilde{\nu}_{e,\mu}$ have hypercharge of $Y = -1/2$, $\tilde{l}_R$ is driven heavier. For the same reason, the spectrum of the left and right squarks of the first and second

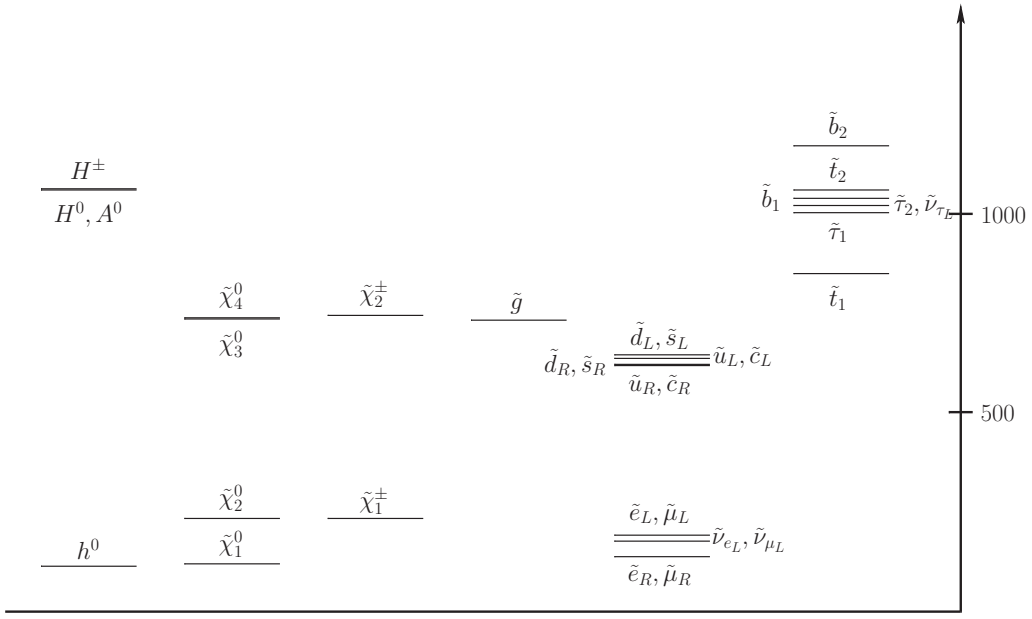


Figure 3.5: Spectrum for benchmark point 2 (BP 2), in GeV.

generations is brought closer together than in CP. Unfortunately, the size of this effect is difficult to estimate analytically since $M_{H_u}$ and $M_{H_d}$ are themselves subject to significant running due to $S$.

Benchmark point 2 (BP 2) in Figure 3.5 is similar to BP 1, except that $(M_{H_u}^2 - M_{H_d}^2)$ is smaller, so the slepton hierarchy is narrowed but remains non-inverted. Benchmark point 3 (BP 3) in Figure 3.6 is also similar, with $(M_{H_u}^2 - M_{H_d}^2)$ being even smaller. Except, in addition to a non-inverted and narrowed slepton hierarchy, because it is in the bridge branch it exhibits typical small-$\mu$ neutralino and chargino hierarchies. In fact, $\tilde{\chi}_2^0$ and $\tilde{\chi}_1^\pm$ are lighter than $\tilde{\nu}_{e,\mu}$, closing off that decay channel.

In the next section, we discuss how these points can be identified at a collider, and use simulated events to demonstrate that this can be done early in 14 TeV running at the LHC.

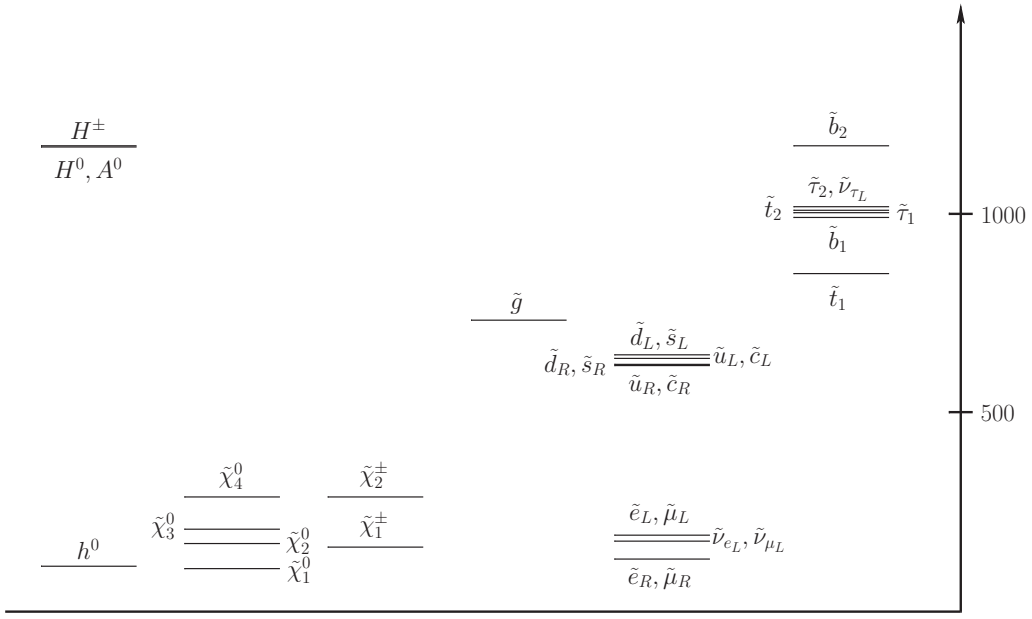


Figure 3.6: Spectrum for benchmark point 3 (BP 3), in GeV.

## 3.4 LHC physics

### 3.4.1 Discrimination at the LHC

We now consider the distinguishing characteristics of NG hypothesis model points and their prospects for detection at the LHC.

Under the NG hypothesis, the third generation scalars are significantly heavier than both the $\tilde{g}$ and the first and second generation squarks, which will result in very few $b$- and $\tau$-jets. Nearly all the squarks produced at the LHC will be of the first and second generation, both from $\tilde{g}$ decay and direct production. By contrast, at CP many $b$- and $\tau$-jets would be produced because all three generations are of comparable mass.

Turning to leptons, because $\tilde{\chi}_2^0 \to \tilde{\tau}\tau$ is closed, there will be many more events with the number of leptons $n_l \geq 2$ than for conventional mSUGRA points. In the bridge branch, $\tilde{\chi}_2^0 \to \tilde{\nu}_{e,\mu}\nu_{e,\mu}$ is closed as well, and $\tilde{q} \to q\tilde{\chi}_4^0$ and $\tilde{q}_L \to q_L\tilde{\chi}_2^{\pm}$ are open due to gaugino mixing caused by small $\mu$; however, most importantly, the right

squarks have a large branching ratio to $\tilde{\chi}_2^0$ due to bino mixing. Thus for BP 3 the number of $n_l \geq 2$ events is greatly enhanced, even over BP 1 and BP 2. Overall, NG hypothesis model points require less integrated luminosity than conventional points in order to reconstruct two-lepton decay chains.

In short, $b$-jet, $\tau$-jet and lepton multiplicities can broadly distinguish NG hypothesis model points from conventional model points.

For greater precision, the effects of the $S$-term on the slepton mass hierarchy should be visible at the LHC. At BP 1 and BP 2, the left squarks will decay mostly to $q_L\tilde{\chi}_2^0$ and $q_L\tilde{\chi}_1^\pm$ because these gauginos are mostly wino, and these in turn will decay mostly into left sleptons. The right squarks will decay mostly to $q_R\tilde{\chi}_1^0$ because $\tilde{\chi}_1^0$ is mostly bino, so no leptons will be produced. Thus, at these points we expect the leptons produced in the squark decay chains to be mostly left-handed. By comparison, at CP $\tilde{\chi}_2^0 \to \tilde{l}_R^\pm l^\mp$ and $\tilde{\chi}_1^\pm \to \tilde{\nu}_L l^\pm$ exclusively since $\tilde{l}_L$ is too heavy — most of these leptons will be right-handed.

This difference can be inferred by measuring the charge asymmetry of the $m_{jl}$ invariant mass distributions from the squark decay chains [152]. In squark decay, $\tilde{\chi}_2^0$ is back-to-back with the quark in the squark rest frame and carries the same polarization as the quark since the squark is scalar. Then, when $\tilde{\chi}_0^2$ decays, the lepton carries its polarization in the same direction. Thus, the chirality of this lepton is positively correlated with the chirality of the quark. Since the LHC is a $p$-$p$ collider, more $\tilde{q}$ is produced than $\tilde{q}^*$, so if the chiralities of the lepton and quark are the same then we expect a positive charge asymmetry. The lepton from the slepton decay is not correlated since the slepton is scalar. Then, for BP 1 and BP 2 there will be a large positive charge asymmetry since most of the $\tilde{\chi}_2^0$ are from $\tilde{q}_L$ rather than $\tilde{q}_R$, and $\tilde{\chi}_2^0$ decays predominantly to $\tilde{l}_L l_L$ .

The situation is more complicated at BP 3 because so many different squark decay channels are open. Moreover, because $\tilde{\chi}_2^0$ is so light, it can only decay to $\tilde{l}_R$. In order to determine the charge asymmetry, we first note that the gluino prefers decays to right squarks (branching ratio 59%) because they are lighter than the left squarks (40%). Then, we observe that the right squarks produce leptons mostly through $\tilde{\chi}_2^0$ (22%), whereas the left squarks produce leptons through $\tilde{\chi}_2^0$ (17% for up, 10% for

down), $\tilde{\chi}_4^0$ ($\sim 15\%$) and $\tilde{\chi}_{1,2}^{\pm}$ ($\sim 65\%$); $\tilde{\chi}_4^0$ decays to $l_L\tilde{l}_L$ only 21% of the time, and $\tilde{\chi}_{1,2}^{\pm}$ to $l_L^{\pm}\nu_L(\tilde{\chi}_1^0)$ only $\sim 35\%$ of the time. Multiplying the branching ratios, one finds that the charge asymmetry from right squarks is positive, but the charge asymmetry from left squarks is largely canceled between $\tilde{\chi}_2^0$ and $\tilde{\chi}_{1,2}^{\pm}$. Thus, overall charge asymmetry of BP 3 will be positive, though not as large as that of BP 1 and BP 2. Then, to clearly distinguish BP 3 from BP 1 and BP 2, its small-$\mu$ character can be seen by observing the tight neutralino mass hierarchy through the small $\tilde{\chi}_2^0$-$\tilde{\chi}_1^0$ mass splitting. being small.

Lastly, at all the benchmark points the heavy states in the Higgs sector will not be produced in sufficient quantities to be identified because their mass is too high. However, if $\tan\beta > 15$, a heavy Higgs of $\mathcal{O}(500$ GeV) may be observed at a CP-like model point [153].

### 3.4.2 Simulation and reconstruction

To demonstrate this phenomenology at the LHC, for each of the model points we generated $10^5$ signal events at 14 TeV for inclusive squark production using the `ISAJET` (version 7.72) spectrum calculator [154], `HERWIG` (version 6.5) shower generator [155] and `AcerDET` (version 1.0) [156] fast detector simulation. (MSSM input parameters were tuned slightly such that `ISAJET` would produce the same spectrum as `SOFTSUSY`.) The inclusive production cross section is $\gtrsim 15$ pb, so the integrated luminosity required for the following analysis is only 7 fb$^{-1}$; this should be achievable in roughly one month of running [157].

To grossly distinguish NG hypothesis model points from conventional points we first extract and compare:

- number of $b$-jets $n_b$ with $p_T > 50$ GeV
- number of $\tau$-jets $n_\tau$ with $p_T > 20$ GeV
- number of leptons $n_l$ with $p_T > 15$ GeV and $\eta < 2$ .

Here, the $b$- and $\tau$-jets are the jets labeled as such by `AcerDET`, with an efficiency of around 80%. However, real tagging efficiencies are probably around 60% and

| Model point | % $n_b \geq 1$ | % $n_\tau \geq 1$ | % $n_l \geq 2$ |
|---|---|---|---|
| BP 1 | 2.29 | 0.04 | 15.80 |
| BP 2 | 2.22 | 0.02 | 15.84 |
| BP 3 | 3.17 | 2.284 | 28.97 |
| CP | 31.70 | 16.94 | 4.10 |

Table 3.2: Percentage of events with the given multiplicities (see text for details).

50% for $b$- and $\tau$-jets, respectively [156]. The results are shown in Table 3.2, as a percentage of events. As expected, for the benchmark points there are a few $b$-jets and very few $\tau$-jets from direct production of third generation squarks. BP 3 shows an enhancement in $\tau$-jets from off-shell $\tilde{\chi}_1^\pm$ decays. By contrast, CP has many $b$-jets from both gluino and third generation squark decays, as well as many $\tau$-jets (and therefore fewer multi-leptons) from $\tilde{\chi}_2^0$ decays.

Turning to the other discriminators, in order to obtain the $\tilde{\chi}$-$\tilde{l}$ mass splittings and charge asymmetry, we must study the gluino and squark decay chains

$$(\tilde{g} \rightarrow)\ \tilde{q}j \rightarrow \tilde{\chi}_2^0 jj \rightarrow \tilde{l}^\pm jj l^\mp \rightarrow jj l^\pm l^\mp + \not{E}_T\ . \tag{3.16}$$

Henceforth, we define the lepton from $\tilde{\chi}_2^0$ decay as the "near" lepton, and the lepton from $\tilde{l}$ decay to be the "far" lepton. We use the method of invariant mass distributions and endpoints to reconstruct the masses [153, 158, 159]. This method can determine the $\tilde{l}$-$\tilde{\chi}_1^0$ and $\tilde{\chi}_2^0$-$\tilde{l}$ mass splitting rather precisely, which is useful here; extracting the squark mass scale is less critical because it is mostly determined by $m_0$. We use the `MINUIT2` fitter in `ROOT` [160] to find the endpoints, and the inversion formulas in Ref. [159] to find the mass differences and squark mass.

For each model point we identify events with $n_l \geq 2,\ n_j \geq 2$ where the two highest $p_T$ leptons are same-flavor/opposite-sign (SFOS). To subtract the chargino contribution to SFOS, we also identify $n_l = 2$ events with different-flavor/opposite-sign (DFOS) and subtract these counts from the SFOS invariant mass distributions before fitting. In a given event, we choose the jet among the two highest $p_T$ jets that gives the smallest $m_{jll}$. This identifies the jet from squark decay on the correct branch.

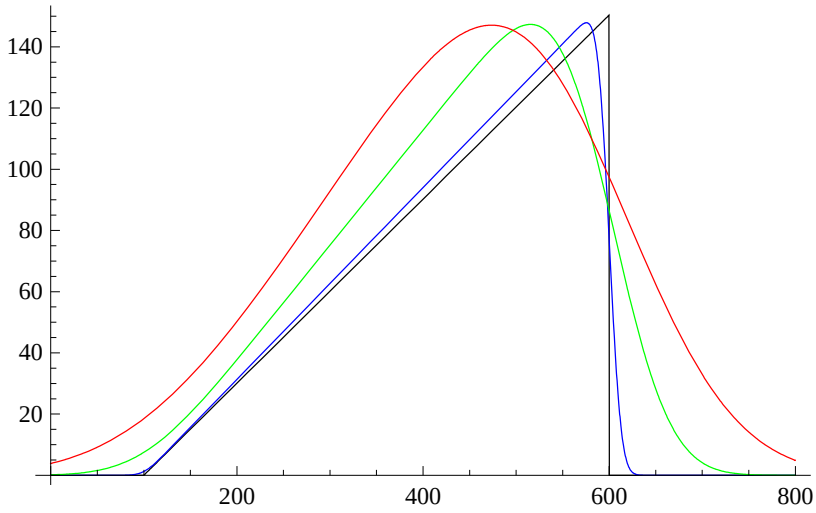


Figure 3.7: Example smeared ramp function with the vertical edge to the right and the sloping edge to the left. Left endpoint = 100, right endpoint = 600, with gaussian smearing widths = 0 (black), 10 (blue), 50 (green) and 100 (red).

Noting the example mass distribution shapes in Ref. [159], we use the vertical edge from a ramp function with gaussian smearing in order to fit the $m_{ll}^{max}$ endpoint, and the sloping edge of a ramp function with gaussian smearing in order to fit the $m_{jll}^{max}$ and $m_{jl(lo)}^{max}$ endpoints (for examples showing both kinds of edges, see Figure 3.7). We also choose a vertical edge for $m_{jl(hi)}^{max}$ instead of a sloping edge because the histogram bins containing this edge usually have few entries, and the resulting broadening obscures any slope. In our fits the smearing width is left as a free parameter to match the broadening of the endpoint due to a finite number of counts; this is most apparent in the $m_{jl(hi)}^{max}$ fits.

For BP 3, however, there are significant tails in the $m_{jl(hi)}$ and $m_{jll}$ distributions due to the decays of $\tilde{\chi}_4^0$ and $\tilde{\chi}_2^{\pm}$. In these fits the fitting function is a left-facing smeared ramp added to a sloping line in piecewise fashion. Moreover, in these functions we set the maximum smearing width to 5 GeV and over a limited mass range to avoid over-fitting to the curves of the edges which are resolvable due to the large statistics.

The $\tilde{\chi}_4^0$ and $\tilde{\chi}_2^{\pm}$ edges of BP 3 can be seen in the $m_{ll}$ mass distribution in Figure 3.8. At 93 GeV is the $\tilde{\chi}_2^{\pm} \rightarrow \tilde{\nu}_L l^{\pm} \rightarrow \tilde{\chi}_1^{\pm} ll$ endpoint, and at 107 GeV is the

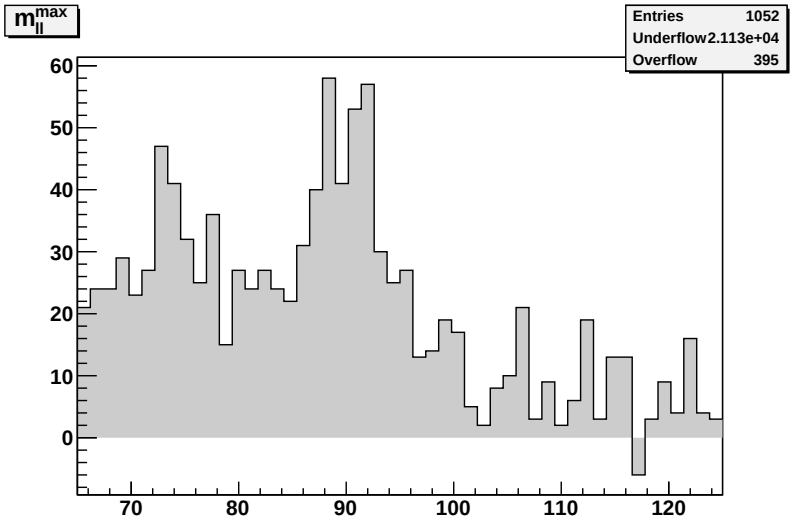


Figure 3.8: Higher range of $m_{ll}$ for BP 3. At 93 GeV is the $\tilde{\chi}_2^{\pm} \to \tilde{\nu}_L l^{\pm} \to \tilde{\chi}_1^{\pm} ll$ endpoint, and at 107 GeV is the $\tilde{\chi}_4^0 \to \tilde{l}_L l \to \tilde{\chi}_2^0 ll$ endpoint.

| Model point | $m_{\tilde{l}} - m_{\tilde{\chi}_1^0}$ | $m_{\tilde{\chi}_2^0} - m_{\tilde{l}}$ | $m_{\tilde{q}} - m_{\tilde{\chi}_2^0}$ | $m_{\tilde{q}}$ |
|---|---|---|---|---|
| BP 1 | $37.7 \pm 1.1$ (37.9) | $73.3 \pm 1.9$ (73.5) | $433 \pm 7$ (428) | $655 \pm 35$ (660) |
| BP 2 | $73.1 \pm 1.4$ (73.5) | $40.8 \pm 0.3$ (40.8) | $414 \pm 5$ (409) | $658 \pm 20$ (643) |
| BP 3 | $29.1 \pm 1.0$ (28.9) | $31.4 \pm 0.9$ (31.6) | $491 \pm 12$ (472) | $693 \pm 88$ (639) |
| CP | $27.7 \pm 3.3$ (25.7) | $76.0 \pm 4.5$ (77.5) | $497 \pm 51$ (444) | $848 \pm 237$ (666) |

Table 3.3: Reconstructed mass differences and squark masses, in GeV. True values are shown in parentheses.

$\tilde{\chi}_4^0 \to \tilde{l}_L l \to \tilde{\chi}_2^0 ll$ endpoint. All the other plots of the mass distributions and their fit endpoints, as well as all the inversion solutions, are shown in the Appendix starting on page 111. Here, we show the correct solutions in Table 3.3, where the values in the parentheses are the true values. The correct solution is chosen by first noting that none of the model points have off-shell decays in the squark decay chains, which would manifest in flat mass distributions. This eliminates Region 4 of $m_{jll}^{max}$, in the terminology of Ref. [159]. Next, among the Region 1 solutions we choose the one with the plausible squark mass that would give the observed production cross-section. If this is ambiguous, looking at the $m_{jl(hi)}$ mass distribution, if there is a secondary edge

| Model point | $A_{c,soft}$ | $A_{c,hard}$ |
|---|---|---|
| BP 1 | $-0.11 \pm 0.02$ | $0.25 \pm 0.02$ |
| BP 2 | $-0.04 \pm 0.02$ | $0.11 \pm 0.02$ |
| BP 3 | $-0.01 \pm 0.01$ | $0.04 \pm 0.01$ |
| CP | $0.04 \pm 0.04$ | $-0.14 \pm 0.06$ |

Table 3.4: Lepton charge asymmetries for each model point.

then the lepton at the fit edge is the far lepton, and so the $\tilde{l}$-$\tilde{\chi}_1^0$ splitting is larger; conversely, if there is no secondary edge, the fit lepton is the near lepton, and the $\tilde{\chi}_2^0$-$\tilde{l}$ splitting is the larger one.

Finally, to calculate the charge asymmetry, we create $m_{jl^\pm}$ distributions separately for both the near and far leptons, where $j$ is the same jet as from $m_{jll}$. This gives us four distributions $m_{jl^\pm(soft)}$ and $m_{jl^\pm(hard)}$ in increasing lepton $p_T$ (these are also shown in the Appendix). Then, we integrate each of the distributions,

$$N(l) = \int_a^b dm' \; m_{jl}(m') \tag{3.17}$$

where $(a, b) = (m_{jl(lo)}^{max} - 100 \text{ GeV}, m_{jl(lo)}^{max})$ for the soft distribution. For the hard distribution, $(a, b) = (m_{jl(near)} - 100 \text{ GeV}, m_{jl(near)})$ where $m_{near}$ is the edge of the $m_{jl(hi)}$ distribution for the near lepton. For our model points, $m_{jl(near)} \neq m_{jl(hi)}^{max}$ only for BP 2, which has a secondary edge at 350 GeV.

This gives us four quantities $N_{soft}(l^\pm)$ and $N_{hard}(l^\pm)$. Finally, we define the charge asymmetry as

$$A_c \equiv \frac{N(l^+) - N(l^-)}{N(l^+) + N(l^-)} \; . \tag{3.18}$$

The soft and hard lepton charge asymmetries, $A_{c,soft}$ and $A_{c,hard}$, are shown for each of the model points in Table 3.4. We see that $|A_{c,soft}| < |A_{c,hard}|$, since more of the soft leptons are from slepton decay.

### 3.4.3 Model point identification

Using the results from the reconstruction procedures above, we describe how to identify the different model points from the data. We will assume universal gaugino

soft masses at high scale, such that $M_3 : M_2 : M_1 \approx 6 : 2 : 1$ at low scale [32].

**BP 1**

The single edge of the $m_{jl(hi)}$ distribution suggests that this is from the near lepton. The large $\tilde{\chi}_2^0$-$\tilde{\chi}_1^0$ mass splitting and non-observation of higher $m_{ll}$ edges from $\tilde{\chi}_4^0$ and $\tilde{\chi}_2^\pm$ decays indicate that $\mu > M_2 - M_1$, so $\tilde{\chi}_2^0$ is gaugino-dominated and the decay chains are primarily from left squarks. Combined with the large positive charge asymmetry, this suggests that the slepton for this edge is $\tilde{l}_L$. Following the mSUGRA mass relations [32], the large $\tilde{\chi}_2^0$-$\tilde{l}_L$ splitting is inconsistent with mSUGRA assumptions; on the other hand, the $\tilde{l}_L$-$\tilde{\chi}_1^0$ splitting is small enough to give the right dark matter relic abundance. Then, we can infer that $\tilde{l}_R$ is heavier than $\tilde{l}_L$. Along with the lack of $b$- and $\tau$-jets, an upper branch point in the NG hypothesis is a plausible candidate.

**BP 2**

Again, the $\tilde{\chi}_2^0$-$\tilde{\chi}_1^0$ splitting is large and no higher $m_{ll}$ edges are observed, so we are not in a small-$\mu$ region and left squark decays produce the most leptons. The secondary edge at 350 GeV in the $m_{jl(hi)}$ distribution suggests that the fitted edge is for the far lepton. Combined with the large $\tilde{l}$-$\tilde{\chi}_1^0$ mass splitting and positive charge asymmetry, we infer that this edge is for the $\tilde{l}_L$ and that there is an unresolved $\tilde{l}_R$ close to $\tilde{\chi}_1^0$, giving the correct dark matter relic abundance. The smaller charge asymmetry than for BP 1 is consistent with the far lepton being more likely to be the hard lepton, contributing roughly 50% below 350 GeV in the $m_{jl(hi)}$ distribution. Thus, in this case, a lower branch point in the NG hypothesis is a plausible candidate.

**BP 3**

The additional edges in the $m_{ll}$ distribution are due to the higher neutralinos and the small $\tilde{\chi}_2^0$-$\tilde{\chi}_1^0$ mass splitting suggest a small-$\mu$ point. These edges can be reconstructed to obtain the masses of these heavy neutralinos [152]. Combining the inferred branching ratios, we can determine that right squark decays contribute more

strongly to the the positive charge asymmetry, suggesting that the reconstructed slepton is $\tilde{l}_R$; we can reconstruct $\tilde{l}_L$ and $\tilde{\nu}_L$ at some specific higher mass. A bridge branch point is consistent with all these features, as well as with the great number of multi-lepton events observed.

**CP**

Unlike the three scenarios above, here we observe a typical number of $b$- and $\tau$-jets along with few multi-lepton events. Since the $\tilde{\chi}_2^0$-$\tilde{\chi}_1^0$ splitting is large, this is not a small-$\mu$ point, so most of the multi-lepton events are from left squark decays. Combined with the negative charge asymmetry, we infer that the slepton for this edge is $\tilde{l}_R$. We also see that the lepton is near, so it is the $\tilde{\chi}_2^0$-$\tilde{l}_R$ splitting which is large. Then, $\tilde{l}_L$ has some mass greater than that of $\tilde{\chi}_2^0$, otherwise the charge asymmetry would be washed out or positive. This is likely a typical mSUGRA point.

In summary, the benchmark points of the NG hypothesis from different regions in the $(M_{H_u}, M_{H_d})$ plane can be readily identified in early 14 TeV running at the LHC, and are easily distinguished from typical mSUGRA points.

## 3.5 Conclusions and outlook

The hierarchy of the Yukawa couplings in the standard model remains an open question. We have presented a class of models wherein the first and second generation fermions are SUSY partners of Nambu-Goldstone bosons which parameterize a non-compact Kähler manifold, such that the first and second generation Yukawa couplings are forbidden by the low-energy theorem. Then we gave an (incomplete) example to show that such a model can be constructed.

Next, we found that many different model points in this scenario can give the correct dark matter abundance while easily evading phenomenological bounds, and examined the spectra of benchmark points in different regions of the allowed parameter space. Finally, we argued that these points can be distinguished from conventional mSUGRA points at the LHC, and demonstrated this assuming only 7 fb$^{-1}$ of inte-

grated luminosity at 14 TeV, with $m_{\tilde{g}} \sim 700$ GeV.

Nonetheless, improvements can be made. First, explicit models should be constructed, and the consequences of their gravitino and novino fields investigated. Also, the running of the soft masses between the SUSY-breaking and GUT scales should be verified to be small. Second, a more expansive simulation (including backgrounds) should be done with higher integrated luminosity to improve the quality of the endpoint fits and increase the significance of the charge asymmetries. Third, observability at LHC should be verified across the entire $(M_{H_u}, M_{H_d})$ plane, not only for specific benchmark points.

Finally, it must be noted that the dark matter candidate here evades all the bounds established in Chapter 2 for the total cosmic-ray $e^{\pm}$ flux. At model points BP 1 and BP 2, the LSP is mostly bino and thus the annihilation cross-section is $p$-wave suppressed, reducing it to $\mathcal{O}(10^{-30})$ cm$^3$ s$^{-1}$ in the present universe. However, at BP 3, the large higgsino component, in addition to enhancing the direct detection cross-section, also gives a large annihilation rate $\mathcal{O}(10^{-26})$ cm$^3$ s$^{-1}$ to $W^+W^-$. Combined with the low mass, the LSP of BP 3 may be able to explain the anomalous rise in the positron fraction (see Figures 1.5 and 2.7). However, the bound from antiprotons must be computed.

In conclusion, we have shown that the NG hypothesis is a promising scenario for explaining the standard model fermion mass hierarchy, as well as providing a dark matter candidate.

# Chapter 4

# Conclusion

While the standard model has been extremely successful in describing the fundamental particles and interactions, there remain a number of important, open questions. These include resolving the hierarchy problem in the renormalization of the Higgs, the hierarchy in the fermion Yukawa couplings, and understanding the nature of dark matter.

In Section 1.1, the standard model was reviewed. Then, in Section 1.2, the shortcomings of the standard model and possible solutions were described. Supersymmetry was one of the solutions argued to have the potential for solving the problems described above. In Section 1.3, supersymmetry was developed from first principles, connected with gravity, then applied to the standard model. Finally, supersymmetric coset spaces were reviewed in order to motivate the work in Chapter 3. In Section 1.4, a broad overview was given on the evidence for dark matter, major candidates for dark matter, and certain aspects of WIMP dark matter detection.

In Chapter 2, novel constraints on the the WIMP dark matter interpretation of the recent cosmic-ray $e^{\pm}$ anomalies were developed using gamma-rays and neutrinos. Then, in Chapter 3, we presented a class of supersymmetric models which can make the first and second generations of the (s)quarks and (s)leptons light, while also providing a dark matter candidate. It is shown by simulation that this class of models can be easily detected at the Large Hadron Collider when it begins to run at 14 TeV. It is also noted that the dark matter candidate here likely evades all

the bounds established in Chapter 2 for the total cosmic-ray $e^{\pm}$ flux, but still may be useful for explaining the anomalous rise in the cosmic-ray positron fraction. However, most importantly, a supersymmetric coset theory provides a dynamical motivation for the masses, generations and representations of the quarks and leptons in the standard model. Future work will involve making an explicit model for quasi-Nambu-Goldstone fermion quarks and leptons, then understanding the astrophysical implications in dark matter and Big Bang nucleosynthesis.

In conclusion, this stands as an important time in particle physics. As the LHC starts up and astrophysical observatories grow more powerful, the critical TeV frontier is beginning to open. We will learn not just about the Higgs, but the TeV particle spectrum and what questions it may answer or create. It is the hope of the author that an elegant dynamical picture will be revealed which resolves the problems addressed in this thesis. As we go higher in energy, peer deeper into the cosmos, and grow more precise in our observations, may we continue to peel back the layers of nature to uncover more profound underlying orders.

# Bibliography

[1] C. Amsler, *et al.* (Particle Data Group), Phys. Lett. B **667**, 1 (2008). 1.1, 1.1, 1.1, 1.1, 1.2, 1.3.4, 1.4.2

[2] J. D. Bjorken, Phys. Rev. **179**, 1547 (1969). 1.1

[3] B. Abbott *et al.*, Eur. Phys. J. C **5**, 687 (1998) [arXiv:hep-ph/9801285]. 1.1

[4] M. E. Peskin and T. Takeuchi, Phys. Rev. D **46**, 381 (1992). 1.1

[5] N. Cabibbo, Phys. Rev. Lett. **10**, 531 (1963). 1.1, 1.1

[6] M. Kobayashi and T. Maskawa, Prog. Th. Phys. **49** No.2, 652 (1973). 1.1

[7] J. Alexander *et al.* [Heavy Flavor Averaging Group (HFAG)], arXiv:hep-ex/0412073. 1.1

[8] L. Wolfenstein, Phys. Rev. Lett. **51**, 1945 (1983). 1.1

[9] M. B. Green, J. H. Schwarz and E. Witten, *Superstring Theory*, Univ. Pr. Cambridge, UK (1987). 1.2

[10] C. T. Hill and E. H. Simmons, Phys. Rept. **381**, 235 (2003) [Erratum-ibid. **390**, 553 (2004)] [arXiv:hep-ph/0203079]. 1.2.1

[11] G. T. Fleming, PoS **LATTICE2008**, 021 (2008) [arXiv:0812.2035 [hep-lat]]. 1.2.1

[12] N. Arkani-Hamed, A. G. Cohen and H. Georgi, Phys. Lett. B **513**, 232 (2001) [arXiv:hep-ph/0105239]; N. Arkani-Hamed, A. G. Cohen, T. Gregoire and

J. G. Wacker, JHEP **0208**, 020 (2002) [arXiv:hep-ph/0202089]; N. Arkani-Hamed, A. G. Cohen, E. Katz and A. E. Nelson, JHEP **0207**, 034 (2002) [arXiv:hep-ph/0206021]. 1.2.1

[13] N. Arkani-Hamed, S. Dimopoulos and G. R. Dvali, Phys. Lett. B **429**, 263 (1998) [arXiv:hep-ph/9803315]; I. Antoniadis, N. Arkani-Hamed, S. Dimopoulos and G. R. Dvali, Phys. Lett. B **436**, 257 (1998) [arXiv:hep-ph/9804398]; N. Arkani-Hamed, S. Dimopoulos and G. R. Dvali, Phys. Rev. D **59**, 086004 (1999) [arXiv:hep-ph/9807344]. 1.2.1

[14] L. Randall and R. Sundrum, Phys. Rev. Lett. **83**, 3370 (1999) [arXiv:hep-ph/9905221]. 1.2.1

[15] S. Dimopoulos and S. Raby, Nucl. Phys. B **192**, 353 (1981); E. Witten, Nucl. Phys. B **188**, 513 (1981); M. Dine, W. Fischler and M. Srednicki, Nucl. Phys. B **189**, 575 (1981); S. Dimopoulos and H. Georgi, Nucl. Phys. B **193**, 150 (1981); N. Sakai, Z. Phys. C **11**, 153 (1981); R. K. Kaul and P. Majumdar, Nucl. Phys. B **199**, 36 (1982). 1.2.1

[16] C. D. Froggatt and H. B. Nielsen, Nucl. Phys. B **147**, 277 (1979). 1.2.2

[17] N. Arkani-Hamed, C. D. Carone, L. J. Hall and H. Murayama, Phys. Rev. D **54**, 7032 (1996) [arXiv:hep-ph/9607298]. 1.2.2

[18] N. Arkani-Hamed and M. Schmaltz, Phys. Rev. D **61**, 033005 (2000) [arXiv:hep-ph/9903417]; E. A. Mirabelli and M. Schmaltz, Phys. Rev. D **61**, 113011 (2000) [arXiv:hep-ph/9912265]. 1.2.2

[19] M. Cvetic, P. Langacker and G. Shiu, Nucl. Phys. B **642**, 139 (2002) [arXiv:hep-th/0206115]. 1.2.2

[20] H. Fanchiotti, C. Garcia-Canal and W. A. Ponce, Europhys. Lett. **72**, 733 (2005) [arXiv:hep-ph/0601101]. 1.2.2

[21] S. L. Adler, Phys. Rev. **137**, B1022 (1965). 1.2.2, 1.3.4, 3.1

[22] B. Pontecorvo, Sov. Phys. JETP **7**, 172 (1958) [Zh. Eksp. Teor. Fiz. **34**, 247 (1957)]; Z. Maki, M. Nakagawa and S. Sakata, Prog. Theor. Phys. **28**, 870 (1962). 1.2.3

[23] L. Wolfenstein, Phys. Rev. D **17**, 2360 (1978); S. P. Mikheyev and A. Y. Smirnov, Prog. Part. Nucl. Phys. **23**, 41 (1989). 1.2.3

[24] J. Dunkley, *et al.*, Astrophys. J. Suppl. **180**, 306 (2009) [arXiv:0803.0586v1 [astro-ph]]. 1.2.3, 1.2.4, 2.1, 2.2.1, 2.3.1

[25] E. Komatsu *et al.*, arXiv:1001.4538 [astro-ph.CO]. 1.2.3, 1.2.4, 1.4.1, 3.3

[26] M. Gell-Mann, P. Ramond, and R. Slansky, *Supergravity*, North Holland, Amsterdam, 315 (1979); T. Yanagida, *Proceedings of the Workshop on Unified Theory and Baryon Number in the Universe*, KEK, Tsukuba, Japan (1979); R. Mohapatra and G. Senjanovic, Phys. Rev. Lett. **44**, 912 (1980); R. Mohapatra and G. Senjanovic, Phys. Rev. D **23**, 165 (1981). 1.2.3, 3

[27] G. 't Hooft, Phys. Rev. D **14**, 3432 (1976) [Erratum-ibid. D **18**, 2199 (1978)]. 1.2.4

[28] C. A. Baker, Phys. Rev. Lett. **97**, 131801 (2006). 1.2.4

[29] R. D. Peccei and H. R. Quinn, Phys. Rev. Lett. **38**, 1440 (1977); R. D. Peccei and H. R. Quinn, Phys. Rev. D **16**, 1791 (1977). 1.2.4

[30] S. Perlmutter *et al.* [Supernova Cosmology Project Collaboration], Astrophys. J. **517**, 565 (1999) [arXiv:astro-ph/9812133]. 1.2.4

[31] J. Wess and J. Bagger, *Supersymmetry and Supergravity*, Princeton, USA: Univ. Pr. (1992). 1.3.1

[32] S. P. Martin, arXiv:hep-ph/9709356. 1.3.3, 3.3, 3.4.3, 3.4.3

[33] R. D. Peccei, "Quarks And Leptons As A Coset Space Phenomenon." 1.3.4

[34] B. Zumino, Phys. Lett. **878**, 203 (1979). 1.3.4, 1.3.4

[35] T. Kugo, I. Ojima and T. Yanagida, Phys. Lett. B **135**, 402 (1984); W. Lerche, Nucl. Phys. B **238**, 582 (1984). 1.3.4, 3.2

[36] G. Jungman, M. Kamionkowski and K. Griest, Phys. Rept. **267**, 195 (1996) [arXiv:hep-ph/9506380]. 1.4, 1.4.3, 2.1

[37] G. Bertone, D. Hooper and J. Silk, Phys. Rept. **405**, 279 (2005) [arXiv:hep-ph/0404175]. 1.4, 2.1

[38] H. Murayama, arXiv:0704.2276 [hep-ph]. 1.4

[39] V. C. Rubin and W. K. J. Ford, Astrophys. J. **159**, 379 (1970); V. C. Rubin, N. Thonnard and W. K. . Ford, Astrophys. J. **238**, 471 (1980). 1.4.1

[40] K. G. Begeman, A. H. Broeils and R. H. Sanders, Mon. Not. Roy. Astron. Soc. **249**, 523 (1991). 1.4.1, 1.3

[41] M. Mateo, Ann. Rev. Astron. Astrophys. **36**, 435 (1998) [arXiv:astro-ph/9810070]. 1.4.1

[42] D. Clowe, M. Bradac, A. H. Gonzalez, M. Markevitch, S. W. Randall, C. Jones and D. Zaritsky, Astrophys. J. **648**, L109 (2006) [arXiv:astro-ph/0608407]. 1.4, 1.4.1

[43] A. Friedmann, Z. Phys. **21**, 326 (1924) [Gen. Rel. Grav. **31**, 2001 (1999)]; G. Lemaitre, Gen. Rel. Grav. **29**, 641 (1997) [Annales Soc. Sci. Brux. Ser. I Sci. Math. Astron. Phys. A **53**, 51 (1933)]; H. P. Robertson, Astrophys. J. **82**, 284 (1935); A. G. Walker, Proc. of the Lon. Math. Soc. **s2-42(1)**, 90 (1937).

[44] D. J. Eisenstein *et al.* [SDSS Collaboration], Astrophys. J. **633**, 560 (2005) [arXiv:astro-ph/0501171]. 1.4.1

[45] M. Viel, J. Lesgourgues, M. G. Haehnelt, S. Matarrese and A. Riotto, Phys. Rev. D **71**, 063534 (2005) [arXiv:astro-ph/0501562]. 1.4.2

[46] B. J. Carr, Astrophys. J. **201**, 1 (1975). 1.4.2

[47] C. Alcock *et al.* [MACHO Collaboration and EROS Collaboration], arXiv:astro-ph/9803082; P. Tisserand *et al.* [EROS-2 Collaboration], Astron. Astrophys. **469**, 387 (2007) [arXiv:astro-ph/0607207]. 1.4.2

[48] K. Jedamzik, Phys. Rev. D **55**, 5871 (1997) [arXiv:astro-ph/9605152]. 1.4.2

[49] L. J. Hall and S. Hsu, Phys. Rev. Lett. **64**, 2848 (1990). 1.4.2

[50] K. Griest and M. Kamionkowski, Phys. Rev. Lett. **64**, 615 (1990). 1.4.2

[51] J. N. Bahcall and R. M. Soneira, Astrophys. J. Suppl. **44**, 73 (1980). 1.4.3

[52] J. F. Navarro, C. S. Frenk and S. D. M. White, Astrophys. J. **490**, 493 (1997) [arXiv:astro-ph/9611107]. 1.4.3, 2.2.1, 2.3.1

[53] J. Diemand, B. Moore and J. Stadel, Mon. Not. Roy. Astron. Soc. **353**, 624 (2004) [arXiv:astro-ph/0402267]. 1.4.3

[54] M. Srednicki, K. A. Olive and J. Silk, Nucl. Phys. B **279**, 804 (1987). 1.4.3, 2.1

[55] K. Freese, Phys. Lett. B **167**, 295 (1986); L. M. Krauss, M. Srednicki and F. Wilczek, Phys. Rev. D **33**, 2079 (1986). 1.4.3, 2.1

[56] J. R. Ellis, R. A. Flores, K. Freese, S. Ritz, D. Seckel and J. Silk, Phys. Lett. B **214**, 403 (1988); M. S. Turner and F. Wilczek, Phys. Rev. D **42**, 1001 (1990); M. Kamionkowski and M. S. Turner, Phys. Rev. D **43**, 1774 (1991); J. Silk and M. Srednicki, Phys. Rev. Lett. **53**, 624 (1984); L. Bergstrom, P. Ullio and J. H. Buckley, Astropart. Phys. **9**, 137 (1998) [arXiv:astro-ph/9712318]. 1.4.3, 2.1

[57] N. W. Evans, F. Ferrer and S. Sarkar, Phys. Rev. D **69**, 123501 (2004) [arXiv:astro-ph/0311145]; L. Bergstrom and D. Hooper, Phys. Rev. D **73**, 063510 (2006) [arXiv:hep-ph/0512317]. 1.4.3, 2.1

[58] P. Gondolo, Phys. Lett. B **295**, 104 (1992) [arXiv:hep-ph/9207261]. 1.4.3, 2.1

[59] O. Adriani *et al.* [PAMELA Collaboration], Nature **458**, 607 (2009) [arXiv:0810.4995 [astro-ph]]. 1.4.3, 2.1

[60] J. Chang *et al.* [ATIC Collaboration], Nature **456**, 362 (2008). 1.4.3, 2.1

[61] S. Torii *et al.*, arXiv:0809.0760 [astro-ph]. 1.4.3, 2.1

[62] A. A. Abdo *et al.* [The Fermi LAT Collaboration], Phys. Rev. Lett. **102**, 181101 (2009) [arXiv:0905.0025 [astro-ph.HE]]. 1.4.3, 2.1

[63] D. Hooper, P. Blasi, P. D. Serpico, JCAP **0901**, 025 (2009) [arXiv:0810.1527 [astro-ph]]; S. Profumo, arXiv:0812.4457 [astro-ph]. 2.1

[64] C. R. Chen, F. Takahashi and T. T. Yanagida, Phys. Lett. B **671**, 71 (2009) [arXiv:0809.0792 [hep-ph]]; Phys. Lett. B **673**, 255 (2009) [arXiv:0811.0477 [hep-ph]]. C. R. Chen, M. M. Nojiri, F. Takahashi and T. T. Yanagida, Prog. Theor. Phys. 122 (2009), 553 [arXiv:0811.3357 [astro-ph]]. 2.1, 2.2, 109

[65] C. R. Chen and F. Takahashi, JCAP **0902**, 004 (2009) [arXiv:0810.4110 [hep-ph]]. 2.1, 2.2

[66] P. f. Yin, Q. Yuan, J. Liu, J. Zhang, X. j. Bi and S. h. Zhu, Phys. Rev. D **79**, 023512 (2009) [arXiv:0811.0176 [hep-ph]]. 2.1

[67] K. Ishiwata, S. Matsumoto and T. Moroi, Phys. Lett. B **675**, 446 (2009) [arXiv:0811.0250 [hep-ph]]. 2.1

[68] S. Shirai, F. Takahashi and T. T. Yanagida, Phys. Lett. B **675**, 73 (2009) [arXiv:0902.4770 [hep-ph]]; arXiv:0902.4770 [hep-ph]. 2.1

[69] A. Ibarra, A. Ringwald, D. Tran and C. Weniger, JCAP **0908**, 017 (2009) [arXiv:0903.3625 [hep-ph]]; see also A. Ibarra, A. Ringwald and C. Weniger, JCAP **0901**, 003 (2009) [arXiv:0809.3196 [hep-ph]]. 2.1

[70] M. Ibe, H. Murayama, S. Shirai and T. T. Yanagida, arXiv:0908.3530 [hep-ph]. 2.1

[71] V. Barger, W. Y. Keun, D. Marfatia and G. Shaughnessy, Phys. Lett. B **672**, 141 (2009) [arXiv:0809.0162 [hep-ph]]. 2.1

[72] I. Cholis, L. Goodenough, D. Hooper, M. Simet and N. Weiner, Phys. Rev. D **80**, 123511 (2009) [arXiv:0809.1683 [hep-ph]]. 2.1

[73] L. Bergstrom, J. Edsjo and G. Zaharijas, Phys. Rev. Lett. **103**, 031103 (2009) [arXiv:0905.0333 [astro-ph.HE]]. 2.1

[74] A. Sommerfeld, Annalen der Physik **403**, 257 (1931); M. Cirelli, A. Strumia, arXiv:0808.3867 [astro-ph]; M. Cirelli, M. Kadastik, M. Raidal and A. Strumia, Nucl. Phys. B **813**, 1 (2009) [arXiv:0809.2409 [hep-ph]]. 2.1

[75] R. Harnik and G. D. Kribs, Phys. Rev. D **79**, 095007 (2009) [arXiv:0810.5557 [hep-ph]]; A. E. Nelson and C. Spitzer, arXiv:0810.5167 [hep-ph]; I. Cholis, D. P. Finkbeiner, L. Goodenough and N. Weiner, JCAP **0912**, 007 (2009) [arXiv:0810.5344 [astro-ph]]; K. M. Zurek, Phys. Rev. D **79**, 115002 (2009) [arXiv:0811.4429v3 [hep-ph]]; P. J. Fox and E. Poppitz, Phys. Rev. D **79**, 083528 (2009) [arXiv:0811.0399 [hep-ph]]; I. Cholis, G. Dobler, D. P. Finkbeiner, L. Goodenough and N. Weiner, Phys. Rev. D **80**, 123518 (2009) [arXiv:0811.3641 [astro-ph]]; S. C. Park and J. Shu, Phys. Rev. D **79**, 091702(R) (2009) [arXiv:0901.0720 [hep-ph]]; D. Hooper and K. M. Zurek, Phys. Rev. D **79**, 103529 (2009) [arXiv:0902.0593 [hep-ph]]; D. Hooper and T. M. P. Tait, Phys. Rev. D **80**, 055028 (2009) [arXiv:0906.0362 [hep-ph]]. 2.1

[76] P. Meade, M. Papucci, A. Strumia and T. Volansky, arXiv:0905.0480 [hep-ph]. 2.1, 2.2.1, 2.2.1, 2.3, 2.3, 2.6, 2.3.2, 2.7

[77] C.-R. Chen, S. K. Mandal, F. Takahashi, arXiv:0910.2639 [hep-ph]. 2.1, 2.3.1

[78] O. Adriani *et al.*, Phys. Rev. Lett. **102**, 051101 (2009) [arXiv:0810.4994 [astro-ph]]. 2.1, 2.2.3

[79] N. Arkani-Hamed, D. P. Finkbeiner, T. R. Slatyer and N. Weiner, Phys. Rev. D **79**, 015014 (2009) [arXiv:0810.0713 [hep-ph]]. 2.1

[80] D. Feldman, Z. Liu and P. Nath, Phys. Rev. D **79**, 063509 (2009) [arXiv:0810.5762 [hep-ph]]. 2.1

[81] M. Ibe, H. Murayama and T. T. Yanagida, Phys. Rev. D **79**, 095009 (2009) [arXiv:0812.0072 [hep-ph]]. 2.1

[82] G. Bertone, M. Cirelli, A. Strumia and M. Taoso, JCAP **0903**, 009 (2009) [arXiv:0811.3744 [astro-ph]]. 2.1

[83] M. Kuriyama, H. Nakajima and T. Watari, Phys. Rev. D **79**, 075002 (2009) [arXiv:0802.2584 [hep-ph]]. 2.2

[84] I. Cholis, L. Goodenough and N. Weiner, Phys. Rev. D **79**, 123505 (2009) [arXiv:0802.2922 [astro-ph]]; N. Arkani-Hamed, D. P. Finkbeiner, T. R. Slatyer and N. Weiner, Phys. Rev. D **79**, 015014 (2009) [arXiv:0810.0713 [hep-ph]]; M. Pospelov and A. Ritz, Phys. Lett. B **671**, 391 (2009) [arXiv:0810.1502 [hep-ph]]. 2.2

[85] N. Okada and T. Yamada, arXiv:0905.2801 [hep-ph]. 2.2

[86] J. Hisano, S. Matsumoto, O. Saito and M. Senami, Phys. Rev. D **73**, 055004 (2006) [arXiv:hep-ph/0511118]. 2.2, 4

[87] P. Sreekumar *et al.* [EGRET Collaboration], Astrophys. J. **494**, 523 (1998) [arXiv:astro-ph/9709257]. 2.2

[88] A. W. Strong, I. V. Moskalenko and O. Reimer, Astrophys. J. **613**, 956 (2004) [arXiv:astro-ph/0405441]. 2.2

[89] T. A. Porter [Fermit LAT Collaboration], [arXiv:0907.0294v1 [astro-ph.HE]]. 2.2, 2.2.1

[90] M. Ackermann [Fermi LAT Collaboration], presented at International Cosmic Ray Conference 2009 and TeV Particle Astrophysics 2009. 2.2, 2.2.1

[91] F. Aharonian, *et al.* [HESS Collaboration], Astron.Astrophys. **425**, L13 (2004) [arXiv:astro-ph/0408145]. 2.2, 2.2.1

[92] T. Sjostrand, S. Mrenna and P. Skands, JHEP **0605**, 026 (2006) [arXiv:hep-ph/0603175]. 2.2.1, 2.3.1

[93] J. F. Beacom, N. F. Bell and G. Bertone, Phys. Rev. Lett. **94**, 171301 (2005) [arXiv:astro-ph/0410359]; L. Bergstrom, T. Bringmann, M. Eriksson, M. Gustafsson, Phys. Rev. Lett. **94**, 131301 (2005); A. Birkedal, K. Matchev, M. Perelstein, A. Spray, [arXiv:hep-ph/0507194]; T. Bringmann, L. Bergstrom, J. Edsjo, JHEP **0801**, 049 (2008) [arXiv:0710.3169 [hep-ph]]. 2.2.1

[94] R. Catena and P. Ullio, arXiv:0907.0018 [astro-ph.CO]. 2.2.1, 2.2.1, 2.3.1

[95] A. Ibarra, D. Tran, Phys. Rev. Lett. **100**, 061301 (2008) [arXiv:0709.4593 [astro-ph]]. 2.2.1, 2.3.1

[96] K. Ishiwata, S. Matsumoto and T. Moroi, Phys. Lett. B **679**, 1 (2009) [arXiv:0905.4593 [astro-ph.CO]]. 2.2.1

[97] T. Delahaye, R. Lineros, F. Donato, N. Fornengo and P. Salati, Phys. Rev. D **77**, 063527 (2008) [arXiv:0712.2312 [astro-ph]]. 2.2.1

[98] G. R. Blumenthal, R. J. Gould, Rev. Mod. Phys. **42**, 237 (1970). 2.2.1

[99] GALPROP Homepage, `http://galprop.stanford.edu`; T. A. Porter, A. W. Strong, [arXiv:astro-ph/0507119]. 2.2.1

[100] A. V. Belikov and D. Hooper, arXiv:0906.2251 [astro-ph.CO]. 2.2.1

[101] S. Profumo and T. E. Jeltema, JCAP **0907**, 020 (2009) [arXiv:0906.0001 [astro-ph.CO]]. 2.2.1

[102] F. Aharonian, *et al.* [HESS Collaboration], Nature **439**, 695 (2006). 2.2.1

[103] G. D. Mack, T. D. Jacques, J. F. Beacom, N. F. Bell, H. Yuksel, Phys. Rev. D **78**, 063542 (2008) [ arXiv:0803.0157 [astro-ph]]. 2

[104] C. Amsler, *et al.* [Particle Data Group], Phys. Lett. **B667**, 1 (2008). 2.2.1

[105] A. Ibarra, D. Tran, C. Weniger, arXiv:0909.3514 [hep-ph]. 2.2.1

[106] S. Palomares-Ruiz, Phys. Lett. **B665**, 50 (2008) [ arXiv:0712.1937 [astro-ph]]; J. Hisano, M. Kawasaki, K. Kohri, K. Nakayama, Phys. Rev. D. **79**, 043516 (2009) [arXiv:0812.0219 [hep-ph]]. 2.2.2, 2.3

[107] M. R. Buckley, K. Freese, D. Hooper, D. Spolyar, H. Murayama, arXiv:0907.2385 [astro-ph.HE]; S. K. Mandal, M. R. Buckley, K. Freese, D. Spolyar and H. Murayama, arXiv:0911.5188 [hep-ph]. 2.2.2

[108] Y. Inoue and T. Totani, Astrophys. J. **702**, 523 (2009) [arXiv:0810.3580 [astro-ph]]. 2.2.2

[109] C. R. Chen, F. Takahashi and T. T. Yanagida, in Ref. [64]. 2.2.3

[110] T. Yangida, in Proceedings of the *"Workshop on the Unified Theory and the Baryon Number in the Universe"*, Tsukuba, Japan, Feb. 13-14, 1979, edited by O. Sawada and A. Sugamoto, KEK report KEK-79-18, p. 95, and *"Horizontal Symmetry And Masses Of Neutrinos"* , Prog. Theor. Phys. **64** (1980) 1103; M. Gell-Mann, P. Ramond and R. Slansky, in *"Supergravity"* (North-Holland, Amsterdam, 1979) *eds.* D. Z. Freedom and P. van Nieuwenhuizen, Print-80-0576 (CERN); see also P. Minkowski, Phys. Lett. B **67**, 421 (1977). 1.2.3, 3

[111] A. Bhadra and R. K. Dey, Mon. Not. R. Astron. Soc. **395**, 1371 (2009) [arXiv:0812.1845 [astro-ph]]; W. Bednarek, Phys. Rev. D **79**, 123010 (2009) [arXiv:0906.0084 [astro-ph.HE]]. 2.3

[112] J. F. Beacom, N. F. Bell and G. D. Mack, Phys. Rev. Lett. **99**, 231301 (2007) [arXiv:astro-ph/0608090]. 2.3

[113] H. Yuksel, S. Horiuchi, J. F. Beacom and S. Ando, Phys. Rev. D **76**, 123506 (2007) [arXiv:0707.0196 [astro-ph]]. 2.3

[114] A. Gould, Astrophys. J. **388**, 338 (1992); G. Jungman, M. Kamionkowski and K. Griest, Phys. Rep. **267**, 195 (1996); D. Hooper and J. Silk, New Journ. of Phys. **6**, 23 (2004). 2.3

[115] M. Kowalski, JCAP **0505**, 010 (2005) [arXiv:astro-ph/0505506]. 2.3

[116] L. Gerhardt [IceCube Collaboration], Proc. of the 30th ICRC (2007) [arXiv:0711.0353 [astro-ph]]. 2.3, 2.3.1

[117] J. Kiryluk [IceCube Collaboration], Proc. of the 31st ICRC (2009) [arXiv:0909.0989 [astro-ph.HE]]. 2.3, 2.3.1

[118] S. R. Klein [IceCube Collaboration], IEEE Trans. Nulc. Sci. **56**, 1141 (2009) [arXiv:0807.0034 [astro-ph]]. 2.3

[119] E. Resconi [IceCube Collaboration], Nucl. Instrum. Meth. A **602**, 7 (2009) [arXiv:0807.3891 [astro-ph]]. 2.3, 2.3.1, 2.3.1, 2.3.1

[120] D. Spolyar, M. Buckley, K. Freese, D. Hooper and H. Murayama, [arXiv:0905.4764 [astro-ph.CO]]. 2.3

[121] M. R. Buckley, K. Freese, D. Hooper, D. Spolyar and H. Murayama, [arXiv:0907.2385 [astro-ph.HE]]. 2.3

[122] E. Middell, J. McCartin and M. D'Agostino [IceCube Collaboration], Proc. of the 31st ICRC (2009). 2.3, 2.3.1

[123] D. Grant, D. J. Koskinen and C. Rott [IceCube Collaboration], Proc. of the 31st ICRC (2009). 2.3, 2.3.3

[124] M. Honda, T. Kajita, K. Kasahara, S. Midorikawa and T. Sanuki, Phys. Rev. D **75**, 043006 (2007) [arXiv:astro-ph/0611418]; J. G. Learned and K. Mannheim, Ann. Rev. Nucl. Part. Sci. **50**, 679 (2000). 2.3, 2.3.1

[125] F.-F. Lee and G.-L. Lin, Astropart. Phys. **25**, 64 (2006). 2.3, 2.3.1

[126] R. Gandhi, C. Quigg, M. H. Reno and I. Sarcevic, Phys. Rev. D **58**, 093009 (1998) [arXiv:hep-ph/9807264]. 2.3, 2.5

[127] J. F. Beacom and J. Candia, JCAP **0411**, 009 (2004) [arXiv:hep-ph/0409046]. 2.3

[128] R. Gandhi, C. Quigg, M. H. Reno and I. Sarcevic, Astropart. Phys. **5**, 81 (1996) [arXiv:hep-ph/9512364]. 5

[129] A. B. McDonald, C. Spiering, S. Schoenert, E. T. Kearns and T. Kajita, Rev. Sci. Instrum. **75**, 293 (2004) [arXiv:astro-ph/0311343]. 2.3.1

[130] R. Abbasi *et al.* [IceCube Collaboration], Phys. Rev. D **79**, 102005 (2009) [arXiv:0902.0675 [astro-ph.HE]]. 2.3.1

[131] W. Buchmüller, S. T. Love, R. D. Peccei and T. Yanagida, Phys. Lett. B **115**, 233 (1982). 3.1

[132] W. Buchmüller, R. D. Peccei and T. Yanagida, Nucl. Phys. B **227**, 503 (1983). 3.1, 3.2, 3.2

[133] J. Bagger and E. Witten, Phys. Lett. B **118**, 103 (1982). 3.1

[134] T. Kugo and T. T. Yanagida, arXiv:1003.5985 [hep-th]. For a-ther recent discussion of coupling rigid SUSY to supergravity, see Z. Komargodski and N. Seiberg, arXiv:1002.2228 [hep-th]. 1

[135] J. L. Evans, D. E. Morrissey and J. D. Wells, Phys. Rev. D **75**, 055017 (2007) [arXiv:hep-ph/0611185]. 2

[136] J. Ellis, A. B. Lahanas, D. V. Nanopoulos and K. Tamvakis, Phys. Lett. B **134**, 429 (1984); J. Ellis, C. Kounnas and D. V. Nanopoulas, Phys. Lett. B **247**, 373 (1984). 2

[137] T. Kugo, S. Uehara and T. Yanagida, Phys. Lett. B **147**, 321 (1984). 3.2

[138] M. Bando, T. Kuramoto, T. Maskawa and S. Uehara, Prog. Theor. Phys. **72**, 313 (1984). 3.2

[139] T. Goto and T. Yanagida, Prog. Theor. Phys. **83**, 1076 (1990). 3.2

[140] S. Weinberg, Phys. Rev. Lett. **48**, 1303 (1982). 3.2

[141] J. Ellis, D. V. Nanopoulos and S. Sarkar, Nucl. Phys. B **259**, 275 (1985); M. H. Reno and D. Seckel, Phys. Rev. D **37**, 3441 (1988); S. Dimopoulos, R. Esmailzadeh, L. J. Hall and G. D. Starkman, Nucl. Phys. B **311**, 699 (1989); M. Kawasaki, K. Kohri and T. Moroi, Phys. Rev. D **71**, 083502 (2005). 3.2

[142] A. H. Chamseddine, R. Arnowitt and P. Nath, Phys. Rev. Lett. **49**, 970 (1982). 3.3

[143] B. C. Allanach, Comput. Phys. Commun. **143**, 305 (2002), [arXiv:hep-ph/0104145]. 3.3

[144] P. Gondolo, J. Edsjo, P. Ullio, L. Bergstrom, M. Schelke and E. A. Baltz, JCAP **0407**, 008 (2004) [arXiv:astro-ph/0406204]; L. Bergström and P. Gondolo, Astropart. Phys. **5**, 263 (1996) [arXiv:hep-ph/9510252]; P. Gondolo and G. Gelmini, Nucl. Phys. B **360**, 145 (1991); J. Edsjö and P. Gondolo, Phys. Rev. D **56**, 1879 (1997) [arXiv:hep-ph/9704361]. 3.3

[145] B. Allanach *et al.*, Comput. Phys. Commun. **180**, 8 (2009) [arXiv:0801.0045 [hep-ph]]; 3.3

[146] S. Heinemeyer, W. Hollik and G. Weiglein, Comput. Phys. Commun. **124**, 76 (2000) [arXiv:hep-ph/9812320]; S. Heinemeyer, W. Hollik and G. Weiglein, Eur. Phys. J. C **9**, 343 (1999) [arXiv:hep-ph/9812472]; G. Degrassi, S. Heinemeyer, W. Hollik, P. Slavich and G. Weiglein, Eur. Phys. J. C **28**, 133 (2003) [arXiv:hep-ph/0212020]; M. Frank, T. Hahn, S. Heinemeyer, W. Hollik, H. Rzehak and G. Weiglein, JHEP **0702**, 047 (2007) [arXiv:hep-ph/0611326]. 3.3

[147] P. Bechtle, O. Brein, S. Heinemeyer, G. Weiglein and K. E. Williams, Comput. Phys. Commun. **181**, 138 (2010) [arXiv:0811.4169 [hep-ph]]. 3.3

[148] J. Kopp, T. Schwetz and J. Zupan, JCAP **1002**, 014 (2010) [arXiv:0912.4264 [hep-ph]]. 3.3

[149] M. Drees, Y. G. Kim, M. M. Nojiri, D. Toya, K. Hasuko and T. Kobayashi,

Phys. Rev. D **63**, 035008 (2001) [arXiv:hep-ph/0007202]; J. Hisano, M. M. Nojiri and W. Sreethawong, JHEP **0906**, 044 (2009) [arXiv:0812.4496 [hep-ph]]. 3.3

[150] J. Hisano, K. Nakayama and M. Yamanaka, Phys. Lett. B **684**, 246 (2010) [arXiv:0912.4701 [hep-ph]]. 3.3

[151] J. Ellis and K. A. Olive, arXiv:1001.3651 [astro-ph.CO]. 3.3

[152] P. Richardson, JHEP **0111**, 029 (2001) [arXiv:hep-ph/0110108]; A. J. Barr, Phys. Lett. B **596**, 205 (2004) [arXiv:hep-ph/0405052]; Phys. Rev. D **70**, 075016 (2004) T. Goto, K. Kawagoe and M. M. Nojiri, [Erratum-ibid. D **71**, 059902 (2005)] [arXiv:hep-ph/0406317]. 3.4.1, 3.4.3

[153] ATLAS Collaboration, "ATLAS detector and physics performance. Technical design report. Vol. 2," ATLAS-TDR-15. 3.4.1, 3.4.2

[154] F. E. Paige, S. D. Protopopescu, H. Baer and X. Tata, arXiv:hep-ph/0312045. 3.4.2

[155] G. Corcella *et al.*, arXiv:hep-ph/0210213. 3.4.2

[156] E. Richter-Was, arXiv:hep-ph/0207355. 3.4.2

[157] O. S. . Bruning, *et al.* (ed.), "LHC design report. Vol. I: The LHC main ring," CERN-2004-003-V-1. 3.4.2

[158] I. Hinchliffe, F. E. Paige, M. D. Shapiro, J. Soderqvist and W. Yao, Phys. Rev. D **55**, 5520 (1997) [arXiv:hep-ph/9610544]; H. Bachacou, I. Hinchliffe and F. E. Paige, Phys. Rev. D **62**, 015009 (2000) [arXiv:hep-ph/9907518]. 3.4.2

[159] B. K. Gjelsten, D. J. . Miller and P. Osland, JHEP **0412**, 003 (2004)[arXiv:hep-ph/0410303]. 3.4.2, 3.4.2, A, A, A, A

[160] F. James and M. Roos, Comput. Phys. Commun. **10**, 343 (1975). R. Brun and F. Rademakers, Nucl. Instrum. Meth. A **389**, 81 (1997). 3.4.2

# Appendix A

# Appendix for Chapter 3

In this section we give miscellaneous data on the model points:

- Plots of invariant mass distributions, with edge fits
- Expected and fit endpoints (as well as secondary endpoints)
- All mass solutions
- Notable branching ratios

**Note:** All mass units are in GeV.

## Benchmark point 1 (BP 1)

### True masses

$$m_{\tilde{\chi}_1^0} = 120.3, \quad m_{\tilde{l}} = 158.2, \quad m_{\tilde{\chi}_2^0} = 231.7, \quad m_{\tilde{q}} = 660.4$$

### Endpoint values

| | $m_{ll}^{max}$ | $m_{jll}^{max}$ | $m_{jl(lo)}^{max}$ | $m_{jl(hi)}^{max}$ |
|---|---|---|---|---|
| Expected | 109.9 | 528.5 | 336.8 | 451.8 |
| Fit | $109.7 \pm 0.4$ | $533.3 \pm 3.0$ | $341.2 \pm 6.0$ | $457.1 \pm 2.4$ |

### Mass solutions

| Region [159] | $m_{\tilde{l}} - m_{\tilde{\chi}_1^0}$ | $m_{\tilde{\chi}_2^0} - m_{\tilde{l}}$ | $m_{\tilde{q}} - m_{\tilde{\chi}_2^0}$ | $m_{\tilde{q}}$ |
|---|---|---|---|---|
| Expected | 37.9 | 73.5 | 429 | 660 |
| (1,1) | $73.0 \pm 1.7$ | $43.1 \pm 1.0$ | $459 \pm 11$ | $876 \pm 62$ |
| (1,2) | Imaginary | | | |
| **(1,3)** | $\mathbf{37.7 \pm 1.1}$ | $\mathbf{73.3 \pm 1.9}$ | $\mathbf{433 \pm 7}$ | $\mathbf{655 \pm 35}$ |
| (4,1) | Imaginary | | | |
| (4,2) | $33.3 \pm 3.5$ | $76.5 \pm 3.0$ | $423 \pm 3.2$ | $551 \pm 5$ |
| (4,3) | $37.2 \pm 1.3$ | $73.5 \pm 2.0$ | $423 \pm 3.0$ | $621 \pm 15$ |

Correct solution is in bold.

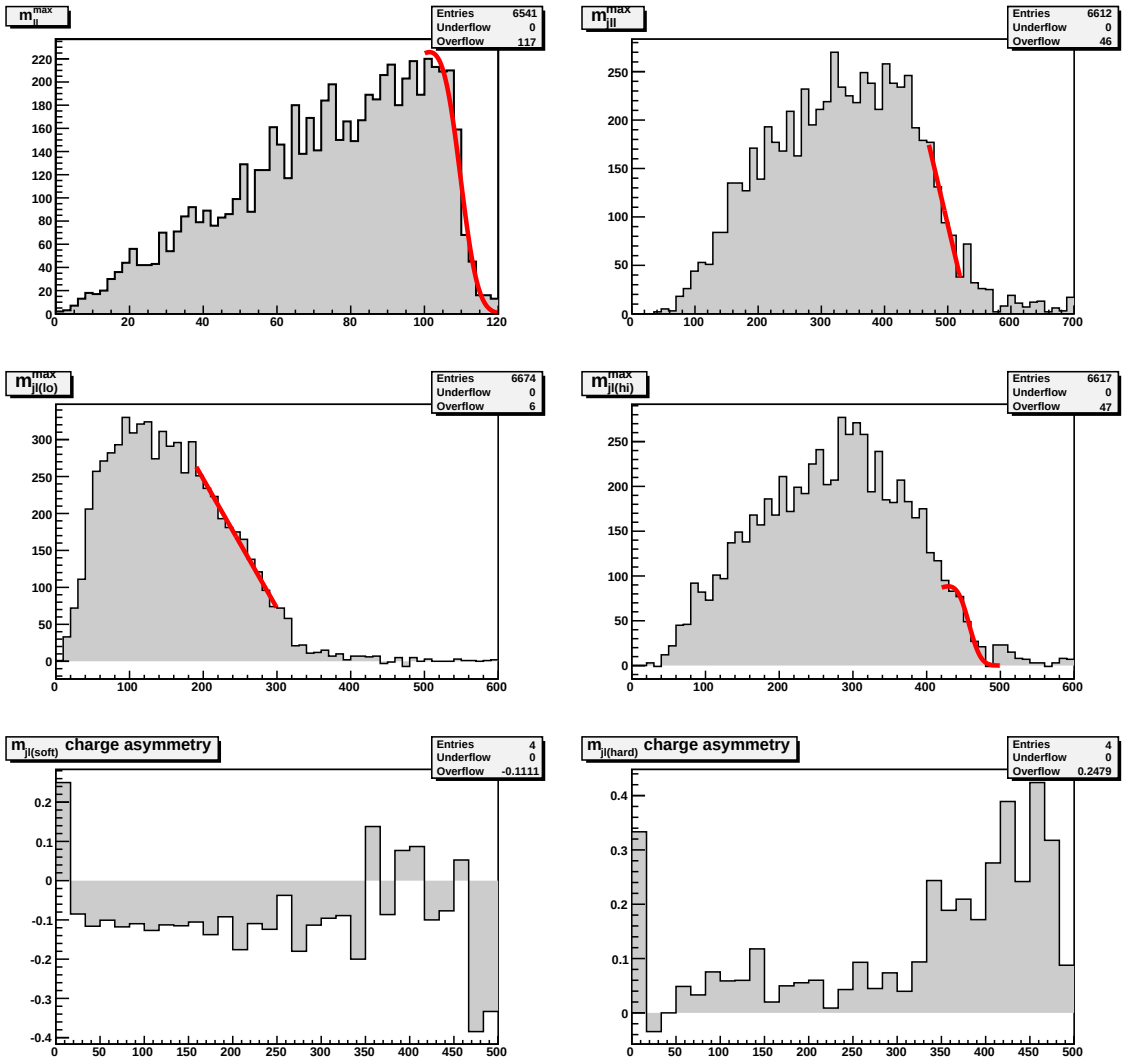


Figure A.1: BP 1 invariant mass distributions and endpoint fits. Upper left, $m_{ll}$; upper right, $m_{jll}$; middle left, $m_{jl(lo)}$; middle right, $m_{jl(hi)}$. Lower left, $m_{jl^+(soft)} - m_{jl^-(soft)}$; lower right, $m_{jl^+(hard)} - m_{jl^-(hard)}$.

**Notable branching ratios**

| Parent | Daughters | Branching ratio |
|---|---|---|
| $\tilde{u}_L$ | $u_L\tilde{\chi}_2^0$ | 0.33 |
| | $d_L\tilde{\chi}_1^{\pm}$ | 0.66 |
| $\tilde{u}_R$ | $u_R\tilde{\chi}_1^0$ | 1.0 |
| | $u_R\tilde{\chi}_2^0$ | $1.1 \times 10^{-3}$ |
| $\tilde{\chi}_2^0$ | $l_L^{\pm}\tilde{l}_L^{\mp}$ | 0.42 |
| | $l_R^{\pm}\tilde{l}_R^{\mp}$ | $5.8 \times 10^{-5}$ |
| | $\nu_L\tilde{\nu}_L$ | 0.58 |

## Benchmark point 2 (BP 2)

### True masses

$$m_{\tilde{\chi}_1^0} = 120.1, \quad m_{\tilde{l}} = 193.7, \quad m_{\tilde{\chi}_2^0} = 234.5, \quad m_{\tilde{q}} = 643.5$$

### Endpoint values

| | $m_{ll}^{max}$ | $m_{jll}^{max}$ | $m_{jl(lo)}^{max}$ | $m_{jl(hi)}^{max}$ |
|---|---|---|---|---|
| Expected | 103.7 | 514.6 | 337.8 | 470.0 |
| Fit | $103.7 \pm 0.3$ | $516.7 \pm 1.2$ | $338.0 \pm 1.2$ | $469.1 \pm 4.8$ |

For calculating charge asymmetry: $m_{jl(near)} = 349.5 \pm 2.8$

### Mass solutions

| Region [159] | $m_{\tilde{l}} - m_{\tilde{\chi}_1^0}$ | $m_{\tilde{\chi}_2^0} - m_{\tilde{l}}$ | $m_{\tilde{q}} - m_{\tilde{\chi}_2^0}$ | $m_{\tilde{q}}$ |
|---|---|---|---|---|
| Expected | 73.5 | 40.8 | 409 | 643 |
| **(1,1)** | $\mathbf{73.1 \pm 1.4}$ | $\mathbf{40.8 \pm 0.3}$ | $\mathbf{414 \pm 5}$ | $\mathbf{658 \pm 20}$ |
| (1,2) | Imaginary | | | |
| (1,3) | $29.9 \pm 1.5$ | $75.0 \pm 1.8$ | $412 \pm 1.5$ | $562 \pm 6$ |
| (4,1) | Imaginary | | | |
| (4,2) | $23.4 \pm 2.4$ | $80.3 \pm 2.6$ | $413 \pm 1$ | $528 \pm 2$ |
| (4,3) | $29.8 \pm 1.5$ | $75.0 \pm 1.7$ | $412 \pm 1$ | $561 \pm 5$ |

Correct solution is in bold.

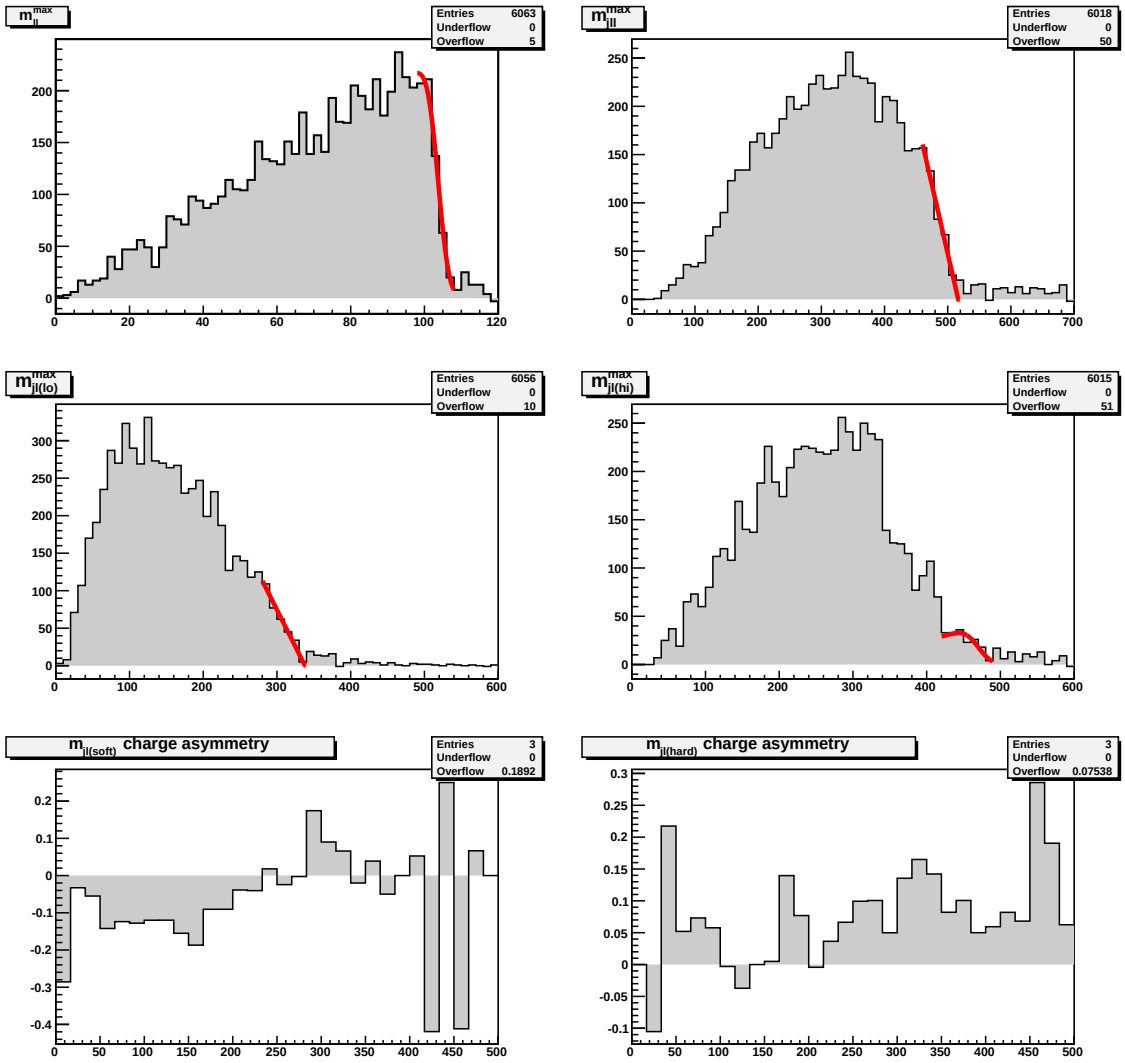


Figure A.2: BP 2 invariant mass distributions and endpoint fits. Upper left, $m_{ll}$; upper right, $m_{jll}$; middle left, $m_{jl(lo)}$; middle right, $m_{jl(hi)}$. Lower left, $m_{jl^+(soft)} - m_{jl^-(soft)}$; lower right, $m_{jl^+(hard)} - m_{jl^-(hard)}$.

**Notable branching ratios**

| Parent | Daughters | Branching ratio |
|---|---|---|
| $\tilde{u}_L$ | $u_L\tilde{\chi}_2^0$ | 0.33 |
| | $d_L\tilde{\chi}_1^{\pm}$ | 0.66 |
| $\tilde{u}_R$ | $u_R\tilde{\chi}_1^0$ | 1.0 |
| | $u_R\tilde{\chi}_2^0$ | $5.0 \times 10^{-4}$ |
| $\tilde{\chi}_2^0$ | $l_L^{\pm}\tilde{l}_L^{\mp}$ | 0.36 |
| | $l_R^{\pm}\tilde{l}_R^{\mp}$ | $5.7 \times 10^{-4}$ |
| | $\nu_L\tilde{\nu}_L$ | 0.64 |

## Benchmark point 3 (BP 3)

### True masses

$$m_{\tilde{\chi}_1^0} = 106.4, \quad m_{\tilde{l}} = 135.3, \quad m_{\tilde{\chi}_2^0} = 166.9, \quad m_{\tilde{q}} = 639.2$$

### Endpoint values

| | $m_{ll}^{max}$ | $m_{jll}^{max}$ | $m_{jl(lo)}^{max}$ | $m_{jl(hi)}^{max}$ |
|---|---|---|---|---|
| Expected | 60.4 | 475.6 | 324.4 | 381.4 |
| Fit | $60.4 \pm 0.1$ | $473.2 \pm 4.5$ | $323.3 \pm 0.9$ | $370.2 \pm 4.4$ |

| Secondary edge | $m_{ll}^{max}$ |
|---|---|
| $\tilde{\chi}_2^{\pm} \to \tilde{\nu}_L l^{\pm} \to \tilde{\chi}_1^{\pm} ll$ | 93.0 |
| $\tilde{\chi}_4^0 \to \tilde{l}_L l \to \tilde{\chi}_2^0 ll$ | 107.4 |
| $\tilde{\chi}_4^0 \to \tilde{l}_L l \to \tilde{\chi}_1^0 ll$ | 176.4 |

### Mass solutions

| Region [159] | $m_{\tilde{l}} - m_{\tilde{\chi}_1^0}$ | $m_{\tilde{\chi}_2^0} - m_{\tilde{l}}$ | $m_{\tilde{q}} - m_{\tilde{\chi}_2^0}$ | $m_{\tilde{q}}$ |
|---|---|---|---|---|
| Expected | 28.9 | 31.6 | 472 | 639 |
| (1,1) | $33.8 \pm 0.4$ | $27.3 \pm 0.3$ | $580 \pm 48$ | $988 \pm 170$ |
| **(1,2)** | $\mathbf{29.1 \pm 1.0}$ | $\mathbf{31.4 \pm 0.9}$ | $\mathbf{491 \pm 12}$ | $\mathbf{693 \pm 31}$ |
| (1,3) | $28.7 \pm 1.0$ | $32.1 \pm 0.6$ | $437 \pm 24$ | $558 \pm 50$ |
| (4,1) | Imaginary | | | |
| (4,2) | $38.1 \pm 2.2$ | $30.1 \pm 0.6$ | $404 \pm 6$ | $480 \pm 7$ |
| (4,3) | $30.6 \pm 1.0$ | $31.5 \pm 0.6$ | $411 \pm 5$ | $506 \pm 10$ |

Correct solution is in bold.

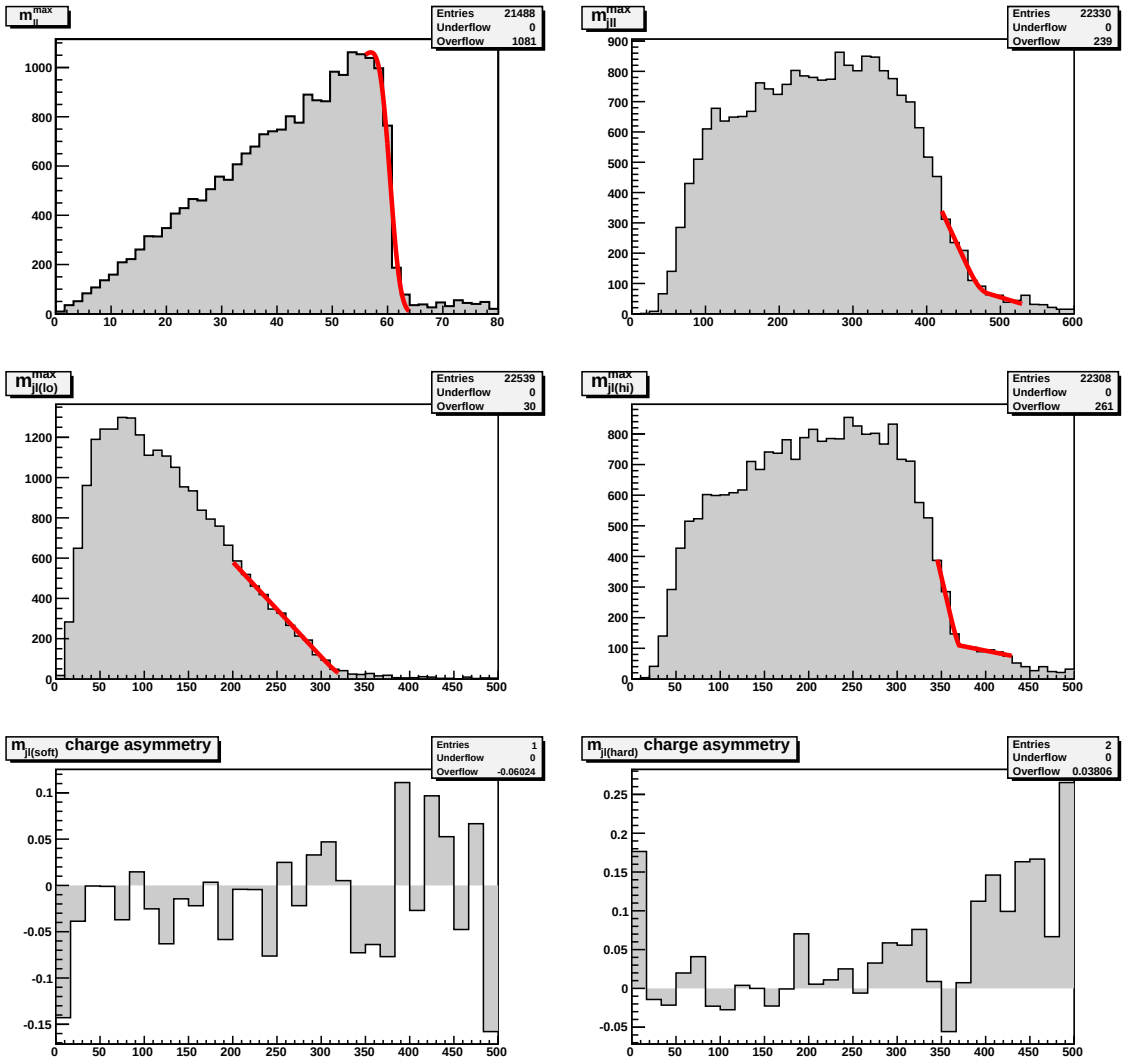


Figure A.3: BP 3 invariant mass distributions and endpoint fits. Upper left, $m_{ll}$; upper right, $m_{jll}$; middle left, $m_{jl(lo)}$; middle right, $m_{jl(hi)}$. Lower left, $m_{jl^+(soft)} - m_{jl^-(soft)}$; lower right, $m_{jl^+(hard)} - m_{jl^-(hard)}$.

**Notable branching ratios**

| Parent | Daughters | Branching ratio |
|---|---|---|
| $\tilde{g}$ | $q\tilde{q}_L$ | 0.40 |
| | $q\tilde{q}_R$ | 0.59 |
| $\tilde{u}_L$ | $u_L\tilde{\chi}_2^0$ | 0.17 |
| | $u_L\tilde{\chi}_4^0$ | 0.16 |
| | $d_L\tilde{\chi}_1^\pm$ | 0.37 |
| | $d_L\tilde{\chi}_2^\pm$ | 0.30 |
| $\tilde{d}_L$ | $d_L\tilde{\chi}_2^0$ | 0.095 |
| | $d_L\tilde{\chi}_4^0$ | 0.19 |
| | $u_L\tilde{\chi}_1^\pm$ | 0.20 |
| | $u_L\tilde{\chi}_2^\pm$ | 0.45 |
| $\tilde{u}_R$ | $u_R\tilde{\chi}_1^0$ | 0.76 |
| | $u_R\tilde{\chi}_2^0$ | 0.22 |
| $\tilde{\chi}_2^0$ | $l_R^\pm\tilde{l}_R^\mp$ | 1.0 |
| $\tilde{\chi}_4^0$ | $l_L^\pm\tilde{l}_L^\mp$ | 0.21 |
| | $l_R^\pm\tilde{l}_R^\mp$ | 0.02 |
| | $\nu_L\tilde{\nu}_L$ | 0.4 |
| $\tilde{\chi}_1^\pm$ | $l_L^\pm\nu_L\tilde{\chi}_1^0$ | 0.36 |
| $\tilde{\chi}_2^\pm$ | $l_L^\pm\tilde{\nu}_L$ | 0.33 |

## Comparison point (CP)

### True masses

$$m_{\tilde{\chi}_1^0} = 118.8, \quad m_{\tilde{l}} = 144.5, \quad m_{\tilde{\chi}_2^0} = 222.0, \quad m_{\tilde{q}} = 666$$

### Endpoint values

| | $m_{ll}^{max}$ | $m_{jll}^{max}$ | $m_{jl(lo)}^{max}$ | $m_{jl(hi)}^{max}$ |
|---|---|---|---|---|
| Expected | 95.9 | 530.3 | 310.4 | 476.6 |
| Fit | $95.3 \pm 0.4$ | $547.6 \pm 6.2$ | $309.0 \pm 2.7$ | $479.6 \pm 15.5$ |

### Mass solutions

| Region [159] | $m_{\tilde{l}} - m_{\tilde{\chi}_1^0}$ | $m_{\tilde{\chi}_2^0} - m_{\tilde{l}}$ | $m_{\tilde{q}} - m_{\tilde{\chi}_2^0}$ | $m_{\tilde{q}}$ |
|---|---|---|---|---|
| Expected | 25.7 | 77.5 | 444 | 666 |
| (1,1) | $75.2 \pm 3.8$ | $31.6 \pm 0.7$ | $526 \pm 67$ | $1080 \pm 400$ |
| (1,2) | Imaginary | | | |
| **(1,3)** | $\mathbf{27.6 \pm 3.3}$ | $\mathbf{76.0 \pm 4.5}$ | $\mathbf{497 \pm 51}$ | $\mathbf{848 \pm 236}$ |
| (4,1) | Imaginary | | | |
| (4,2) | $14.9 \pm 3.8$ | $89.0 \pm 7.9$ | $444 \pm 7$ | $574 \pm 10$ |
| (4,3) | $24.9 \pm 2.5$ | $78.3 \pm 45.3$ | $444 \pm 6$ | $664 \pm 30$ |

Correct solution is in bold.

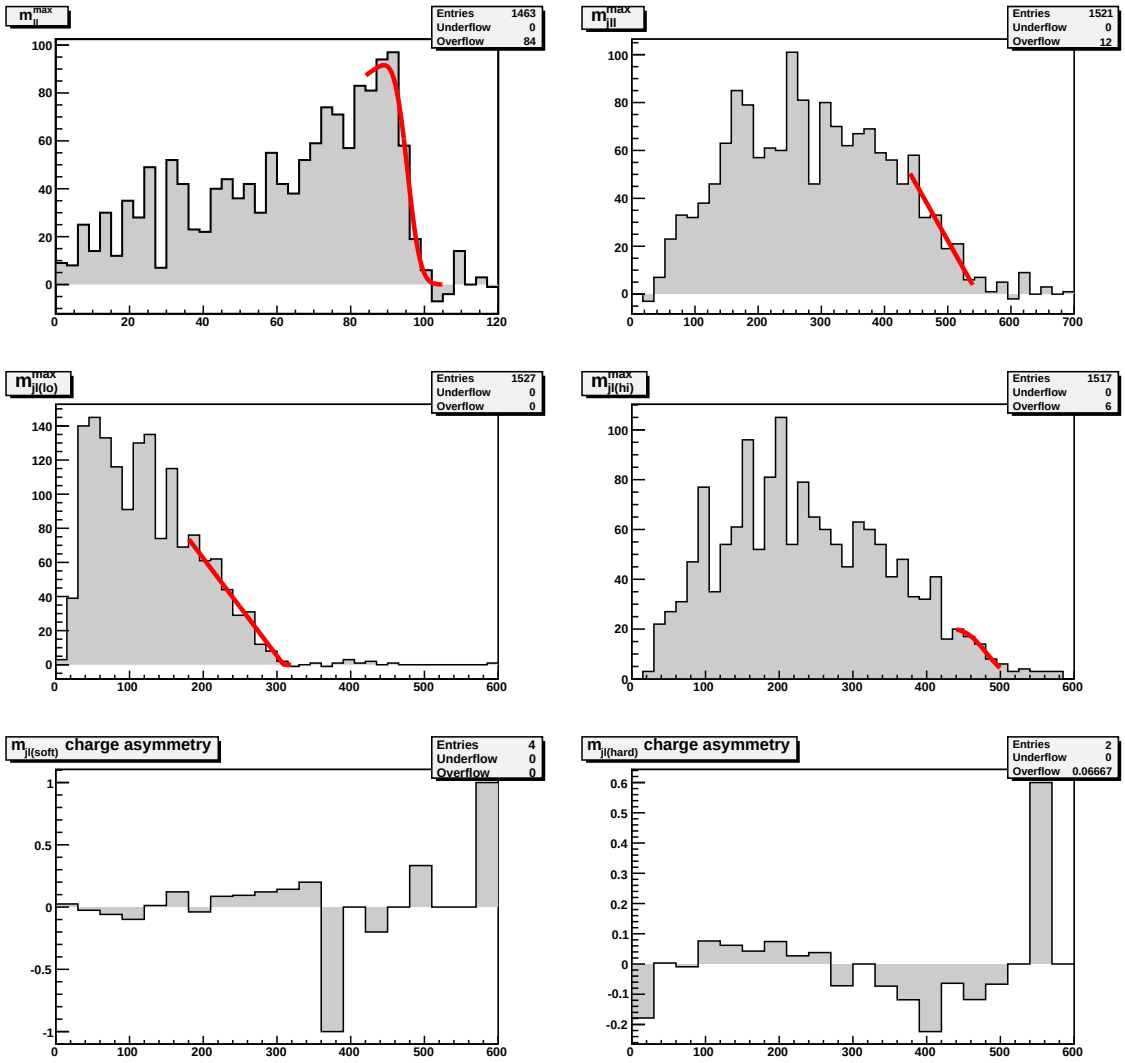


Figure A.4: Comparison point invariant mass distributions and endpoint fits. Upper left, $m_{ll}$; upper right, $m_{jll}$; middle left, $m_{jl(lo)}$; middle right, $m_{jl(hi)}$. Lower left, $m_{jl^+(soft)} - m_{jl^-(soft)}$; lower right, $m_{jl^+(hard)} - m_{jl^-(hard)}$.

**Notable branching ratios**

| Parent | Daughters | Branching ratio |
|---|---|---|
| $\tilde{u}_L$ | $u_L\tilde{\chi}_2^0$ | 0.32 |
| | $d_L\tilde{\chi}_1^\pm$ | 0.65 |
| $\tilde{u}_R$ | $u_R\tilde{\chi}_1^0$ | 0.99 |
| | $u_R\tilde{\chi}_2^0$ | $4.7 \times 10^{-3}$ |
| $\tilde{\chi}_2^0$ | $l_R^\pm\tilde{l}_R^\mp$ | 0.052 |
| | $\tau^\pm\tilde{\tau}_1^\mp$ | 0.44 |
| | $\nu_L\tilde{\nu}_L$ | 0.50 |